LAWRENCE
LIVERMORE
NATIONAL
LABORATORY

UCRL-TH-206583

Structural and Functional Studies of the Protamine 2-Zinc Complex from Syrian Gold Hamster (Mesocricetus Auratus) Spermatids and Sperm

C. E. Dolan

September 16, 2004

This work was performed under the auspices of the U.S. Department of Energy by University of California, Lawrence Livermore National Laboratory under Contract W-7405-Eng-48.

Structural and Functional Studies of the Protamine 2-Zinc Complex from Syrian Gold Hamster (*Mesocricetus auratus*) Spermatids and Sperm

Cheryl E. Dolan

B.S. (California State University, Hayward) 1994

Submitted in partial satisfaction of the requirements for the degree of Doctor of Philosophy in Biochemistry and Molecular Biology from the University of California, Davis

June 2004

Approved:

_____

_____

_____

Dissertation Committee (2004)

ABSTRACT

The research described in this dissertation consists of four major areas: (1) sequence analysis of protamine 2 from Muroid rodents to identify potential zinc-binding domain(s) of protamine 2; (2) structural studies of the protamine 2-zinc complex from Syrian Gold hamster sperm and spermatids to elucidate the role of zinc during spermiogenesis; (3) structural studies of an unique protamine 2-zinc complex from chinchilla sperm; and (4) Nuclear Magnetic Resonance (NMR) studies of soluble complexes of hairpin oligonucleotides with synthetic arginine-rich peptides or protamine 1 isolated from bull sperm. First, zinc was quantitated in spermatids and sperm by Proton-Induced X-ray Emission (PIXE) to determine whether zinc is present in the early stages of spermiogenesis. The PIXE results revealed the zinc content varies proportionately with the amount of protamine 2 in both spermatid and sperm nuclei. An exception was chinchilla sperm containing twice the amount of protamine 2 than zinc. Further analyses by PIXE and X-ray Absorption Spectroscopy (XAS) of zinc bound to protamines isolated from hamster sperm confirmed the majority of the zinc is bound to protamine and identified the zinc ligands of protamine 2 in hamster spermatids and sperm *in vivo*. These studies established that zinc is bound to the protamine 2 precursor in hamster spermatids and the coordination of zinc by protamine 2 changes during spermiogenesis. Finally, the sequence analysis combined with the XAS results suggest that the zinc-binding domain in protamine 2 resides in the amino-terminus. Similar analyses of chinchilla sperm by XAS were performed to clarify the unusual PIXE results and revealed that chinchilla has an atypical protamine

2-zinc structure. Two protamine 2 molecules coordinate one zinc atom, forming homodimers that facilitate the binding of protamine 2 to DNA and provide an organizational scheme that would accommodate the observed species-specific protamine stoichiometry in mammalian sperm. Based on these results, we propose the binding of zinc to protamine 2 molecules stabilizes a dimerization domain in other mammalian sperm. Future experiments will use the knowledge we gained of the interactions between protamine 1 and DNA from the NMR studies to obtain structural data for the DNA-protamine 2-zinc complex.

TABLE OF CONTENTS

ACKNOWLEDGEMENTS

I would like to gratefully acknowledge the following individuals for their valuable assistance throughout my graduate research. My advisors and mentors, Dr. Rod Balhorn and Dr. Morton Bradbury, for the opportunity to study the interdisciplinary area of protein structure. Thank you, Rod, for encouraging me and exchanging ideas regarding my research anytime I could catch you in your office! Shelley Corzett, for giving technical and intellectual support beyond measure, taught me there is no such thing as a "simple experiment", and exemplifies true friendship. Don Hoffman, my awesome Student-Employee Graduate Research Fellowship advocate! I appreciate the efforts of my collaborators, Drs. Graham Bench, Katrina Peariso, Larry Brewer and Monique Cosman - you made the project more exciting because of your expertise and enthusiasm for science. Thank you to my colleagues, friends, and the Student-Employee Graduate Research Fellowship staff at Lawrence Livermore National Laboratory for their tremendous support.

I am grateful to my parents, Virginia and Joseph Kramer, for imparting the fun of learning and the importance of education to their children - thank you, Mom and Dad!

I am immensely grateful for the grants and fellowships I was awarded for the support of my research project: from the University of Davis, California, the National Institute of Health Molecular & Cellular Biology Training Grant, the Alexander and Henrietta Hollaender Institute Fellowship, and the Floyd and Mary Schwall Fellowship; and from the Lawrence Livermore National Laboratory, the Student-Employee Graduate Research Fellowship.

This work was performed at Lawrence Livermore National Laboratory under the auspices of the U.S. Department of Energy under contract W-7405 ENG-48.

DEDICATION

This dissertation is dedicated to my wonderful family who sacrificed their time with me so I could complete this project. To my two beautiful daughters, Hannah and Serena, I know there were mornings that you wanted to stay in your jammies, but you went to school instead. I am very proud of both of you. To my understanding husband, Christopher, who listened to endless conversations about my research AND provided ideas! Thank you for your sincere interest, encouragement, and sense of humor.

We did it!!!

GENERAL INTRODUCTION

Chromatin remodeling in mammalian sperm.

At the onset of spermatogenesis in the testes, proliferating diploid spermatogonia in the epithelium of the seminiferous tubules enter one of three pathways: remain as undifferentiated stem cells; differentiate to spermatozoa; or terminate by apoptosis (1). Each spermatogonia committed to the differentiative pathway completes two meiotic divisions, producing haploid spermatids that will differentiate into four mature sperm. During this maturation phase of sperm, spermiogenesis, the haploid round spermatids undergo complex morphological and biochemical modifications that enable the successful transmission of the paternal genome to the next generation.

The most notable of these nuclear modifications is the extensive chromatin remodeling that occurs during mammalian spermiogenesis. The supercoiled, nucleosomal chromatin of the haploid round spermatid is eliminated in the elongated spermatid by the replacement of histones with intermediary transition proteins, TP1 and TP2 (2-5). The mechanism of histone removal from the sperm chromatin is unknown, but it is preceded by chemical modifications of the highly conserved and accessible N-terminal tails of the core histones. These modifications - phosphorylation,

acetylation, methylation, and ubiquitination – are initial events for destabilizing the interactions between the histones and DNA as well as creating a signaling "code" to recruit the factors that participate in chromatin remodeling during spermatogenesis (6-11). Additionally, the transition proteins may also facilitate histone removal and repair the DNA strand breaks that occur during chromatin remodeling, therefore contributing both functional and structural roles in the exchange of chromatin proteins in the elongating spermatid nucleus (12,13).

Toward the end of spermiogenesis, protamines complete the dynamic process of sperm chromatin remodeling by replacing the transition proteins. The molecular events have yet to be elucidated, but protamines 1 and 2 also utilize transient and reversible modifications to promote DNA binding, such as phosphorylation, that decrease basicity and/or increase mass (14). Protamines remain as the predominant nuclear protein in mammalian sperm, condensing the sperm nucleus to 5% the volume of a somatic cell nucleus (15-17). This extremely compact packaging unique to sperm nuclei is due to the neutralization of the acidic DNA by the basic protamines, creating polymers that form bundles held together by van der Waals forces, and coiling the nucleoprotamine into 60nm toroids (18-22). One consequence of the highly condensed packaging of DNA by protamine is that the majority of

transcription ceases (23). It has been proposed that this quiescent and highly condensed sperm cell increases hydrodynamic efficiency crucial for sperm motility and protects the DNA from mutagenesis and other damaging agents (1).

The time-course of the sperm chromatin proteins binding to DNA has been characterized by examining the developmental stages of the *R. norvegicus* spermatid. Grimes et al. (24) used cell and nuclei separation techniques to determine the stage-specific synthesis and binding of transition proteins 1 and 2, protamine 1, and protamine 2 precursor during spermiogenesis (25). These results indicated that histones were present in step 1-8 spermatid nuclei, transition proteins 1 and 2 were present in steps 13-15, and protamine 1 and protamine 2 precursors were bound to DNA in step 16-19 spermatids. Further refinement of the isolation of the stage-specific rat spermatids demonstrated the sequential appearance of TP2 (steps 9-14) followed by TP1 (steps 12-15) with protamine 1 in spermatids steps 11-19 (26). Since the molecular events that occur during spermatogenesis are evolutionarily conserved, it is not surprising that the order of appearance of nuclear proteins is identical in human sperm (23). The analyses of human spermatids by *in situ* hybridization and immunohistochemistry revealed that protamines 1 and 2 were present in step 4-8 spermatid nuclei (27).

Regulation of protamine expression in mammalian sperm.

Protamine 1 is expressed in the mature spermatozoa of all mammalian species whereas P2 expression is limited to the sperm nuclei of rodents and primates (16,28-41). However, the P2 gene appears to be present in the genome of all eutherian mammals. Restriction maps of the protamine genes of human, mouse, rat and bull demonstrate that the protamine genes are organized on a chromosomal gene cluster with TP-2 (42-46). The presence of this tandem array of protamine genes does not coincide with the level of P2 expression, since the percentage of P2 varies between different genera even in sperm that contain both protamines. Thus, while the gene cluster contributes to the regulation of protamine expression by shared regulatory factors, each gene is further regulated by its own specific controls, most of which remain to be identified.

Both protamines are transcribed from a single copy gene and studies using transgenic mice and *in vitro* transcription assays have identified a number of the promoter sequences that regulate protamine gene expression (47-49). Some of the factors involved in the regulation of protamine gene expression have been identified using gel mobility shift assays, although regulation by the cAMP-response element modulator (CREM) is the best characterized to date (49-51). During spermatogenesis, there is a switch in

CREM gene expression from an inhibitor to an activator generated by alternative exon splicing. Transgenic studies using CREM-mutant mice demonstrate that round spermatids fail to differentiate into spermatozoa and protamine 1 and 2 were not expressed (52,53). Similarly, maturation of round spermatids is arrested when sperm from infertile humans do not express CREM (54).

The expression of spermatid nucleoproteins is also translationally regulated. During spermiogenesis in the mouse, protamine mRNA is transcribed in haploid round spermatids and not translated until one week later in the elongating spermatid (55,56). Studies using transgenic mice have established that translation of protamine mRNA is controlled by the 3'UTR region (57-59). TPs and protamine mRNAs in the round spermatid are stored as ribonucleoprotein particles that are translationally repressed and a number of protein repressors that bind to the poly-A tail or other specific sequences located in the 3'UTR region have been identified (27). This translational delay provides a powerful means of spatial and temporal regulation by which the large amounts of protamines required for condensing the sperm genome can be synthesized quickly despite cessation of transcription of the protamine genes (60,61).

Structure of protamines.

Both protamines contain arginine-rich domains that bind to DNA, but unlike the central domain of P1, the polyarginine regions are interspersed throughout the P2 molecule (19). Mammalian protamines contain cysteine residues that form intra- and inter-molecular disulfide bonds. Disulfide formation is initiated in the testicular sperm nuclei after protamines bind to DNA and is completed during descent of the sperm through the epididymis (62-65). Consequently, isolation of protamines from mature sperm requires reduction of the disulfide bonds that crosslink the protamines around the DNA helix whereas protamines can be isolated from spermatids without a reducing agent.

Although presently the precise functions of P1 and P2 are unknown, structural differences alone suggest the protamines have unique roles as DNA packaging proteins. Protamine 2 differs from protamine 1 in that it is synthesized as a larger precursor protein that is processed through a series of specific proteolytic cleavages after incorporation into the sperm chromatin complex (36). Also, amino acid composition and sequence analyses of the protamine 2 molecules isolated from various species of mammals have shown them to be extremely rich in histidine e.g. 13-21% (19). Protamine 1, by comparison, usually contains 5% or less histidine. These two differences

in structure and metabolism suggest that protamines 1 and 2 might perform different functions in sperm chromatin. Indeed, results from recent transgenic experiments in which either the protamine 1 or 2 gene was eliminated from the mouse genome revealed that protamines do not have redundant functions since both protamines are essential for fertility (66).

Structural studies of the mammalian sperm chromatin.

The arginine domains of protamines appear to mediate the condensation of DNA through the formation of toroids, elliptical subunits 50-100 nm in diameter, as revealed by topological analyses of intact sperm chromatin from bull, rat, and mouse using scanning probe microscopy (SPM) (67). SPM analyses of human sperm chromatin, containing both histones and protamines, demonstrated higher order structures of nucleosomes and toroids. Optical trapping experiments using single DNA molecules suggested that the number of polyarginine domains affects the rate of toroid formation (68). To date, no other model based on experimental evidence has been proposed to describe the higher order structure of nucleoprotamine.

Objective of study.

In addition to elucidating the function of protamine 2 in mammalian sperm, the objective of this project was to design novel structural

experiments to gain understanding of protamine organization in the sperm chromatin by examining the specific interactions between the protamines and DNA, P1 and P2, as well as P2 and zinc. Rodent protamines were selected as the model system for these experiments instead of human for practical reasons. First, because of the substantial amount of material required for optimizing the sample preparation and conditions for the experiments, hamster epididymides are an ideal source, yielding 150-fold more sperm and protamines than can be obtained from comparable rat or mouse tissue. Second, transgenic mice provide an experimental system that can be altered to test theories *in vivo* developed from the earlier hamster data, such as substitution of amino acids in protamine 2 proposed to coordinate zinc.

Designing our structural studies required knowledge of the amino acid sequences of protamines 1 and 2 present in the sperm of rodents, but because of the number of consecutive arginine residues present in these two proteins, only the amino-terminal sequences could be obtained by direct protein sequencing of isolated protamines. Since only the laboratory rat (*Rattus norvegicus*) and mouse (*Mus musculus*) protamine gene sequences were known, the initial step was to sequence protamine 1 and 2 genes from hamster by using polymerase chain reaction (PCR). This proved to be quite

challenging as the N-terminal sequences for protamine 2 are not conserved and the protamine gene sequences are extremely GC-rich. The 5' primer was designed using conserved promoter sequences to flank the beginning of the P1 gene and the 3' primer to flank the end of the P2 gene, the hamster P1 and P2 genes were amplified by PCR as a unit using a high-fidelity polymerase mix (40). In retrospect, formation of secondary structures adjacent to the 5' region of the P2 gene may have interfered with primer binding, thereby preventing amplification of the P2 gene from isolated genomic DNA. Regardless, the amplification of the protamine genes as a primary reaction followed by secondary reactions amplifying the individual protamine genes yielded a PCR method for easily obtaining other rodent protamine gene sequences from which the amino acid sequences could be derived and compared, improving the prediction of key amino acids involved in zinc coordination and thus the design of structural studies of protamines.

Importance of structural studies of protamine 2 and zinc: advancing our understanding of male infertility for clinical applications.

While the protamine 2 content of sperm varies widely among different genera of mammals, a number of studies have correlated male infertility in humans with alterations in the proportion of P1 and P2 in the sperm nuclei

and decreased amounts of either or both protamines (69-74). Protamine-deficient sperm chromatin is decondensed and the DNA is frequently damaged (75-83). Thus, perturbations in P1:P2 stoichiometry may result in susceptibility to DNA damage in the sperm nucleus and contribute to current idiopathic infertility cases.

Additionally, zinc appears to play an important function in fertility. Zinc content is elevated in the male reproductive tract, compared with blood plasma, and has been proposed to function in maintaining the stability of sperm DNA during epididymal storage and ejaculation. Decondensation of DNA has been correlated *in vitro* in sperm with the addition of zinc chelators and *in vivo* in sperm from infertile males with impaired secretion of zinc from the prostate (84-88). Conversely, zinc must be depleted from hamster sperm for capacitation and penetration of the zona pellucida to occur (89,90). Recent studies of zinc in rodent testes demonstrate that both deficiency and excessive intake of zinc adversely affects testicular tissue and sperm function (91,92). Hence, although it is evident that zinc contributes to the stability of the chromatin required for normal sperm function, secretion of zinc by the prostate may be required to regulate the amount of zinc present during spermiogenesis. Until zinc function is better understood, the use of zinc supplements may be toxic and thereby unsuitable for treating

male infertility.

Infertility treatment is a $1 billion per year industry and of the 2.6 million couples seeking reproductive assistance, 40% of the infertility cases are male-related. Abnormal sperm chromatin packaging and nuclear DNA damage are linked and the fertilization rates decline when the spermatozoa nuclei contain fragmented DNA (93). Increasing our understanding of the molecular mechanisms underlying male infertility, including protamine function and structure, is necessary to prevent inappropriate use of costly procedures as well as to decrease the risks to the developing embryo. In addition, the information obtained from these protamine 2-zinc studies will be useful in developing the next generation of male contraceptives in which specific interactions are disrupted between protamines, zinc, and DNA.

REFERENCES

1. Hecht NB. Molecular mechanisms of male germ cell differentiation. BioEssays 1998; 20:555-561.
2. Ward WS, Partin AW, Coffey DS. DNA loop domains in mammalian spermatozoa. Chromosoma 1989; 98:153-159.
3. Risley MS, Einheber S, Bumcrot DA. Changes in DNA topology during spermatogenesis. Chromosoma 1986; 94:217 -227.
4. Meistrich ML. Histone and basic nuclear protein transitions in

mammalian spermatogenesis. In: Hnilica LS, Stein GS, Stein JL (eds), Histones and other basic nuclear proteins. Florida: CRC Press; 1989: 165-182.

5. Levesque D, Veilleux S, Caron N, Boissonneault G. Architectural DNA-binding properties of the spermatidal transition proteins 1 and 2. Biochem Biophys Res Commun 1998; 252:602-609.
6. Cheung P, Allis CD, Sassone-Corsi P. Signaling to chromatin through histone modifications. Cell 2000; 103:263-271.
7. Strahl BD, Allis CD. The language of covalent histone modifications. Nature 2000; 403:41-45.
8. Robertson KD. DNA methylation and chromatin - unraveling the tangled web. Oncogene 2002; 21:5361-5379.
9. Jason LJ, Moore SC, Lewis JD, Lindsey G, Ausio J. Histone ubiquitination: a tagging tail unfolds? Bioessays 2002; 24:166-174.
10. Moore SC, Jason L, Ausio J. The elusive structural role of ubiquitinated histones. Biochem Cell Biol 2002; 80:311-319.
11. Baarends WM, Hoogerbrugge JW, Roest HP, Ooms M, Vreeburg J, Hoeijmakers JH, Grootegoed JA. Histone ubiquitination and chromatin remodeling in mouse spermatogenesis. Dev Biol 1999; 207:322-333.

12. Meistrich M, Mohapatra B, Shirley C, Zhao M. Roles of transition nuclear proteins in spermiogenesis. Chromosoma 2003; 111:483-488.

13. Boissonneault G. Chromatin remodeling during spermiogenesis: a possible role for the transition proteins in DNA strand break repair. FEBS Lett 2002; 514:111-114.

14. Green GR, Balhorn R, Poccia DL, Hecht NB. Synthesis and processing of mammalian protamines and transition proteins. Mol Reprod Dev 1994; 37:255-263.

15. Balhorn R, Weston S, Thomas C, Wyrobek A. DNA packaging in mouse spermatids: synthesis of protamine variants and four transition proteins. Exp Cell Res 1984; 150:298-308.

16. Pogany GC, Corzett M, Weston S, Balhorn, R. DNA and protein content of mouse sperm: implications regarding sperm chromatin structure. Exp Cell Res 1981; 136:127-136.

17. Corsi-Sassone P. Unique chromatin remodeling and transcriptional regulation in spermatogenesis. Science 2002; 296:2176-2178.

18. Balhorn R. A model for the structure of chromatin in mammalian sperm. J Cell Biol 1982; 93:298-305.

19. Balhorn R. Mammalian protamines: structure and molecular interactions. In: Adolph KW (ed), Molecular biology of chromosome

function. New York: Springer-Verlag; 1989: 366-395.

20. Allen MJ, Bradbury EM, Balhorn R. AFM analysis of DNA-protamine complexes bound to mica. Nucleic Acids Res 1997; 25:2221-2226.

21. Hud NV, Allen MJ, Downing KH, Lee J, Balhorn R. Identification of the elemental packing unit of DNA in mammalian sperm cells by atomic force microscopy. Biochem Biophys Res Commun 1993; 193:1347-1354.

22. Ward WS, Zalensky AO. The unique, complex organization of the transcriptionally silent sperm chromatin. Crit Rev Eukaryot Gene Expr 1996; 6:139-147.

23. Hecht NB. The making of a spermatozoon: a molecular perspective. Dev Genet 1995; 16:95-103.

24. Grimes SR, Meistrich ML, Platz RD, Hnilica LS. Nuclear protein transitions in rat testis spermatids. Exp Cell Res 1977; 110:31-39.

25. Unni E, Zhang Y, Meistrich ML, Balhorn R. Rat spermatid basic nuclear protein TP3 is the precursor of protamine 2. Exp Cell Res 1994; 210:39-45.

26. Kistler WS, Henriksen K, Mali P, Parvinen M. Sequential expression of nucleoproteins during rat spermiogenesis. Exp Cell Res 1996;

225:374-381.

27. Steger K. Transcriptional and translational regulation of gene expression in haploid spermatids. Anat Embryol 1999; 199:471-487.

28. Balhorn R, Gledhill BL, Wyrobek AJ. Mouse sperm chromatin proteins: quantitative isolation and partial characterization. Biochemistry 1977; 16:4074-4080.

29. Bellve AR, Carraway RJ. Characterization of two basic chromosomal proteins isolated from mouse spermatozoa. Cell Biol 1978; 79:177a.

30. Kleene LC, Distel RJ, Hecht NB. Nucleotide sequence of a cDNA clone encoding mouse protamine 1. Biochemistry 1985; 24:719-722.

31. McKay DJ, Renaux BS, Dixon GH. The amino acid sequence of human sperm protamine P1. Biosci Rep 1985; 5:383-391.

32. Ammer H, Henschen A, Lee C-H. Isolation and amino acid sequence analysis of human sperm protamines P2 and P2: occurrence of two forms of protamine 2. Biol Chem Hoppe-Seyler 1986; 367:515-522.

33. Gusse M, Sautiere P, Belaiche D, Martinage A, Roux C, Dadoune J-P, Chevaillier P. Purification and characterization of nuclear basic proteins of human sperm. Biochim Biophys Acta 1986; 884:124-134.

34. McKay DJ, Renaux BS, Dixon GH. Human sperm protamines: amino-acid sequences of two forms of protamine P2. Eur J Biochem

1986; 156:5-8.

35. Corzett M, Mazrimas JA, Balhorn, R. Protamine 1:protamine 2 stoichiometry in the sperm of eutherian mammals. Mol Reprod Dev 2002; 61:519-527.

36. Yelick PC, Balhorn R, Johnson M, Corzett M, Mazrimas JA, Kleene KC, Hecht NB. Mouse protamine is synthesized as a precursor whereas mouse protamine 1 is not. Mol Cell Biol 1987; 7:2173-2179.

37. Bellve AR, McKay DJ, Renaux BS, Dixon GH. Purification and characterization of mouse protamines P1 and P2: amino acid sequence of P2. Biochemistry 1988; 27:2890-2897.

38. Johnson PA, Yelick PC, Liem H, Hecht NB. Differential distribution of the P1 and P2 protamine gene sequences in eutherian and marsupial mammals and a monotreme. Gamete Res 1988; 19:169-175.

39. Retief JD, Winkfein RJ, Dixon GH, Adroer R, Queralt R, Ballabriga J, Oliva R. Evolution of protamine P1 genes in primates. J Mol Evol 1993; 37:426-434.

40. Corzett M, Kramer C, Blacher R, Mazrimas J, Balhorn R. Hamster protamines sequence and distribution. Mol Reprod Dev 1999; 54:273-282.

41. Dolan CE, Fabes SE, Mazrimas JA, Corzett MH, Breed WG, Balhorn

R. Variable regulation of protamine 2 gene expression in Muroid rodents. (manuscript in preparation).

42. Hecht NB, Kleene KC, Yelick PC, Johnson PA, Pravtcheva DD, Ruddle FH. Mapping of haploid expressed genes: genes for both mouse protamines are located on chromosome 16. Somat Cell Mol Genet 1986; 12:203-208.

43. Adham IM, Szpirer C, Kremling H, Keime S, Szpirer J, Levan G, Engel W. Chromosomal assignment of four rat genes coding the spermatid-specific proteins proacrosin (ACR), transition proteins 1 (TNP1) and 2 (TNP2), and protamine 1 (PRM1). Cytogenet Cell Genet 1991; 57:47-50.

44. Reinhart N, Kremling H, Luerseen H, Adham IM, Engel W. Characterization of a gene encoding a basic protein of the spermatid nucleus, TNP2, and its close linkage to the protamine genes in the bull. Biol Chem Hoppe Seyler 1991; 372:431-436.

45. Schluter G, Kremling H, Engel W. The gene for human transition protein 2: nucleotide sequence, assignment to the protamine gene cluster, and evidence for its low expression. Genomics 1992; 14:377-38.

46. Keime S, Heitland K, Kumm S, Schlosser M, Hroch N, Holtz W,

Engel W. Characterization of four genes encoding basic proteins of the porcine spermatid nucleus and close linkage of three of them. Biol Chem Hoppe Seyler 1992; 373:261-270.

47. Peschon JJ, Behringer RR, Brinster RL, Palmiter RD. Spermatid-specific expression of protamine 1 in transgenic mice. Proc Natl Acad Sci USA 1987; 84:5316-5319.

48. Zambrowicz BP, Harendza CJ, Zimmermann JW, Brinster RL, Palmiter RD. Analysis of the mouse protamine 1 promoter in transgenic mice. Proc Natl Acad Sci USA 1993; 90:5071-5075.

49. Yiu GK, Hecht NB. Novel testis-specific protein-DNA interactions activate transcription of the mouse protamine 2 gene during spermatogenesis. J Biol Chem 1997; 272:26926-26933.

50. Hummelke GC, Meistrich ML, Cooney AJ. Mouse protamine genes are candidate targets for the novel orphan nuclear receptor, germ cell nuclear factor. Mol Reprod Dev 1998; 50:396-405.

51. Foulkes NS, Mellstrom BR, Benusiglio E, Sassone-Corsi P. Developmental switch of CREM function during spermatogenesis: from antagonist to activator. Nature 1992; 355:80-84.

52. Nantel F, Monaco L, Foulkes NS, Masquilier D, LeMeur M, Henriksen K, Dierich A, Parvinen M, Sassone-Corsi P.

Spermiogenesis deficiency and germ-cell apoptosis in CREM-mutant mice. Nature 1996; 380:159-162.

53. Blendy JA, Kaestner KH, Weinbauer GF, Nieschlag E, Schutz G. Severe impairment of spermatogenesis in mice lacking the CREM gene. Nature 1996; 380:162-165.

54. Weinbauer GF, Behr R, Bergmann M, Nieschlag E. Testicular cAMP responsive element modulator (CREM) protein is expressed in round spermatids but is absent or reduced in men with round spermatid maturation arrest. Mol Hum Reprod 1998; 4:9-15.

55. Kleene KC, Distel RJ, Hecht NB. cDNA clones encoding cytoplasmic poly(A)+ RNAs which first appear at detectable levels in haploid phases of spermatogenesis in the mouse. Dev Biol 1983; 98:455-464.

56. Kleene KC, Distel RJ, Hecht NB. Translational regulation and coordinate deadenylation of a protamine mRNA during spermiogenesis in the mouse. Dev Biol 1984; 105:71-79.

57. Braun RE, Peschon JJ, Behringer RR, Brinster RL, Palmiter RD. Protamine 3'-untranslated sequences regulate temporal translational control and subcellular localization of growth hormone in spermatids of trangenic mice. Genes Dev 1989; 3:793-802.

58. Kwon YK, Hecht NB. Cytoplasmic protein binding to highly

conserved sequences in the 3’ untranslated region of mouse protamine 2 mRNA, a translationally regulated gene of male germ cells. Proc Natl Acad Sci USA 1991; 88:3584-3588.

59. Fajardo MA, Butner KA, Lee K, Braun RE. Germ cell-specific proteins interact with the 3’-untranslated regions of Prm-1 and Prm-2 mRNA. Dev Biol 1994; 166:643-653.

60. Dadoune JP. Expression of mammalian spermatozoal nucleoproteins. Microsc Res Tech 2003; 61:56-75.

61. Steger K. Haploid spermatids exhibit translationally repressed mRNAs. Anat Embryol 2001; 203:323-334.

62. Calvin HI, Yu CC, Bedford JM. Effects of epididymal maturation, zinc (II) and copper (II) on the reactive sulfhydryl content of structural elements in rat spermatozoa. Exp Cell Res 1973; 81:333-341.

63. Bedford JM, Calvin HI. The occurrence and possible functional significance of -S-S- crosslinks in sperm heads, with particular reference to eutherian mammals. J Exp Zool 1974; 188:137-156.

64. Marushige Y, Marushige K. Transformation of sperm histone during formation and maturation of rat spermatozoa. J Biol Chem 1975; 250:39-45.

65. Saowaros W, Panyim S. The formation of disulfide bonds in human protamines during sperm maturation. Experientia 1979; 35:191-192.

66. Cho C, Willis WD, Goulding EH, Jung-Ha H, Choi YC, Hecht NB, Eddy EM. Haploinsufficiency of protamine-1 or –2 causes infertility in mice. Nat Genet 2001; 28:82-86.

67. Allen MJ, Dong XF, O'Neill TE, Yau P, Kowalczykowski SC, Gatewood J, Balhorn R, Bradbury EM. Atomic force microscope measurements of nucleosome cores assembled along defined DNA sequences. Biochemistry 1993; 32:8390-8396.

68. Brewer LR, Corzett MH, Balhorn R. Protamine-induced condensation and decondensation of the same DNA molecule. Science 1999; 286:120-123.

69. Balhorn R, Reed S, Tanphaichitr N. Aberrant protamine 1/protamine 2 ratios in sperm of infertile human males. Experientia 1988; 44:52-55.

70. Belokopytova IA, Kostyleva EI, Tomilin AN, Vorobev VI. Human male infertility may be due to a decrease of the protamine-P2 content in sperm chromatin. Mol Reprod Dev 1993; 34:53-57.

71. Blanchard Y, Lescoat D, Le Lannou D. Anomalous distribution of nuclear basic proteins in round-headed human spermatozoa. Andrologia 1990; 22:549-555.

72. de Yebra L, Ballesca JL, Vanrell JA, Bassas L, Oliva R. Complete selective absence of protamine-P2 in humans. J Biol Chem 1993; 268:10553-10557.

73. Bench G, Corzett MH, de Yebra L, Oliva R, Balhorn R. Protein and DNA contents in sperm from an infertile human male possessing protamine defects that vary over time. Mol Reprod Dev 1998; 50:345-353.

74. de Yebra L, Ballesca JL, Vanrell JA, Corzett M, Balhorn R, Oliva R. Detection of P2 precursors in the sperm cells of infertile patients who have reduced protamine P2 levels. Fertil Steril 1998; 69:755-759.

75. Razavi S, Nasr-Esfahani MH, Mardani M, Mafi A, Moghdam A. Effect of human sperm chromatin anomalies on fertilization outcome post-ICSI. Andrologia 2003; 35:238-243.

76. Nasr-Esfahani MH, Razavi S, Mardani M. Relation between different human sperm nuclear maturity tests and *in vitro* fertilization. J Assist Reprod Genet 2001; 18:219-225.

77. Iranpour FG, Nasr-Esfahani MH, Valojerdi MR, al-Taraihi TM. Chromomycin A3 staining as a useful tool for evaluation of male fertility. J Assist Reprod Genet 2000; 17:60-66.

78. Sakkas D, Urner F, Bizzaro D, Manicardi G, Bianchi PG, Shoukir Y,

Campana A. Sperm nuclear DNA damage and altered chromatin structure: effect on fertilization and embryo development. Hum Reprod 1998; 13:11-19.

79. Bianchi PG, Manicardi GC, Urner F, Campana A., Sakkas D. Chromatin Packaging and Morphology in Ejaculated Human Spermatozoa: Evidence of Hidden Anomalies in Normal Spermatozoa. Mol Hum Reprod 1996; 2:139-144.

80. Lolis D, Georgiou I, Syrrou M, Zikopoulos K, Konstantelli M, Messinis I. Chromomycin A3-staining as an indicator of protamine deficiency and fertilization. Int J Androl 1996; 19:23-27.

81. Sailer BL, Jost LK, Evenson DP. Mammalian sperm DNA susceptibility to in situ denaturation associated with the presence of DNA strand breaks as measured by the terminal deoxynucleotidyl transferase assay. J Androl 1995; 16:80-87.

82. Manicardi GC, Bianchi PG, Pantano S, Azzoni P, Bizzaro D, Bianchi U, Sakkas D. Presence of endogenous nicks in DNA of ejaculated human spermatozoa and its relationship to chromomycin A3 accessibility. Biol Reprod 1995; 52:864-867.

83. Gorczyca W, Traganos F, Jesionowska H, Darzynkiewicz Z. Presence of DNA strand breaks and increased sensitivity of DNA *in situ* to

denaturation in abnormal human sperm cells: analogy to apoptosis of somatic cells. Exp Cell Res 1993; 207:202-205.

84. Bjorndahl L, Kvist U. Loss of an intrinsic capacity for human sperm chromatin decondensation. Acta Physiol Scand 1985; 124:189-194.

85. Kvist U, Bjorndahl L. Zinc preserves an inherent capacity of chromatin decondensation of human spermatozoa. Acta Physiol Scand 1985; 124:195-200.

86. Kvist U, Bjorndahl L, Kjellberg S. Sperm nuclear zinc, chromatin stability, and male fertility. Scanning Microsc 1987; 1:1241-1247.

87. Bjorndahl L, Kjellberg S, Roomans GM, Kvist U. The human sperm nucleus takes up zinc at ejaculation. Int J Androl 1986; 9:77-80.

88. Kvist U, Bjorndahl L. Zinc in sperm chromatin and chromatin stability in fertile men and men in barren unions. Scand J Urol Nephrol 1988; 22:1-6.

89. Andrews JC, Bavister BD. Capacitation of hamster spermatozoa with the divalent cation chelators D-penicillamine, L-histidine, and L-cysteine in a protein-free culture medium. Gamete Res 1989; 23:159-170.

90. Andrews JC, Nolan JP, Hammerstedt RH, Bavister BD. Role of zinc during hamster sperm capacitation. Biol Reprod 1994; 51:1238-1247.

91. Ozturk A, Baltaci AK, Bediz CS, Mogulkoc R, Gungor S. 2003. Effects of zinc and melatonin deficiency on testicular tissue of rats. Biol Trace Elem Res 96:255-262.

92. Turgut G, Abban G, Turgut S, Take G. Effect of overdose zinc on mouse testis and its relation with sperm count and motility. Biol Trace Elem Res 2003; 96:271-279.

93. Lopes S, Sun JG, Jurisicova A, Meriano J, Casper RF. Sperm deoxyribonucleic acid fragmentation is increased in poor-quality semen samples and correlates with failed fertilization in intracytoplasmic sperm injection. Fertil Steril 1998; 69:528-532.

CHAPTER ONE

A Comparative Sequence Analysis of Protamine 2 from Muroid Rodents

Abstract

Sequence comparisons provide insight into the key amino acids that contribute to the structural domains of proteins. We obtained and compared protamine 2 sequences from a variety of rodents from the Muridae family to elucidate potential amino acid residues that coordinate zinc. We also used the data to examine how different mechanisms for organizing protamines 1 and 2 might dictate the relative proportion of protamines that package the DNA in sperm chromatin. We discovered that differences in protamine primary sequence do relate to the coordination of zinc, but they do not appear to influence protamine stoichiometry in sperm chromatin. Instead, the results suggest that the formation of protamine 2 homodimers on sperm DNA may provide a mechanism for regulating the proportion of protamines observed in Muroid rodent sperm.

Introduction

Chromatin condensation in mammalian spermatids.

The final stages of mammalian spermiogenesis are characterized by the dramatic compaction of the chromatin in elongating spermatids (1,2). The transformation of the spermatid chromatin begins when histones, which organize early spermatid chromatin into nucleosomes, are replaced with transition proteins (3). In late-step spermatids, the transition proteins are displaced by smaller, highly basic protamines, creating the extremely condensed nucleoprotamine complex characteristic of the mature spermatozoan (4,5).

Characteristics of protamines 1 & 2.

Two types of protamines, protamines 1 (P1) and 2 (P2), have been isolated from the sperm nuclei of rodents and primates (Figure 1)(5-8). P1 has a molecular weight of approximately 7kD, a highly conserved amino-terminal sequence, and a central DNA binding domain consisting of multiple polyarginine domains (9,10). In contrast, P2 is synthesized as an approximately 13kD precursor from which one-third of the amino-terminus of P2 is sequentially removed after the precursor is deposited onto DNA in late-step spermatids (11). The remaining 8.5kD protein is histidine-rich with arginine-rich regions interspersed throughout the protein (10). Both

A.

HUMAN P1
MARYRCCRSQSRSRYYRQRQRSRRRRRRSCQTRRRAMRCCRPRYRPRCRRH

MOUSE P1
MARYRCCRSKSRSRCRRRRRRCRRRRRRCCRRRRRRCCRRRRSYTIRCKKY

B.

HUMAN P2
MVRYRVRSLSERSHEVYRQQLHGQEQGHHGQEEQGLSPEHVEVYE
RTHGQSHYRRRHCSRRRLHRIHRRQHRSCRRRKRRSCRHRRRHRRGCRTRKRTC
RRH

MOUSE P2
MVRYRMRSPSEGPHQGPGQDHEREEQGQGQGLSPERVEDYGRTH
RGHHHHRHRRCSRKRLHRIHKRRRSCRRRRRHSCRHRRRHRRGCRRSRRRRRCR
CRKCRRHHH

Figure 1. Primary sequences of (A) human and mouse protamine 1 and (B) human and mouse protamine 2. The leader sequence of the protamine 2 precursor is shown in red.

protamines bind inside the major groove of DNA to the phosphate backbone via a series of arginine-rich domains (12-16). Using data derived from DNA and total protamine masses in individual mammalian sperm, the DNA binding sites of P1 and P2 were estimated to cover 11 and 15 base pairs, respectively (17). This study also revealed that the total protamine mass to DNA mass ratio was similar in the different mammalian sperm examined, even though the relative proportion of protamines 1 and 2 vary between the species (17).

Organization of protamine genes & expression.

Although only the sperm chromatin of rodents and primates contain P2, DNA sequences homologous to both protamine genes appear to be present in the genomes of all eutherian mammals (18). Restriction maps of human, mouse, rat and bull genomes demonstrated that the protamine genes and transition protein 2 are organized as a chromosomal gene cluster (19-23). Despite the presence of a similar tandem array of protamine 1 and 2 genes, the amount of P2 in spermatids differs widely among mammalian species. While P1 comprises 100% of total protamine in the sperm of many mammals, rodent and primate sperm contain variable amounts of protamines 1 and 2. However, the amount of P2 has not been observed to exceed 80% of total protamine in the sperm of any species examined to date (24). This

limited P2 expression suggests that, while P1 can function independently, P2 may require P1 for some function that stabilizes the haploid genome to promote fertilization and/or embryonic development.

Objectives of this study.

To accomplish our goal of identifying how P2 binds zinc, we needed to identify those ligands (amino acid side chains) that bind zinc within P2. We began by obtaining P2 sequences from the rodent family, Muridae, for a comparative analysis of conserved amino acids. When we initiated this study, P2 sequences from rodents had only been determined for *Mus musculus* (11,25) and *Rattus norvegicus* (26), also of the Muridae family. In addition to obtaining P2 sequences from a variety of hamsters and rats, we isolated and purified basic nuclear proteins from the sperm chromatin of these animals to quantitate protamine stoichiometry. Based on the variability in P2 content and sequences we observed in these rodents, we speculated that both of these features must govern the protein interactions that affect how the two protamines are organized on sperm chromatin. This chapter describes the results of our comparison of P2 sequences and the differences observed in the stoichiometry of protamines isolated from the sperm of two closely related hamsters, Syrian Gold (*M. auratus*) and Chinese (*C. griseus*), and eight rat species.

Materials and Methods

Accession numbers. The GenBank database accession numbers for hamster genes and cDNAs (respectively) are: Syrian Gold hamster, *Mesocricetus auratus* (AF268203), (AF268204) and Chinese hamster, *Cricetulus griseus* (AF269065), (AF269066). The GenBank database accession numbers for rat genes and cDNAs (respectively) are: *Rattus fuscipes* (AF268201), (AF268202); *Rattus tunneyi* (AF268199), (AF268200).

Tissue Sources. Chinese hamster and *Rattus norvegicus* were purchased from Simonsen Laboratory (Gilroy, CA). Other *Rattus* species were collected in the wild in Australia. *Mesocricetus auratus* (Syrian hamster) were bred in our animal facility at Lawrence Livermore National Laboratory. The testes and epididymides were removed from each species and immediately frozen.

Fractionation of Rattus Protamines. Epididymal sperm were obtained from sexually mature rats and the basic nuclear proteins were isolated as previously described for the mouse (6). The basic nuclear proteins were solubilized in 3M GuCl, 50mM Tris-HCl pH 8.0, and 10mM DTT, and separated from the other basic nuclear proteins by HPLC using a Nucleosil RP-C18 column and the following multi-step acetonitrile gradient:

linear increase of Buffer B (60% acetonitrile, 0.1% trifluoroacetic acid) from 40% to 65% over 10 minutes; isocratic for 20 minutes; and an increase from 65% to 75% Buffer B in only 0.1 minute. Buffer A = aqueous 0.1% trifluoroacetic acid. Protein elution was monitored at 214 nm.

Electrophoretic Analysis. The cysteine residues of the sperm basic nuclear proteins were amino-ethylated using aziridine prior to their separation on acid urea gels as previously described (6,27).

Immunological Detection of Protamine 2 in Western Blots. The protamines of each *Rattus* species were resolved by electrophoresis on a minislab acid-urea gel (10 x 10 cm x 1.5mm) and subsequently blotted onto Immobilon P (Millipore Corporation, Burlington, MA) in 0.0009N acetic acid at 50V for 15 minutes. The dried blots were wetted with methanol, rinsed in water, and blocked with 5% bovine serum albumin containing calf thymus DNA (10mg/ml) in solution 1 (10mM Tris-HCl, [pH 7.4], 0.9% saline, 0.1% Tween-20) at 37°C for one hour. After washing three times in solution 1, the blots were incubated at room temperature for two hours with either Hup1N or Hup2B, antibodies specific for protamine 1 or protamine 2, respectively (1 μl in 10 ml solution 1) (28). The blots were washed three times with solution 1 and then incubated for 30 minutes at room temperature with biotinylated goat anti-mouse IgG (final concentration 5μg per ml of

solution 1) (Sigma Chemicals, St. Louis, MO). After three washes in solution 1, the antibodies were intensified using the VectaStain ABC-AP system (Vector Labs, Burlingame, CA), washed with solution 2 (solution 1 without Tween-20), and visualized using Vector Red.

Amplification of the Protamine 2 Gene. Genomic DNA was isolated from 10mg of frozen testes using a Puregene kit (Gentra, Research Triangle Park, NC) as per the manufacturer's instructions. All PCR reactions were performed in a MJ Research PTC-100 thermal cycler. The protamine gene cluster was amplified from 750 nanograms of hamster genomic DNA as previously described for Syrian Gold hamster (27). The PCR reactions resulted in a 1.7kb product from Chinese hamster and a 3.0kb product from Syrian Gold hamster. Half a microliter of each "primary" reaction was used as the template for a nested reaction to amplify the P2 gene as previously described for Syrian Gold hamster (27). These reactions yielded a 500bp product from Chinese hamster and a 700bp product from Syrian Gold hamster, and the DNA was extracted from a Nusieve gel (FMC BioProducts, Rockland, ME) using a Qiaquick kit (QIAGEN, Inc., Santa Clarita, CA). The extracted amplicons were sequenced by dye terminator cycle sequencing (U.C. Davis Sequencing Facility, Davis, CA). Triplicate samples of each PCR reaction were sequenced in both the forward and

reverse directions.

The protamine genes of *Rattus norvegicus*, *R. tunneyi*, and *R. fuscipes* were amplified from 750ng genomic DNA with the primer pair 5'-CCATGGCCAGATACAGATGCTG-3' and 5'-GCTTTATTTGGCAGGTGGCTT-3' using an Elongase kit (Gibco/Life Technologies, Grand Island, NY) and the following program: 94°C for 2 minutes; 5 cycles at 94°C for 1.5 minutes and 68°C for 6 minutes; 30 cycles at 94°C for 1 minute, 63°C for 1.5 minutes, and 68°C for 5 minutes; and ending with 1 cycle at 72°C for 10 minutes. The size of the PCR product obtained from all *Rattus* species was 5.2kb. One microliter of these reactions was used as template for subsequent nested reactions using an Elongase kit (Gibco/Life Technologies, Grand Island, NY). The program for the nested reactions was: 94°C for 2 minutes; 3 cycles at 94°C for 1 minute, 65°C for 1 minute, and 68°C for 1 minute; 2 cycles at 94°C for 1 minute, 64°C for 1 minute, and 68°C for 1 minute; 20 cycles at 94°C for 45 seconds, 63°C for 1 minute, and 68°C for 1 minute. The primer pair 5'-GTGTGCAGGCTACCGACCCTC-3' and TTGGCTTGGGCAGGTGACTTC-3') yielded a 575bp product for all three *Rattus* species. The DNA was extracted from the gel and sequenced by dye

terminator cycle sequencing (U.C. Davis Sequencing Facility, Davis, CA). Each PCR reaction was amplified twice more and sequenced in both the forward and reverse directions.

Amplification of Protamine 2 cDNA. Total RNA was isolated from the testes of *R. norvegicus*, *R. tunneyi*, *R. fuscipes*, Chinese hamster and Syrian Gold hamster using a GlassMax kit (Gibco/Life Technologies, Grand Island, NY) as per the manufacturer's instructions. DNase was added to the RNA samples to remove contaminating genomic DNA. One microgram of the total RNA was used as the template for RT-PCR using a Superscript II kit (Gibco/Life Technologies, Grand Island, NY). The protocol for RNA containing high GC sequences was followed per manufacturer's instructions using oligo(dT)16-18. The cDNAs obtained from the reverse transcriptase reactions from both Chinese hamster and Syrian Gold hamster were subsequently PCR-amplified using the primer pair 5'-TCTTCATCCCATCCAGGTCAG-3' and 5'-GCTTACTGCCTCCTACACCT-3' and the following program: 94°C for 1 minute; one cycle at 94°C for 1 minute, 63°C for 1 minute, and 72°C for 1 minute; one cycle at 94°C for 45 seconds, 62°C for 45 seconds, and 72°C for 45 seconds; 30 cycles at 94°C for 30 seconds, 61°C for 30 seconds, and 72°C for 40 seconds; and ending with 1 cycle at 68°C for 3 minutes. The

cDNAs from *R. norvegicus*, *R. tunneyi*, and *R. fuscipes* were amplified with the primer pair 5'-TCTCCTGGCACTATGGTTCGCT-3' and 5'-TTGGCTTGGGCAGGTGACTTC-3'. The program used was: 94°C for 2 minutes; 1 cycle at 94°C for 30 seconds, 65°C for 1 minute, and 72°C for 1 minute; 1 cycle at 94°C for 30 seconds, 64°C for 1 minute, and 72°C for 1 minute; 28 cycles at 94°C for 30 seconds, 63°C for 1 minute, and 72°C for 1 minute; and ending with 1 cycle at 72°C for 5 minutes. All reactions generated a 400bp product and the amplified cDNAs were sequenced using the dye terminator method (U.C. Davis Sequencing Facility, Davis, CA).

Results

Chinese hamster P2 mRNA is frameshifted.

The DNA sequence (and derived amino acid sequence) was obtained for the protamine 2 gene of Chinese hamster (*Cricetulus griseus*) by amplifying the P2 gene and sequencing the PCR product (Figure 2). The P2 gene sequence for Syrian Gold hamster (*Mesocricetus auratus*) was obtained by the same method (GenBank accession number AF268203) (27). Analyses of the sequencing data confirmed that the Chinese hamster genome does contain the P2 gene, but also revealed several deletions within the first 4 codons that create a transcript which, when translated, codes for a

hydrophobic protein that is terminated at the 28th codon (TGA). Because the sequence was vastly different from that which has been observed

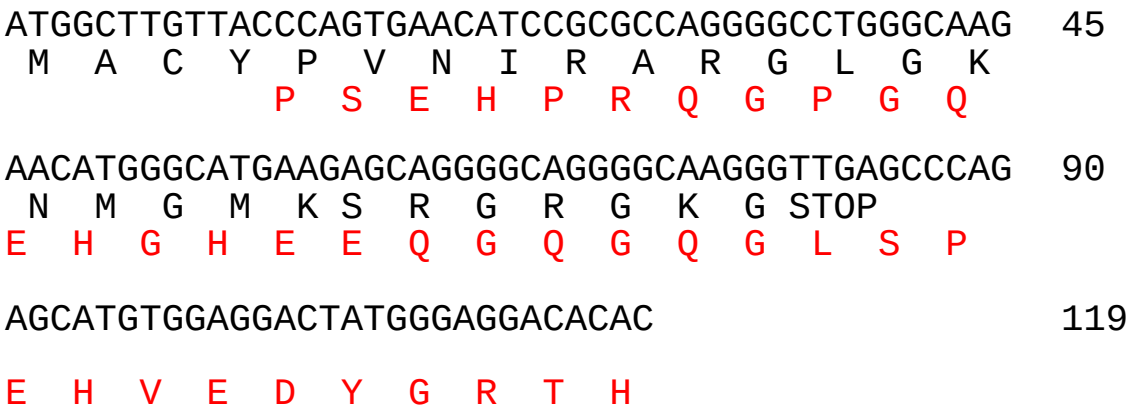

Figure 2. Partial sequence of Chinese Hamster protamine 2 gene (terminated at stop codon) and derived amino acid sequence frameshifted beginning with 11th base (in red).

previously for P2, it did not initially appear that we had isolated the P2 gene. However, when the gene sequence was frame-shifted at the 11th base, it became evident that it was the leader sequence of the P2 gene (Figure 2).

To determine if the Chinese hamster P2 gene is transcribed, we amplified cDNA obtained from the testes of Chinese hamster using Syrian Gold hamster as a control. Figure 3 (lane 3) shows that P2 mRNA isolated from the testes of Syrian Gold hamster is highly transcribed and efficiently processed - only fully spliced P2 cDNA was amplified. Unexpectedly, the majority of cDNA amplified from RNA isolated from the testes of Chinese hamster was unspliced (Figure 3, lane 2), as confirmed by sequencing the cDNA amplified from the testes of this hamster (Figure 4A). The unspliced cDNA cannot be attributed to the absence of conserved splice sites since the sequences for acceptor and donor sites were identical for hamster, mouse, and *R. norvegicus*, *R. tunneyi* and *R. fuscipes*. The cDNA also had a pyrimidine-rich consensus sequence at the 3' splice junction (Figure 4). In addition to treating the total RNA from Chinese hamster with DNase, duplicate samples were incubated without reverse transcriptase as negative controls to verify the RT-PCR results from Chinese hamster were not due to genomic contamination. A genomic PCR product was not amplified from

the mRNA sample (Figure 3, lane 4). Also, as a positive control, P1 cDNA

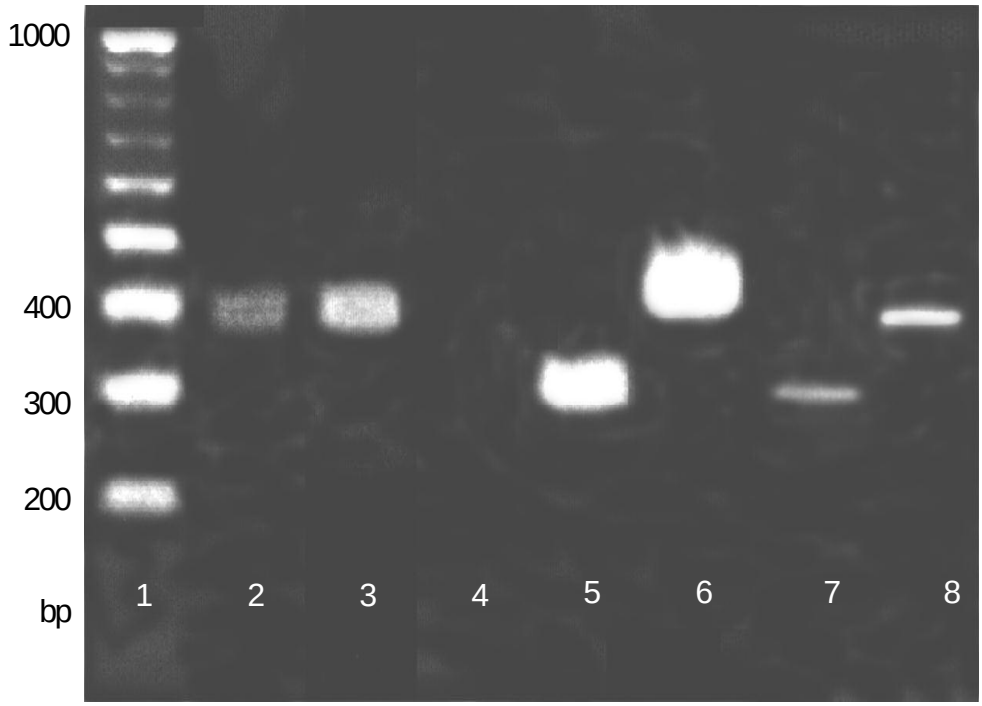

Figure 3. DNA gel comparing amplification yields of cDNA and genomic DNA from the testis of Chinese and Syrian Gold hamsters using the same primer pair. Lane 1: DNA 100-base pair ladder; 2: Chinese hamster P2 from cDNA; 3: Syrian hamster P2 from cDNA; 4: Chinese hamster cDNA without reverse transcriptase; 5: Chinese hamster P2 gene from genomic DNA; 6: Syrian hamster P2 gene from genomic DNA; 7: Chinese hamster P1 cDNA; 8: Syrian hamster P1 cDNA.

A.

```
ATGGCTTGTTACCCAGTGAACATCCGCGCCAGGGGCCTGGGCAAGAACATGGGC 54
 M  A  C  Y  P  V  N  I  R  A  R  G  L  G  K  N  M  G

ATGAAGAGCAGGGGCAGGGGCAAGGGTTGATCTTGCAGCCATCGCAGATGTAAG 108
 M  K  S  R  G  R  G  K  G STOP

CACCCAAGAACCTCAGACCCCTGGCCACCTGTGTTGCCCAGCAAGGCAGGAGTG 162
CTCCCATCTACCCTGCTGCCTCCCAGACAGCAAACCAGAACTTTTCTTCCCCAA 216
AGGCTGCAGAAGACGCAGGTGCAGGAGGTGTAGGAGGCACTAA             262
```

B.

```
ATGGTTCGTTACCGAATGAGGAGCCCCAGTGAGCGTCCGCACCAGGGGCCTGGG 54
 M  V  R  Y  R  M  R  S  P  S  E  R  P  H  Q  G  P  G

CAAGAACATGGACGTGAAGAGCAAGGGCAGGGGCAAGGGTTGAGCCCAGAGCGT 108
 Q  E  H  G  R  E  E  Q  G  Q  G  Q  G  L  S  P  E  R

GTGGAGGACTATACACACGGGAGGAGGGGCCAACACCACCACAGACGTCGCTGC 162
 V  E  D  Y  G  R  T  H  R  G  Q  H  H  H  R  R  R  C

TCGCGTAGGAAGCTGTACCGAATCCACAGGAGGCGCCGGTCATGCAGGAGGCGG 216
 S  R  R  K  L  Y  R  I  H  R  R  R  R  S  C  R  R  R

AGGAGACACTCCTGCCGTCACAGGAGACGGCATCGCAGAGGCTGCAGAAGATCA 262
 R  R  H  S  C  R  H  R  R  R  H  R  R  G  C  R  R  S

CGCAGGAGGAGGAGATGCAGGTGCAGGAGGTGTAGGAGGCACCACCACTAA    316
 R  R  R  R  R  C  R  C  R  R  C  R  R  H  H  H STOP
```

Figure 4. Complete cDNA and derived protein sequences for (A) Chinese and (B) Syrian hamsters. Predicted consensus sequences for splicing in Chinese hamster P2 are underlined.

was amplified from Chinese hamster, sequenced, and determined to be spliced (Figure 3, lane 7).

Steady state levels of Chinese hamster P2 mRNA are low.

Figure 3 also shows that less P2 cDNA is amplified from Chinese hamster compared with Syrian Gold hamster as an additional 10 cycles were needed to amplify Chinese hamster cDNA to visualize it on a gel. This result does not appear to reflect a reduced efficiency of amplification since similar yields were obtained when the same primers were used to amplify the genomic DNA from Chinese and Syrian Gold hamsters (Figure 3, lanes 5 and 6).

Expression levels of fully processed P2 varies within Rattus species.

Gel electrophoresis and HPLC analyses of *Rattus* protamines revealed marked intraspecies variation in P2 expression. Mature, fully processed P2 was not detected in *R. norvegicus* or *R. rattus* sperm (representatives of southeast Asian species) chromatin, whereas six Australian *Rattus* species (*R. tunneyi, R. villossimus, R. sordidus, R. colletti, R. lutreolus,* and *R. fuscipes*) were all observed to have fully processed P2 in their sperm chromatin (see representative HPLC data for two species, *R. fuscipes* and *R. norvegicus,* Figure 5). Immunoblots of the protamines isolated from the sperm of each species show fully processed protamine 2 is present in all of

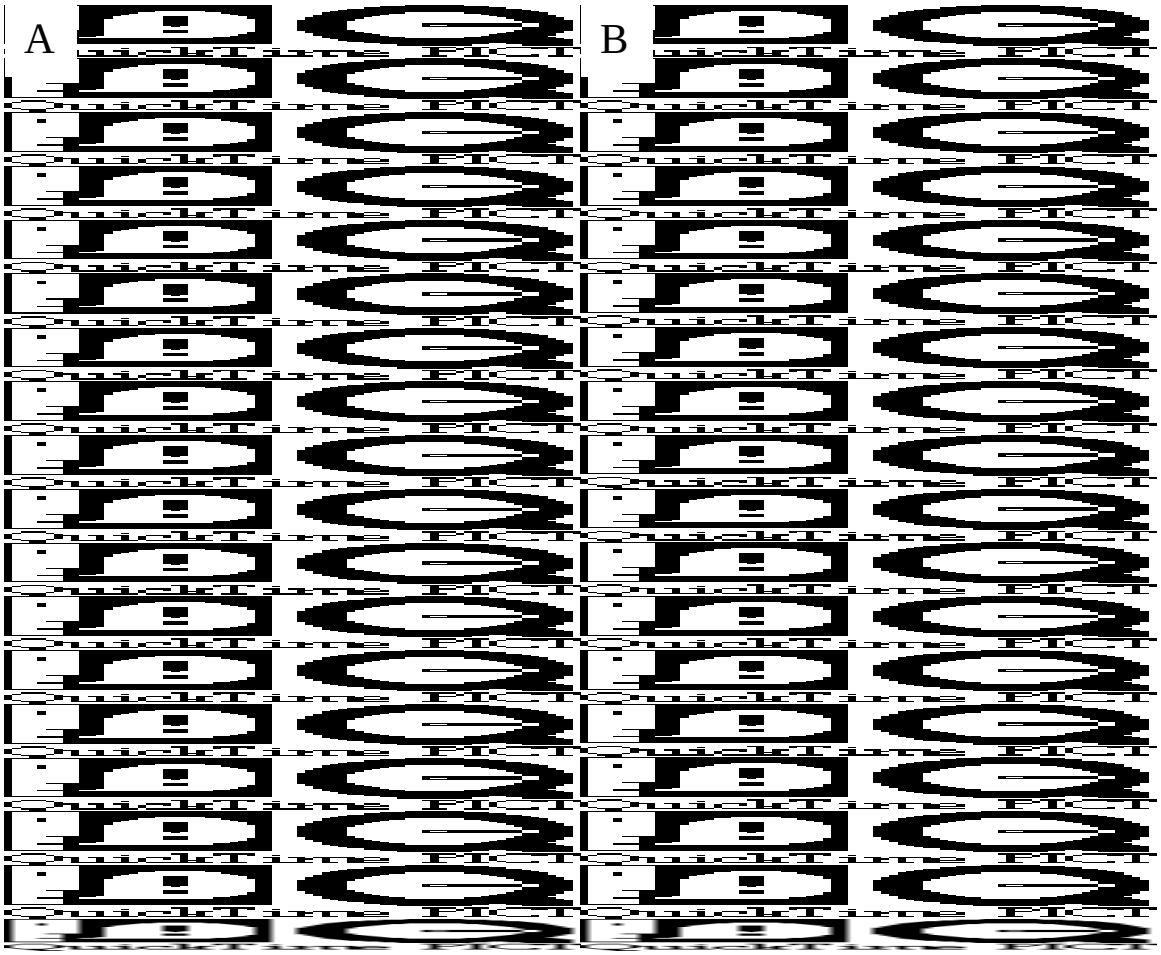

Figure 5. Fractionation of *Rattus norvegicus* and *Rattus fuscipes* protamines by HPLC shown in upper panel (A) *R. norvegicus* and (B) *R. fuscipes*. Fractions were analyzed by ELISA using the protamine 1-specific antibody Hup1N and protamine 2-specific antibody Hup2B shown in lower panel (A) *R. norvegicus* and (B) *R. fuscipes.*

the Australian *Rattus* species, but is absent in *R. norvegicus* and *R. rattus* sperm chromatin (Figure 6). The sperm of *R. norvegicus* and the Australian *Rattus* species contained detectable levels of partially processed P2 precursor, whereas *R. rattus* sperm did not appear to contain any P2 precursor (Figure 6, lanes 1 and 2).

To examine the mechanism regulating P2 expression within the *Rattus* genus, we amplified and sequenced the P2 genes from two *Rattus* species, *R. tunneyi, and R. fuscipes* (data not shown). The P2 gene sequence for *R. norvegicus* was reported earlier (GenBank accession number Z46939) (26). We also sequenced the P2 cDNAs obtained from the testes of these same three species of *Rattus* (Figure 7). Our results for *R. norvegicus* protamine 2 mRNA were identical to the sequence reported previously (GenBank accession number NM012873) (26). The rat P2 cDNA sequences showed that the transcripts were fully spliced and the putative amino acid sequences were highly conserved when compared with the P2 sequences of Syrian hamster and mouse, two species that contain abundant P2 in their sperm chromatin (Figure 8). The leader sequence of P2 from *R. norvegicus* has two amino acid changes compared with *R. tunneyi* and *R. fuscipes*: (1) proline (residue 13) is replaced by glutamine, and (2) the histidine residue at the last cleavage site (residue 44) is replaced by glutamic acid.

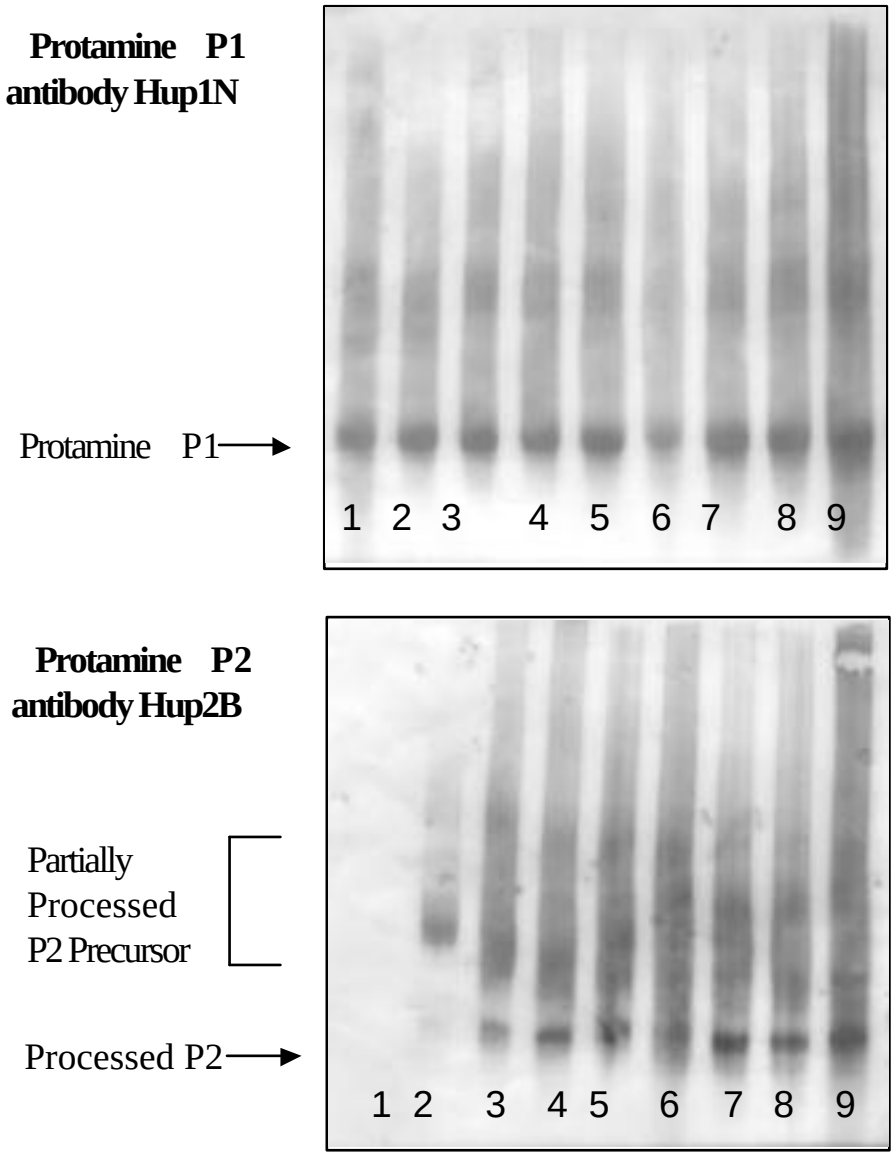

Figure 6. Immunoblots of basic nuclear proteins isolated from epididymal sperm of nine Rattus species. 1: *R. rattus*; 2: *R. norvegicus*; 3: *R. lutreolus*; 4: *R. fuscipes coracious*; 5: *R. fuscipes fuscipes*; 6: *R. tunneyi tunneyi*; 7: *R. sordidus*; 8: *R. colletti*; 9: *R. villosissimus*.

A.

```
ATGGTTCGCTACCGAATGAGGAGCCCCAGTGAGGGTCAGCACCAGGGGCCTGGG 54
 M  V  R  Y  R  M  R  S  P  S  E  G  Q  H  Q  G  P  G
CAAGACCATGAGCGCGAGGAGCAGGGGCAGGGGCAAGAGCTGAGCCCAGAGCGC 108
 Q  D  H  E  R  E  E  Q  G  Q  G  Q  E  L  S  P  E  R
GTGGAGGACTATGGGAGGACAGAAAGGGGCCACCACCACAGACACAGGCGCTGC 162
 V  E  D  Y  G  R  T  E  R  G  H  H  H  R  H  R  R  C
AAGAGGCTTCACAGGATCCACAAGAGGCGCCGGTCATGCAGAAGGCGGAGGAGA 216
 K  R  L  H  R  I  H  K  R  R  R  S  C  R  R  R  R  R
CACTCCTGCCGCCACAGGAGGCGGCATCGCAGAGGCTGCAGAAGATCCCGAAGG 270
 H  S  C  R  H  R  R  R  H  R  R  G  C  R  R  S  R  R
AGGAGGAGCTGCAGGTGCAGGAAATGCAGGTGGCACTATTAT             312
 R  R  S  C  R  C  R  K  C  R  W  H  Y  Y
```

B.

```
ATGGTTCGCTACCGAATGAGGAGCCCCAGTGAGGGTCCTCACCAGGGTCCTGGG 54
 M  V  R  Y  R  M  R  S  P  S  E  G  P  H  Q  G  P  G
CAAGACCATGAACGCGAGGAGGCAGGGCAGGGGCAAGAGCTGAGCCCAGAGCGC 108
 Q  D  H  E  R  E  E  Q  G  Q  G  Q  E  L  S  P  E  R
GTGGAGGACTATGGGAGGACACACAGGGGCCACCACAGACACAGGCGCTGCTCT 162
 V  E  D  Y  G  R  T  H  R  G  H  H  R  H  R  R  C  S
CGTAAGAGGCTTCACAGGATCCACAAGAGGCGCCGATCATGCAGAAGGCGGAGG 216
 R  K  R  L  H  R  I  H  K  R  R  R  S  C  R  R  R  R
AGACACTCCTGCTGCCACAGGAGGCGGCATCGCAGAGGCTGCAGAAGATCCCGA 270
 R  H  S  C  C  H  R  R  R  H  R  R  G  C  R  R  S  R
AGGAGGAGGAGATGCAAGTGCAGGAAATGCAGGAGGCACTGTCAC     303
 R  R  R  R  C  K  C  R  K  C  R  R  H  C  H
```

C.

```
ATGGTTCGCTACCGAATGAGGAGCCCCAGTGAGAGTCCGCACCAGGGTCCTGGG 54
 M  V  R  Y  R  M  R  S  P  S  E  S  P  H  Q  G  P  G
CAAGACCATGAAAGCGAGGAGCAGGGGCAGGGGCAAGAGCTGAACCCAGAGCGC 108
 Q  D  H  E  S  E  E  Q  G  Q  G  Q  E  L  N  P  E  R
GTGGAGGACTATGGGAGGACACACAGGGGCCACCACAGACACAGGCGCTGTTCT 162
 V  E  D  Y  G  R  T  H  R  G  H  H  R  H  R  R  C  S
CGTAAGAGGCTTCACAGGATCCACAAGAGGCGCCGATCATGCAGAAGGCGGAGG 216
 R  K  R  L  H  R  I  H  K  R  R  R  S  C  R  R  R  R
AGACACTCCTGCTGCCACAGGAGGCGGCATCGCAGAGGCTGCAGAAGATCCCGA 270
 R  H  S  C  C  H  R  R  R  H  R  R  G  C  R  R  S  R
AGGAGGAGGAGATGCAGGTGCAGGAAATGCAGGAGGCAGTGTCAC     303
 R  R  R  R  C  R  C  R  K  C  R  R  Q  C  H
```

Figure 7. Complete cDNA and derived protein sequences of (A) *Rattus norvegicus*, (B) *Rattus fuscipes*, and (C) *Rattus tunneyi*. Changes in amino acid sequence in R. norvegicus leader sequence are in red.

These same amino acid substitutions were previously noted when *R. norvegicus* P2 sequence was compared with mouse P2 (29).

Discussion

Identification of potential zinc-binding domain in protamine 2.

Due to the number of consecutive arginine residues present in protamines, amino acid sequencing of these proteins is limited to the N-terminal sequences. Entire sequences for 2 hamsters, Syrian Gold and Chinese, were obtained by amplifying the protamine genes using nested polymerase chain reaction (PCR) and sequencing the amplicons. Similar reactions yielded protamine 2 sequences for 3 rats, *R. norvegicus*, *R. fuscipes* and *R. tunneyi*. An alignment of the Muroid rodent protamine 2 sequences (excluding Chinese hamster) is shown in Figure 8.

We initially optimized the sequencing parameters for protamine 2 from Muroid rodents to identify potential zinc binding domains for our proposed P2-zinc structural studies. Based on the previous hypothesis derived from the calculation of the length of DNA covered by protamines, we assumed the protamines must bind to DNA using the arginine-rich domains in an extended conformation (17). This would preclude the possibility of the entire protamine 2 molecule wrapping around the zinc to form a typical zinc finger conformation as suggested previously (30,31).

M. auratus

RGQHHHRRR-CSRRKLYRIHRRRRSCRRRRRHSCRHRRRHRRGCRRSRRRRRCRCRRCRRHHH

M. musculus

RGHHHHRHRRCSRKRLHRIHKRRRSCRRRRRHSCRHRRRHRRGCRRSRRRRRCRCRKCRRHHH

R. norvegicus

RG-HHHRHRRC--KRLHRIHKRRRSCRRRRRHSCRHRRRHRRGCRRSRRRRSCRCRKCRWHYY

R. fuscipes

RG-HH-RHRRCSRKRLHRIHKRRRSCRRRRRHSCCHRRRHRRGCRRSRRRRRCKCRKCRRHCH

R. tunneyi

RG-HHR-HRRCSRKRLHRIHKRRRSCRRRRRHSCCHRRRHRRGCRRSRRRRRCRCRKCRRQCH

Figure 8. Alignment of mature (fully processed) P2 sequences of *M. auratus* (Syrian Gold hamster), *M. musculus* (laboratory mouse), and *R. norvegicus*, *R. fuscipes* and *R. tunneyi*.

Since the arginine domains are located primarily in the region of the protein sequences extending from the 26th residue to the C-terminal end, we focused our sequence comparison for the zinc-binding region on the N-terminus of the protein. Within the first 25 amino acids of the N-terminus, our alignment revealed a histidine-rich region in the first 8 amino acids as well as 2 cysteine residues and an additional histidine (Figure 8). These findings are consistent with sequences determine for other rodent protamine 2 sequences as well (data not shown) and with our hypothesis that zinc is coordinated at the N-terminal end of protamine 2.

Preliminary chemical crosslinking studies indicated that protamine 2 molecules are clustered in hamster chromatin as dimers (27). If protamine 2 binds to DNA as dimers in the sperm chromatin in all species, it seems highly probable that the monomers that comprise the dimer must be linked in a way that would produce a symmetrical dimer. As the amount of protamine 2 bound to DNA is varied in different species, this could be accomplished through the binding of additional protamine 2 dimers. One possible method for inducing and/or stabilizing the formation of a dimerization site between protamine 2 monomers could be through the coordination of zinc by the amino termini of protamine 2 molecules. One additional advantage of forming protamine 2 homodimers is that the dimers

would have increased affinity for DNA with twice the number of electrostatic interactions with the DNA phosphate backbone as compared with monomers. If dimerization occurred before protamine 2 binds to DNA, the presence of the dimer and its increased affinity for DNA should affect the rate of DNA condensation, which has been observed *in vitro* where zinc facilitated the condensation of DNA by P2 (32).

Number and position of cysteines do not appear to influence stoichiometry.

This alignment also demonstrates the marked similarity that exists between mouse and Syrian hamster protamine 2. From our sequencing data of protamine 1 we discovered the amino acid sequences for protamine 1 of these animals differ by 3 conservative changes at the C-terminus (27). Furthermore, the positions of the cysteine residues in both protamines are comparable. One-third of the total protamine from Syrian hamster is protamine 2 in contrast to mouse sperm, which contains 67% protamine 2. Prior to this study, we proposed that the formation of disulfide bridges between the protamines could account for the organization and thus relative proportion of protamines in sperm chromatin. Since the mouse and Syrian hamster protamine sequences are nearly identical, yet the relative proportion of protamines is vastly different in mouse and hamster sperm, it would

appear unlikely that disulfide bond formation between specific cysteine thiols in protamines 1 and 2 could account for the differences in protamine stoichiometry. However, if protamine 2 homodimers were interspersed among protamine 1 molecules, the formation of specific intra- and inter-molecular protamine disulfides would not need to change among species and we could reconcile this dilemma (27).

Splicing does not occur in defective protamine 2 Chinese hamster transcripts.

Our sequencing data provided additional insight into the variable protamine stoichiometry we observed in hamsters. Sequence analyses of the genomic DNA from Chinese hamster revealed that this hamster has a protamine gene cluster and that the P2 gene is transcribed, but the mRNA contains several mutations that shift the reading frame, producing an internal stop codon approximately 80 bases downstream from the start codon. This nonsense codon terminates the translation of P2 gene after 28 amino acids and produces a hydrophobic protein consisting of only a partial leader sequence and lacking a DNA binding domain. This protein would not be expected to be functional, nor would it be detected using standard techniques for isolating and characterizing protamines (23). P2, a highly basic protein containing approximately 63 amino acids after processing, would have a

very different electrophoretic mobility and a different elution time from an HPLC column than the truncated, hydrophobic protein produced by expression of the Chinese hamster P2 gene.

It has been proposed that the absence of P2 in the sperm chromatin of bull and boar was also caused by deletions in the transcripts (33,34). As for the Chinese hamster, translation of these transcripts would also produce a protein more hydrophobic than the highly basic P2. Together, these findings suggest that, in certain mammalian species including Chinese hamster, bull, and boar, P2 cannot be incorporated into the sperm chromatin because the mutated gene products lack the highly basic DNA-binding domain.

The low steady-state level of mRNA, the nonsense codon, and the unspliced cDNA isolated from Chinese hamster sperm mRNA are all consistent with the nonsense-mediated mRNA decay (NMD) pathway that has been primarily characterized in yeast, but also functions in higher eukaryotes including mammalian cells (35). In this pathway, the nonsense-containing transcript may remain as pre-mRNA, i.e. the intron is not spliced out of the transcript. In some systems, the intron functions to promote the NMD pathway (36,37). Nonsense mutations located at the 5'-proximal end of the gene have also been correlated with reduced levels of steady-state mRNA, which limited the overall expression of specific genes (38). Our

results suggest that when the P2 gene is transcribed in the testes of Chinese hamster, the frameshift mutation creates a nonsense-containing mRNA that remains unspliced and is unstable.

A sequence motif containing two ATG's has been identified in yeast downstream of the nonsense codon that appears to be required for nonsense-mediated mRNA decay (39). Two ATG's are also located downstream of the nonsense mutation in Chinese hamster P2 (data not shown). While inconclusive, these preliminary observations suggest that this decay pathway may be a mechanism used in Chinese hamster spermatids to eliminate the accumulation of potentially deleterious nonsense-containing mRNAs. The advantage a cell would derive by using this pathway is that it would conserve resources and prevent the translation of a hydrophobic protein that would be functionally useless to the cell or that may interfere with cell function. This certainly is applicable to the sperm cell as the accumulation of a hydrophobic protein would not bind to the negatively charged DNA, but it could disrupt the interactions that occur between protamines or the coiling of the neutralized chromatin into toroids. This compaction is essential to the protection of the paternal genome as well as its successful transmission to the next generation.

Changes in protamine 2 leader sequences inhibit processing.

In contrast to Chinese hamster, bull, and boar, the P2 precursor is synthesized and partially processed in the spermatids of *R. norvegicus*, but reduced transcription of the P2 precursor appears to limit the amount of P2 in the chromatin of rat spermatozoa (29,40). The low amount of P2 incorporated into the sperm chromatin of *R. norvegicus* might be explained by the impaired processing of P2 precursor, which could be a consequence of the absence or reduced expression of a functional enzyme required for processing. Alternatively, the processing of P2 precursor may be impaired by changes in the amino acid sequence within, or surrounding, the cleavage sites that alter a specific structure recognized by the processing enzyme. The lack of processing could account for the overall low levels of P2 in *R. norvegicus* sperm, since after the P2 precursor binds to DNA, processing would be expected to be required for elimination of the negatively charged leader sequence to prevent repulsion between the protein and the DNA phosphate backbone, which could hinder toroid formation and condensation of the sperm chromatin.

A comparison of the sequences obtained for several *Rattus* P2 genes revealed that the amino acids immediately adjacent to the cleavage sites of *R. norvegicus*, *R. fuscipes*, and *R. tunneyi* protamine 2 are conserved except

for the last cleavage site (H→E) in *R. norvegicus* (Figure 7). Bunick and colleagues observed this same amino acid substitution when they aligned P2 sequences for *R. norvegicus* and laboratory mouse (29). While there is no direct experimental evidence to suggest this mutation affects processing, it is conceivable that this amino acid substitution might alter the structure of the cleavage site and affect recognition by the processing enzyme.

Processing could also be affected by changes in neighboring sequences, either by preventing access to the cleavage site or by altering its conformation. As one example, the conserved proline neighboring the second cleavage site in mouse (24), *R. tunneyi*, and *R. fuscipes* (Figure 7) is replaced by a glutamine in *R. norvegicus* P2. This change could block the binding of the processing enzyme by steric hindrance or prevent recognition of the site by the enzyme. Since the cleavage process occurs sequentially (11), the efficiency of subsequent cuts would be expected to decrease if binding by the enzyme to the previous site was impaired. The mutation of the proline adjacent to the second processing site in *R. norvegicus* P2 might block downstream processing in this manner. This hypothesis is supported by the results from the immunoblots of *R. norvegicus* protamine since only the larger processed forms of the precursor are present in sperm chromatin (Figure 5). Interestingly, this cleavage site in the P2 precursor of rodents

appears to be absent in primates as indicated by the sequences of human P2 precursor intermediates (41). In seven primate species (including *Homo sapiens*) this proline residue is replaced by serine.

The present studies have also shown that the protamine 2 gene is expressed and the precursor is processed in a number of Australian *Rattus* species. This expression of the P2 gene and its processing in the Australian *Rattus* species are similar to that which occurs in the house mouse, *Mus domesticus* (11,25). The lack of processing in *R. norvegicus* and *R. rattus* may reflect the presence of mutations in the coding region of the leader sequence. Functional studies outside the scope of this project would resolve this speculation, which is currently based almost entirely on sequence comparisons.

Although early work suggested otherwise (42,43), more recent data have indicated that the Australian Rattus are part of the same lineage that gave rise to southeast Asian species, which include *R. norvegicus* and *R. rattus*. Furthermore, electrophoretic and microcomplement fixation data have suggested that the Australian *Rattus* are no more divergent from *R. norvegicus* and *R. rattus* than these two species are from each other (44). The most parsimonius explanation for the present findings would be that the P2 gene was fully expressed in an early *Rattus* ancestor and was retained in

the lineage that gave rise to the Australian species, but the expression of P2 was reduced due to mutations in the lineages that gave rise to *R. norvegicus* and *R. rattus*. Additional studies of the expression of the P2 gene in sperm of other Asian *Rattus* species would be an interesting test of this hypothesis.

The fact that the protamine 2 gene is present in most, if not all, eutherian genomes but often cannot be transcribed into a functional gene product has interesting, albeit perplexing, biological implications. While human males with nonfunctional or disproportionate amounts of P2 are infertile (45-47), Chinese hamster, *R. rattus* and *R. norvegicus* produce nonfunctional P2 gene products, and yet these species retain their ability to produce offspring. The reason for this apparent discrepancy is unclear, but alludes to the presence of multiple factors that must contribute to the regulation of fertility, as well as reproductive isolation between closely related species. Specifically, if this variability in P2 expression actually protects against cross-fertilization and/or regulates the rate of decondensation of sperm genome after fertilization, then this protection must require additional regulatory pathways as indicated by animals with only P1 in their sperm chromatin.

Clinically, deregulation of expression of the protamine genes appear to adversely affect human male fertility: a number of studies in the past

decade have correlated male infertility with alterations in the proportion of P1 and P2 in the sperm nuclei and decreased amounts of either or both protamines (43-45). Understanding the regulation of protamine gene expression will provide information to elucidate the causes of perturbations of protamine stoichiometry involved in human male infertility.

Acknowledgements

We gratefully acknowledge Sarah Fabes for her assistance with the rat protamine 2 PCR amplifications, Dr. William Breed for providing rat tissue, and Shelley Corzett and Joe Mazrimas for their analyses of rat protamine proteins.

References

1. Roosen-Runge EC. The process of spermatogenesis in mammals. Biol Rev Camb Philos Soc 1962; 37:343-377.
2. Dooher GB, Bennett D. Fine structural observations on the development of the sperm head in the mouse. Am J Anat 1973; 136:339-361.
3. Meistrich ML. Histone and basic nuclear protein transitions in mammalian spermatogenesis. In: Hnilica LS, Stein GS, Stein JL (eds), Histones and Other Basic Nuclear Proteins. Boca Raton, FL: CRC Press; 1989: 165-182.

4. Balhorn R, Weston S, Thomas C, Wyrobek A. DNA packaging in mouse spermatids: synthesis of protamine variants and four transition proteins. Exp Cell Res 1984; 150:298-308.

5. Pogany GC, Corzett M, Weston S, Balhorn R. DNA and protein content of mouse sperm: implications regarding sperm chromatin structure. Exp Cell Res 1981; 136:127-136.

6. Balhorn R, Gledhill BL, Wyrobek AJ. Mouse sperm chromatin proteins: quantitative isolation and partial characterization. Biochemistry 1977; 16:4074-4080.

7. Bellve AR, Carraway R. Characterization of two basic chromosomal proteins isolated from mouse spermatozoa. J Cell Biol 1978; 79:177a.

8. Balhorn, R, Corzett M, Mazrimas JA, Stanker LH, Wyrobek A. HPLC separation and partial characterization of human protamines 1, 2 and 3. Biotechnol Appl Biochem 1987; 9:82-88.

9. Belaiche D, Loir M, Kruggle W, Sautiere P. Isolation and characterization of two protamines St1 and St2 from stallion spermatozoa, and amino acid sequence of the major protamine St1. Biochim Biophys Acta 1987; 913:145-149.

10. Balhorn R. Mammalian protamines: structure and molecular interactions. In: Adolph KW (ed), Molecular Biology of Chromosome

Function. New York: Springer-Verlag; 1989: 366-395.

11. Yelick PC, Balhorn R, Johnson M, Corzett M, Mazrimas JA, Kleene KC, Hecht NB. Mouse protamine 2 is synthesized as a precursor whereas mouse protamine 1 is not. Mol Cell Biol 1987; 7:2173-2179.
12. Prieto MC. Structural characterization of DNA-protein complexes by optically detected magnetic resonance and nuclear magnetic resonance. Ph.D. thesis, University of California, 1995.
13. Balhorn R. A model for the structure of chromatin in mammalian sperm. J Cell Biol 1982; 93:298-305.
14. Prieto MC, Maki AH, Balhorn R. Analysis of DNA-protamine interactions by optical detection of magnetic resonance. Biochemistry 1997; 36:11944-11951.
15. Hud NV, Milanovich FP, Balhorn R. Evidence of novel secondary structure in DNA-bound protamine is revealed by raman spectroscopy. Biochemistry 1994; 33:7528-7535.
16. Fita I, Campos JL, Puigjaner LC, Subirana JA. X-ray diffraction study of DNA complexes with arginine peptides and their relation to nucleoprotamine structure. J Mol Biol 1983; 167:157-177.
17. Bench GS, Friz AM, Corzett MH, Morse DH, Balhorn R. DNA and total protamine masses in individual sperm from fertile mammalian

subjects. Cytometry 1996; 23:263-271.

18. Johnson PA, Yelick PC, Liem H, Hecht NB. Differential distribution of the P1 and P2 protamine gene sequences in eutherian and marsupial mammals and a monotreme. Gamete Res 1988; 19:169-175.

19. Hecht NB, Kleene KC, Yelick PC, Johnson PA, Pravtcheva DD, Ruddle FH. Mapping of haploid expressed genes: genes for both mouse protamines are located on chromosome 16. Somat Cell Mol Genet 1986; 12:203-208.

20. Adham IM, Szpirer C, Kremling H, Keime S, Szpirer J, Levan G, Engel W. Chromosomal assignment of four rat genes coding for the spermatid-specific proteins proacrosin (ACR), transition proteins 1 (TNP1) and 2 (TNP2), and protamine 1 (PRM1). Cytogenet Cell Genet 1991; 57:47-50.

21. Reinhart N, Kremling H, Luerseen H, Adham IM, Engel W. Characterization of a gene encoding a basic protein of the spermatid nucleus, TNP2, and its close linkage to the protamine genes in the bull. Biol Chem Hoppe Seyler 1991; 372:431-436.

22. Schluter G, Kremling H, Engel W. The gene for human transition protein 2: nucleotide sequence, assignment to the protamine gene

cluster, and evidence for its low expression. Genomics 1992; 14:377-383.

23. Keime S, Heitland K, Kumm S, Schlosser M, Hroch N, Holtz W, Engel W. Characterization of four genes encoding basic proteins of the porcine spermatid nucleus and close linkage of three of them. Biol Chem Hoppe Seyler 1992; 373:261-270.

24. Corzett M, Mazrimas J, Balhorn R. Protamine 1:protamine 2 stoichiometry in the sperm of eutherian mammals. Mol Reprod Dev 2002; 61:519-527.

25. Bellve AR, McKay DJ, Renaux BS, Dixon GH. Purification and characterization of mouse protamines P1 and P2: amino acid sequence of P2. Biochemistry 1988; 27:2890-2897.

26. Tanhauser SM, Hecht NB. Nucleotide sequence of the rat protamine 2 gene. Nucleic Acids Res 1989; 17:4395.

27. Corzett M, Kramer C, Blacher R, Mazrimas J, Balhorn R. Analysis of hamster protamines: primary sequence and species distribution. Mol Reprod Dev 1999; 54:273-282.

28. Stanker LH, McKeown C, Balhorn R, Lee C, Mazrimas J, Goralka M, Wyrobek A. Immunological evidence for a P2 protamine precursor in mature rat sperm. Mol Reprod Dev 1992; 33:481-488.

29. Bunick D, Balhorn R, Stanker LH, Hecht NB. Expression of the rat protamine 2 gene is suppressed at the level of transcription and translation. Exp Cell Res 1990; 188:147-152.

30. Gatewood JM, Schroth GP, Schmid CW, Bradbury EM. Zinc-induced secondary structure transitions in human sperm chromatin. J Biol Chem 1990; 265:20667-20672.

31. Bianchi F, Rousseaux-Prevost R, Sautiere P, Rousseaux J. P2 protamines from human sperm are zinc-finger proteins with one CYS2/HIS2 motif. Biochem Biophys Res Commun 1992; 182:540-547.

32. Brewer L, Corzett M, Balhorn R. Condensation of DNA by spermatid basic nuclear proteins. J Biol Chem 2002; 277:38895-38900.

33. Maier W-M, Nussbaum G, Domenjoud L, Klemm U, Engel W. The lack of protamine 2 (P2) in boar and bull spermatozoa is due to mutations within the P2 gene. Nucleic Acids Res 1990; 18:1249-1254.

34. Kremling H, Reinhart N, Schlosser M, Engel W. The bovine protamine 2 gene: evidence for alternative splicing. Biochim Biophys Acta 1992; 1132:133-139.

35. Czaplinski K, Ruiz-Echevarria MJ, Gonzalez CI, Peltz SW. Should we kill the messenger? The role of the surveillance complex in

translation termination and mRNA turnover. Bioessays 1999; 21:685-696.

36. Cheng J, Belgrader P, Zhou X, Maquat LE. Introns are cis effectors of the nonsense-codon-mediated reduction in nuclear mRNA abundance. Mol Cell Biol 1994; 14:6317-6325.

37. Zhang J, Sun X, Qian Y, Maquat LE. Intron function in the nonsense-mediated decay of beta-globin mRNA: indications that pre-mRNA splicing in the nucleus can influence mRNA translation in the cytoplasm. RNA 1998; 4:801-815.

38. Zhang S, Ruiz-Echevarria MJ, Quan Y, Peltz SW. Identification and characterization of a sequence motif involved in nonsense-mediated mRNA decay. Mol Cell Biol 1995; 15:2231-2244.

39. He F, Peltz SW, Donahue JL, Rosbash M, Jacobson A. Stabilization and ribosome association of unspliced pre-mRNAs in a yeast upf1-mutant. Proc Natl Acad Sci USA 1993; 90:7034-7038.

40. Bower PA, Yelick PC, Hecht NB. Both P1 and P2 protamine genes are expressed in mouse, hamster, and rat. Biol Reprod 1987; 37:479-488.

41. Retief JD, Dixon GH. Evolution of pro-protamine P2 genes in primates. Eur J Biochem 1993; 214:609-615.

42. Musser GG. The giant rat of Flores and its relatives east of Borneo and Bali. Bull Amer Mus Nat Hist 1981; 169:67-176.

43. Musser GG, Newcomb C. Malaysian murids and the giant rat of Sumatra. Bull Amer Mus Nat Hist 1983; 174:327-578.

44. Baverstock PR, Adams M, Watts CHS. Biochemical differentiation among karyotypic forms of Australian Rattus. Genetica 1986; 71:11-22.

45. Balhorn R, Reed S, Tanphaichitr N. Aberrant protamine 1/protamine 2 ratios in sperm of infertile human males. Experientia 1988; 44:52-55.

46. de Yebra L, Ballesca JL, Vanrell JA, Bassas L, Oliva R. Complete selective absence of protamine-P2 in humans. J Biol Chem 1993; 268:10553-10557.

47. Belokopytova IA, Kostyleva EI, Tomilin AN, Vorobev VI. Human male infertility may be due to a decrease of the protamine-P2 content in sperm chromatin. Mol Reprod Dev 1993; 34:53-57.

CHAPTER TWO

In Vivo Analysis of the Zinc-Binding Domain of Hamster Protamine 2 During Spermiogenesis

Abstract

Conflicting models have been proposed for zinc binding to human protamine 2 (P2) using data obtained from *in vitro* binding experiments. The inconsistent mode of binding when zinc is added to isolated human protamine 2 and synthetic P2 peptides may be explained by the binding of zinc to thiol groups of P2 that do not interact with zinc *in vivo*. The objectives of this *in vivo* study were to: (1) quantitate zinc in hamster spermatids and sperm to determine when the zinc is present in the developing sperm using Proton-Induced X-Ray Emission (PIXE); (2) determine whether zinc is bound to protamine 2 in spermatid and sperm nuclei; and (3) identify the zinc coordination site of P2 bound to DNA using X-ray Absorption Spectroscopy (XAS). The data obtained from these analyses show that zinc is bound to protamine 2 in the developing spermatid prior to or immediately after protamine deposition onto DNA and the coordination of the zinc changes as the spermatid matures. These results

suggest that one function of zinc in sperm may be to stabilize a structural domain that facilitates P2 binding to DNA, as opposed to creating a DNA-binding domain (such as a zinc finger), in the spermatid chromatin.

Introduction

The nucleoprotamine complex of mammalian sperm contains either protamine 1 (P1) or P1 and protamine 2 (P2). Both protamines contain multiple cysteines, but unlike P1, P2 is histidine-rich (1). Although the importance of zinc for stabilizing the sperm chromatin is recognized, its precise role(s) in sperm viability and male fertility is unknown (2-6). It has been demonstrated that isolated human P2 binds zinc *in vitro*, and while no structural domain was identified experimentally, both groups proposed a zinc finger domain in human P2, but with different zinc coordination site(s) (7,8). An attempt to localize the zinc binding site(s) of P2 using partial sequences of human P2 did not resolve the contradictory models, but provided the first evidence that zinc binds to P2 before the zinc-P2 complex binds DNA (9). Furthermore, in another *in vitro* study using optical trapping and a real time analysis of DNA condensation induced by nuclear proteins binding to single DNA molecules, zinc facilitated DNA condensation by P2 3-fold (10). These exciting results suggest one role of zinc in mammalian sperm chromatin may be to modulate the rate of P2 binding to DNA,

thereby directly impacting the rate of DNA condensation.

To gain insight into how P2 interacts with zinc *in vivo*, we quantitated P2 and zinc in individual mammalian sperm using Particle Induced X-ray Emission (PIXE) spectroscopy. For those species with P2 packaging sperm DNA, equimolar amounts of zinc and protamine 2 are present in the nuclei (11). Chinchilla sperm were found to be an exception, containing only enough zinc to yield a stoichiometry of one zinc atom per two P2 molecules. While the PIXE data did not substantiate whether zinc is actually bound to P2 *in vivo*, the results provided evidence that there is enough zinc in the sperm nuclei to interact stoichiometrically with P2.

Currently, the zinc coordination site of P2 *in vivo* remains unidentified. Structural data have been inconclusive due to the insolubility of the protamine/DNA complex. Also, the current methods for extracting protamines from DNA in sperm utilize reducing agents and denaturants, conditions not conducive for protamine 2 to retain zinc. Zinc is abundant in mature sperm, and this high concentration of zinc has been proposed to result from zinc uptake at ejaculation from the zinc-rich prostatic fluid (3,5). However, the presence of zinc in the developing spermatids has not been examined. To this end, we quantitated zinc and protamine 2 in large and small individual spermatids from hamster testes using PIXE. The large

spermatids are a sonication-resistant fraction of cells, representing the earliest stages of spermatids we can isolate with only protamines bound to DNA. Since the spermatids decrease in size as the protamines condense the chromatin, we could exploit differences in the size of the spermatids to discern whether zinc was present in the initial stages of protamine 2 deposition onto sperm DNA. Using X-ray Absorption Near Edge Structure (XANES) and Extended X-ray Absorption Fine Structure spectroscopy (EXAFS), we also examined the structure of the zinc coordination site in native P2 bound to DNA in spermatids and sperm. The data from the EXAFS experiments identified the ligands and coordination distance of the ligands to zinc in Syrian hamster P2 and its precursor in spermatids isolated from the testes and fully processed P2 in epididymal sperm. The results from this study demonstrate that zinc is present and must be bound to the protamine 2 precursor in spermatids, and that it remains bound to the protamine 2 precursor as it is processed during spermiogenesis. Based on this information, we propose the stabilization of sperm chromatin by zinc is due to zinc creating a structural domain in P2 that facilitates protamine binding to DNA, inducing toroidal formation and the subsequent condensation of the chromatin**.**

Materials & Methods

All chemicals were purchased from Sigma Chemical Company (St. Louis, MO) unless otherwise noted. All buffers were screened by PIXE to ensure purity from contaminating metals. All preparative steps were carried out in metal-free conditions (nitric acid cleaned containers and Teflon sonicator tip and metal-free reagents) to prevent contamination.

Syrian hamster (*Mesocricetus auratus*) testes and epididymides from adult males (retired breeders) were purchased from Simonsen Laboratory (Gilroy, CA).

Spermatid/Sperm Isolation for PIXE. Fat and membranes were removed from 1 hamster testis. To prepare sonication resistant spermatids, the teased testicular tissue was resuspended in 5ml ddH2O and the spermatids were filtered through silk to remove cell debris. From the filtered sample, 500µl of spermatids in ddH2O were gently sonicated using a Teflon tip and microfuged at 8000rpm for 3 minutes. To wash the spermatids, the supernatant was removed, 500µl ddH2O added, the sample was sonicated and microfuged. The wash was repeated 3 times. After the last resuspension in 500µl ddH2O, 100µl was dropped on nylon foils, the excess liquid wicked off, and individual spermatids were analyzed by PIXE.

For sperm, the procedure was the same as for spermatids except 0.15M ammonium acetate (ultra-pure, metal-free) was used to tease apart the epididymis and to wash the sperm cells. Sperm from the caput was diluted 10-fold and sperm from the cauda was diluted 20-fold prior to mounting onto nylon foils for PIXE analyses.

PIXE Analysis. PIXE analysis using the nuclear microprobe at LLNL has been previously described (12). In brief, PIXE data of individual spermatid and sperm nuclei were obtained using incident 3 MeV proton beams with beam currents of up to 1.5nA focused down to spot sizes of 3μm scanned over areas of 20 x 19 μm^2. Each irradiated area contained the head from a single sperm of normal morphology and size. Background levels of phosphorus, sulfur, and zinc on the nylon foils were typically below minimum detectable limits of 5ng/cm^2 for each sample. The details of data analysis have been described (11,12).

Isolation of Hamster sperm cells for EXAFS. Epididymal sperm were obtained from mature hamsters as described above (13,14). The sperm were sonicated in Tris-saline, pH 8.0, and the samples placed on ice and sonicated again. This step was repeated 3 times to ensure the tails were removed from the sperm heads. The suspension was centrifuged at 4000Xg for 5 minutes. The sonication and centrifuge steps were repeated 4 times.

After the last centrifugation, the pellet was resuspended in either: (1) 10ml Tris-saline by sonication, and 2ml of suspension was applied to a 10ml 1M sucrose solution (in 10mM Tris-HCl, pH 8.0) and centrifuged at 2500g for 5 minutes; or (2) incubated in β-mercaptoethanol for 15 minutes on ice followed by extraction of membrane proteins by MTAB (13). The sperm heads were pelleted by centrifugation at 5000rpm for 3 minutes at 4°C and the contaminating tails were carefully aspirated off. The sucrose purification was repeated 3 times. The pelleted sperm heads were pooled, washed twice with Tris-saline, pH 8.0, twice with double-deionized water (metal-free) and resuspended in 100 μl double deionized water for analysis by XAS.

XAS data collection and analysis. Suspensions of isolated tris/saline (T/S) and MTAB-treated mature hamster sperm cells and spermatids in double deionized water were centrifuged at 14,000 g for 10 minutes to form a pellet of cells. The supernatant was removed, and the cells were transferred to a Lucite cuvette with a 40μm Kapton window and frozen in liquid nitrogen.

Zinc XAS data were collected for two independently prepared samples of the T/S and MTAB-treated mature sperm and one sample of the T/S spermatids at Stanford Synchrotron Radiation Laboratory (SSRL) on beamline 7-3, under dedicated conditions (3.0 GeV, 55-100 mA), using a

Si(220) double-crystal monochromator detuned to 50% of the maximum intensity for harmonic rejection. EXAFS measurements were also made on two independently isolated samples of MTAB-treated mature sperm cells, T/S spermatids, and MTAB-treated spermatids at SSRL on beamline 9-3 using a Si(220) double crystal monochromator under dedicated conditions (3.0 GeV, 55-100 mA). The monochromator was operated fully tuned, and a rhodium coated upstream mirror was used for harmonic rejection. Samples were held at 10 K throughout the measurements in an Oxford Instruments liquid helium flow cryostat. X-ray energies in the individual scans were calibrated by simultaneous measurement of the absorption spectrum of a zinc foil, with the first inflection point of the foil assigned to be 9659 eV. The spectra were measured using 10 eV steps through the pre-edge region, 0.30 eV steps through the edge region, and 0.05k Å^{-1} steps through the EXAFS region with integration times of 1 s, 1 s, and k^3 weighted times from 1-20 s, respectively, giving a total scan time of ~30 min/scan. Data were collected as fluorescence excitation spectra using a 13-element Ge solid-state detector array on beamline 7-3 and a 30-element Ge solid-state detector array on beamline 9-3. The total count rates for each channel in the detector array and the windowed Zn Kα count rates in the EXAFS region are given in Table 1. All of the channels from each scan were examined for the

Sample	Beamline	Zn Kα	ICR	# FF Channels per scan	# Scans
T/S Sperm (A)	7-3	3600	50000	8	8
T/S Sperm (B)	7-3	10500	90000	11	5
MTAB Sperm (A)	7-3	9000	60000	11	6
MTAB Sperm (B)	7-3	12000	80000	11	8
MTAB Sperm (C)	9-3	15000	55000	24	4
MTAB Sperm (D)	9-3	16000	52000	26	4
T/S Spermatids (A)	7-3	5800	65000	11	6
T/S Spermatids (B)	9-3	17000	48000	18	4
T/S Spermatids (C)	9-3	17000	48000	14	2
MTAB Spermatids (A)	9-3	24000	78000	16	6
MTAB Spermatids (B)	9-3	13000	71000	16	5

Table 1. EXAFS data collection parameters.

presence of glitches, and the good channels (Table 1) were then averaged for each sample to give the final spectrum. Based on the number of channels used and the measured Zn Kα count rates at k =13Å^{-1}, approximately 0.6-2.6 x 10^6 useful counts were collected per scan on beamline 7-3 and 1.7-10.5 x 10^6 on beamline 9-3. The number of scans averaged for each sample is given in Table 1.

X-ray absorption near edge structure (XANES) data normalization and the EXAFS data reduction followed procedures described previously (15). EXAFS data reduction was accomplished by first removing the background using a first-order polynomial in the pre-edge region and a two-region cubic spline above the edge, followed by normalization to a Victoreen function (16). The data were converted to k-space, where k= $[(2m_e/\hbar^2)(E-E_0)]^{1/2}$, with the threshold energy, E_0, defined as 9675 eV. The EXAFS data were Fourier transformed over a range of 2-12.3 Å^{-1} and then backtransformed over the range R=0.8-2.6 Å. Both this filtered data and the raw data were fit to eq. 1 with a nonlinear least-squares algorithm.

$$\chi(k) = \sum_i \frac{N_i S_i(k) A_i(k)}{kR_i^2} \exp(-2k^2\sigma_i^2) \sin(2kR_i + \phi_i(k)) \qquad (1)$$

In eq. 1, $\chi(k)$ is the fractional modulation in the absorption $S_i(k)$ is

coefficient above the edge, N_i is the number of scatterers at a distance R_i, a scale factor unique to the absorber-scatterer pair, $A_i(k)$ is the effective backscattering amplitude, σ^2_i is the mean-square deviation in R_i, and ϕ_i is the phase-shift experienced by the photoelectron wave as it passes through the potentials of the absorbing and scattering atoms. The sum is taken over all scattering interactions.

Theoretical EXAFS amplitudes, $A_i(k)$ and phase functions, $\phi_i(k)$, were calculated using FEFF 6.01 (17,18). The experimental data were fit using single scattering parameters calculated for Zn-N and Zn-S with bond lengths of 2.05 Å and 2.35 Å, respectively. The scale factor, S=0.85 for O and S=1.02 for S, and the threshold energy, E_0=9.0 eV, were calibrated by fitting EXAFS data for structurally characterized Zn model complexes (19). R and σ were varied while holding the coordination number fixed at reasonable integer values (20).

Results and Discussion

The sperm head is a simple structure with relatively few components. Treatment of fertile mammalian sperm with a disulfide reducing agent and detergent to dissolve the tails, acrosome, and membranes yields intact chromatin that maintain the species-specific shape of the sperm head (21,22). The transition proteins are extracted in this process without

removing protamines (22). Additionally, there is no significant difference in zinc, phosphorus, and sulfur contents between intact mouse sperm heads and amembraneous nuclei from mouse sperm (22). Hamster spermatids and sperm were selected for our zinc structural analyses because protamines comprise more than 95% of the nuclear proteins in rodent sperm while approximately 15% of total nuclear proteins in human sperm are histones (22-25). As histone-containing nucleosomes typically represent transcriptionally active regions in sperm, the zinc fingers of transcription factors bound to these regions of DNA might be expected to contribute to the zinc signal in EXAFS, interfering with the metal analyses of protamines. Human sperm are also highly heterogeneous; therefore, analyses of pooled human sperm would be expected to provide mixed absorption spectra that would be extremely difficult to interpret. In contrast, the amembraneous nuclei from hamster sperm is composed primarily of DNA and protamines, 66% P1 and 34% P2 (fully processed), and only P2 binds zinc, thereby providing an ideal system for analyses by PIXE and XAS.

Our data from previous PIXE analyses of individual hamster sperm and isolated protamines revealed that zinc and P2 were present in equal amounts and that the zinc was bound to protamine (11). However, due to the inability to separate protamines 1 and 2 while retaining zinc bound to

protamine 2, we could only infer that zinc was associated with protamine 2. To confirm the zinc was bound to P2 as we expected, and to identify the zinc coordination site in P2, we analyzed sperm heads by XAS. Unlike PIXE, the amount of zinc in the sperm cell is below the detection limit for zinc using single cell analysis; therefore, bulk analysis was used for the XAS analysis, requiring purification of sperm heads from tails.

It has been demonstrated that removing tails from mature sperm, but not spermatids, requires treatment with reducing agents and detergent yet exposure to these chemicals could affect metal binding by disrupting protein structure. To address this possibility, we compared two methods of purifying sperm heads. First, tails were mechanically removed from sperm heads by repeated sonication in tris-saline buffer (T/S). Second, the sperm was sonicated in tris-saline buffer and the tails chemically removed by treatment with β-mercaptoethanol (BME) and mixed alkyl trimethylammonium bromide (MTAB-treated). All samples were rinsed with tris-saline then sedimented by sucrose purification to remove the tails remaining after tris-saline washes. The sperm heads were microscopically examined for purity before analyses by XAS.

Figures 1 and 2 show the XANES and Fourier transforms of the zinc EXAFS data for intact T/S and MTAB-treated mature sperm cells. The

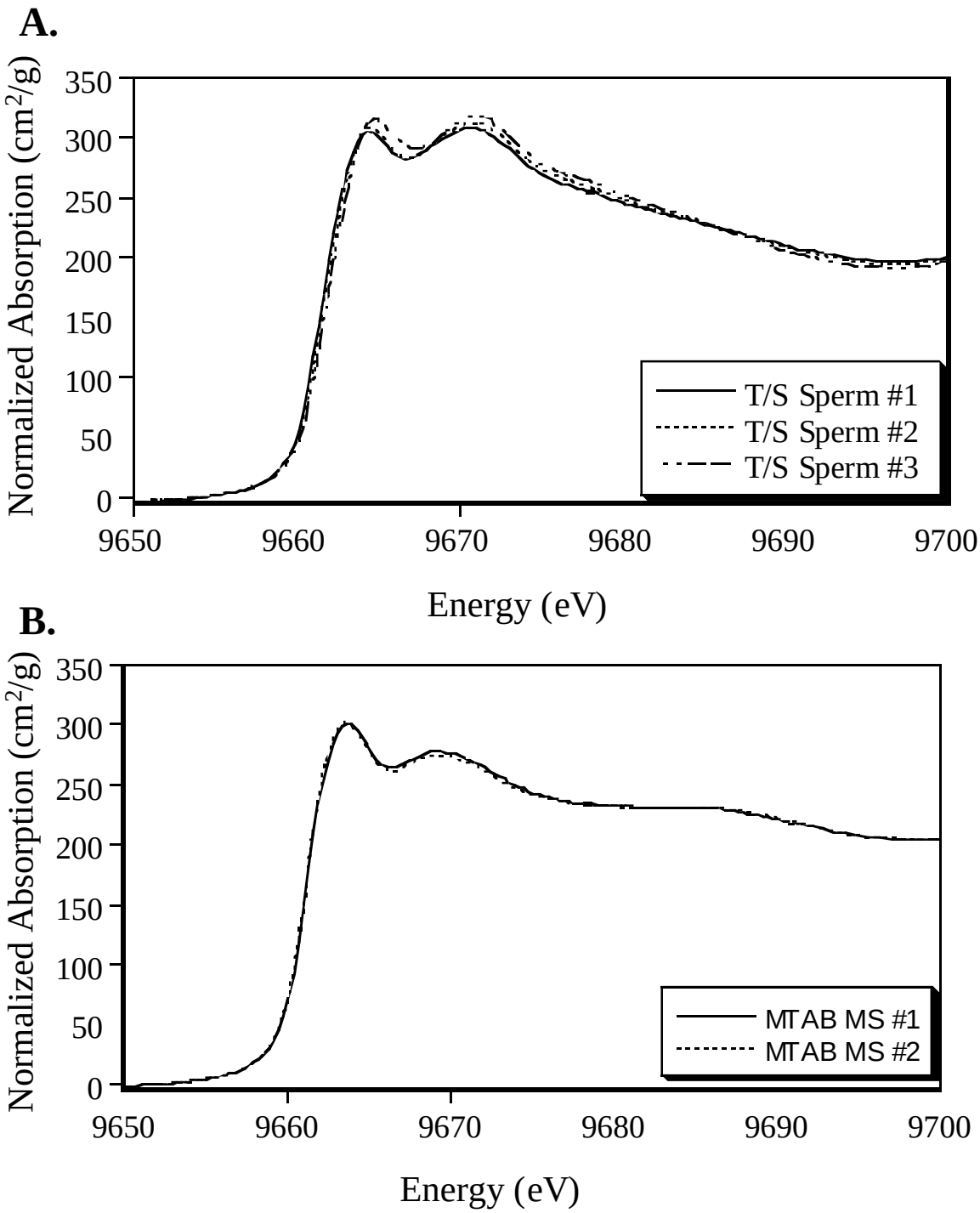

Figure 1. Representative XANES spectra of hamster sperm incubated in (A) tris -saline (T/S) buffer and (B) mixed alkyl trimethylammonium bromide (MTAB) and β-mercaptoethanol.

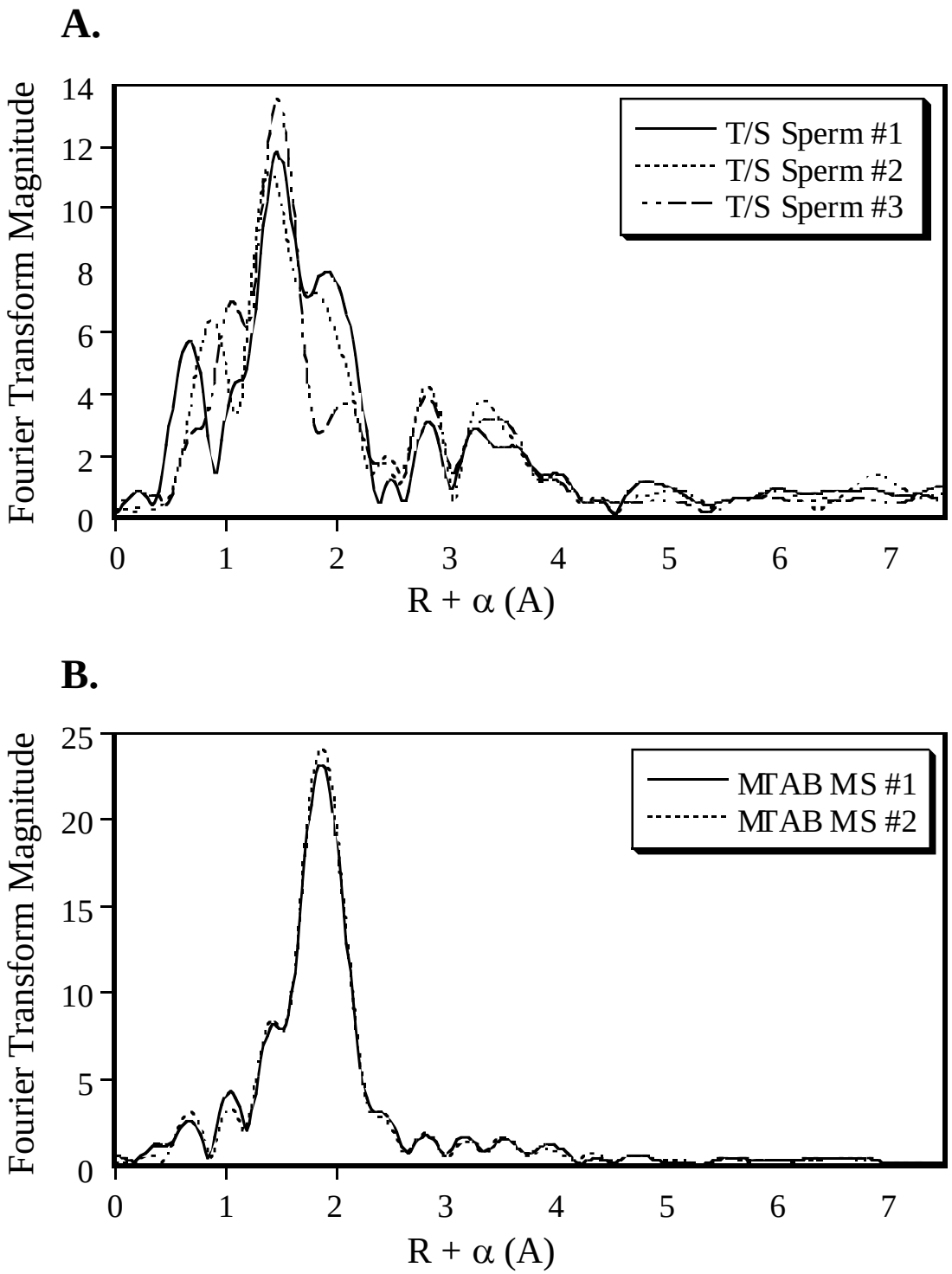

Figure 2. Representative Fourier transformed EXAFS data for hamster sperm incubated in (A) tris -saline (T/S) buffer and (B) mixed alkyl trimethylammonium bromide (MTAB) and β-mercaptoethanol.

XANES spectra for the MTAB-treated sperm samples show a small shift to lower energy and a decrease in the intensity of the feature at ~9669 eV compared with that for the T/S sperm. The differences between the samples are more dramatic in the Fourier transforms. There are 2 peaks of similar amplitude in the T/S spectrum. These become unresolvable, and there is a significant increase in amplitude and shift to longer distance following MTAB treatment. These changes are consistent with the replacement of low-Z ligands by higher-Z ligands in the MTAB-treated sperm cells. These changes are verified in the EXAFS fits (Table 2). Both samples have bond distances consistent with 4-coordinate zinc sites (26,27); however, the T/S sperm samples are best modeled as 1S at 2.31 Å and 3N at 2.00 Å, while the MTAB-treated cells are best fit as 3S at 2.33 Å and 1(N/O) at 2.08 Å. Further analyses of the sample preparation revealed that exposing the sperm heads to disulfide reductants changed the ligands binding zinc in P2 by liberating a thiol group, which is normally sequestered in a disulfide bond, to compete for zinc binding.

(Authors' note: To address minor inconsistencies in the data we obtained from the T/S sperm, we are in the process of analyzing single sperm cells by infrared (IR) analysis in collaboration with Dr. Hoi-Ying Holman from U.C. Berkeley at the Advanced Light Source facility. The

Sample	Ligand	R_{ab} (Å)	$^2 \bullet 10^3$ (Å^2)	F'
T/S Sperm #1	4S	2.28	12.8	0.111
	3S 1N	2.30 1.99	8.6 0	0.051
	2S 2N	2.31 2.00	5.1 2.3	0.032
	1S **3N**	**2.32** **2.02**	**1.0** **4.2**	**0.024**
	4N	2.05	8.9	0.167
T/S Sperm #2	4S	2.27	13.9	0.108
	3S 1N	2.29 1.99	10.2 0.5	0.061
	2S 2N	2.30 2.00	7.1 3.3	0.041
	1S **3N**	**2.31** **2.01**	**2.7** **4.9**	**0.032**
	4N	2.04	8.5	0.122
T/S Sperm #3	4S	2.25	16.1	0.185
	3S 1N	2.24 2.45	13.4 1.1	0.229
	2S 2N	2.29 1.98	9.5 1.3	0.063
	1S **3N**	**2.30** **1.99**	**4.2** **2.9**	**0.044**
	4N	2.01	6.3	0.069
MTAB-Treated Sperm #1	4S	2.33	4.6	0.016
	3S **1N**	**2.33** **2.08**	**2.8** **6.3**	**0.009**
	2S 2N	2.33 2.09	0.6 4.2	0.020
	1S 3N	2.34 2.14	0 3.4	0.157
MTAB-Treated Sperm #2	4S	2.33	4.4	0.012
	3S **1N**	**2.33** **2.09**	**2.7** **5.4**	**0.010**
	2S 2N	2.34 2.10	0.5 3.7	0.029
	1S 3N	2.34 2.14	0 2.9	0.181

Table 2. Representative EXAFS fitting results for hamster sperm. Best-fit data denoted in bold.

variability we observed in these samples can be attributed to either impurities in the sample preparation [i.e. zinc-containing proteins from the tail fragments that sediment with the sperm heads during centrifugation] ordegradation of the sample from the heat generated by excessive sonication. Single cell analysis by IR should allow us to obtain zinc coordination data from the heads only.)

It has been proposed that zinc is secreted into the seminal fluid by the prostate (3,5). To discern whether zinc was present prior to deposition of protamine 2 onto sperm DNA, we quantitated zinc and protamine 2 in large and small individual spermatids from hamster testes using PIXE. The large spermatids contain protamine 2 precursors and as the precursors bind to DNA and are processed, the chromatin compacts, concomitant with the spermatid nucleus condensing. Thus the majority of nuclear protein in the small spermatids is protamine. The majority of the protamine 2 is present in the processed form. Our zinc, protamine and DNA data from the PIXE analysis of large and small spermatids are shown in Table 3. The atom ratios of zinc to protamine 2 is 1:1 in the heads of both large and small spermatids, supporting the presence of zinc in the testes within spermatids long before exposure to the seminal fluid from the prostate.

The purpose of the next set of experiments was to determine whether

	Large	σ	Small	σ
DNA (pg)	3.4	0.1	3.3	0.1
Zinc (10^{-15} mol)	0.18	0.04	0.16	0.04
protamine (pg)	3.6	0.3	3.1	0.2
protamine/DNA	0.86	0.06	0.86	0.06
Prot 2 (10^{-15} mol)	0.160	0.010	0.140	0.010
Zinc/Prot 2 ratio	1.0	0.2	1.0	0.3

Table 3. Values are derived from analysis of 9 large spermatid heads and 9 small spermatid heads from one animal. Values are expressed as a mean ± standard deviation of measurements from 18 heads.

zinc was bound to the P2 precursor and, if so, whether coordination was the same as in the mature, processed P2 in sperm. Sonication-resistant late-step spermatids (stages 16-19) were prepared for EXAFS as previously described for sperm. Late-step spermatids achieve sonication resistance once the protamines are deposited on DNA. Small amounts of TP2 are present in these spermatids, but TP2 is extracted from the cell by MTAB. TP2 has been proposed to contain 3 zinc finger motifs, therefore, presence of TP2 would contribute to the signal (28).

In contrast to the differences observed in the mature sperm cells, the T/S and MTAB-treated spermatids have quite similar XANES spectra (Figure 3). The Fourier transforms of the EXAFS data for both samples show a single peak with an unresolvable low-R shoulder, although the Fourier transforms for the T/S treated spermatids have a slightly smaller main peak amplitude which could be interpreted as a decrease in the number of scatterers at $R + \alpha = 1.9$ Å or an increase in the disorder of the zinc site of the T/S spermatids (Figure 4). Analysis of the EXAFS fitting results show that both T/S and MTAB-treated spermatids have bond distances consistent with tetrahedral zinc model complexes (27) (Table 4). Both T/S and MTAB-treated spermatids are best modeled as 3S + 1(N/O), but the Zn-S Debye-Waller factor for the T/S sample is somewhat higher than that in the

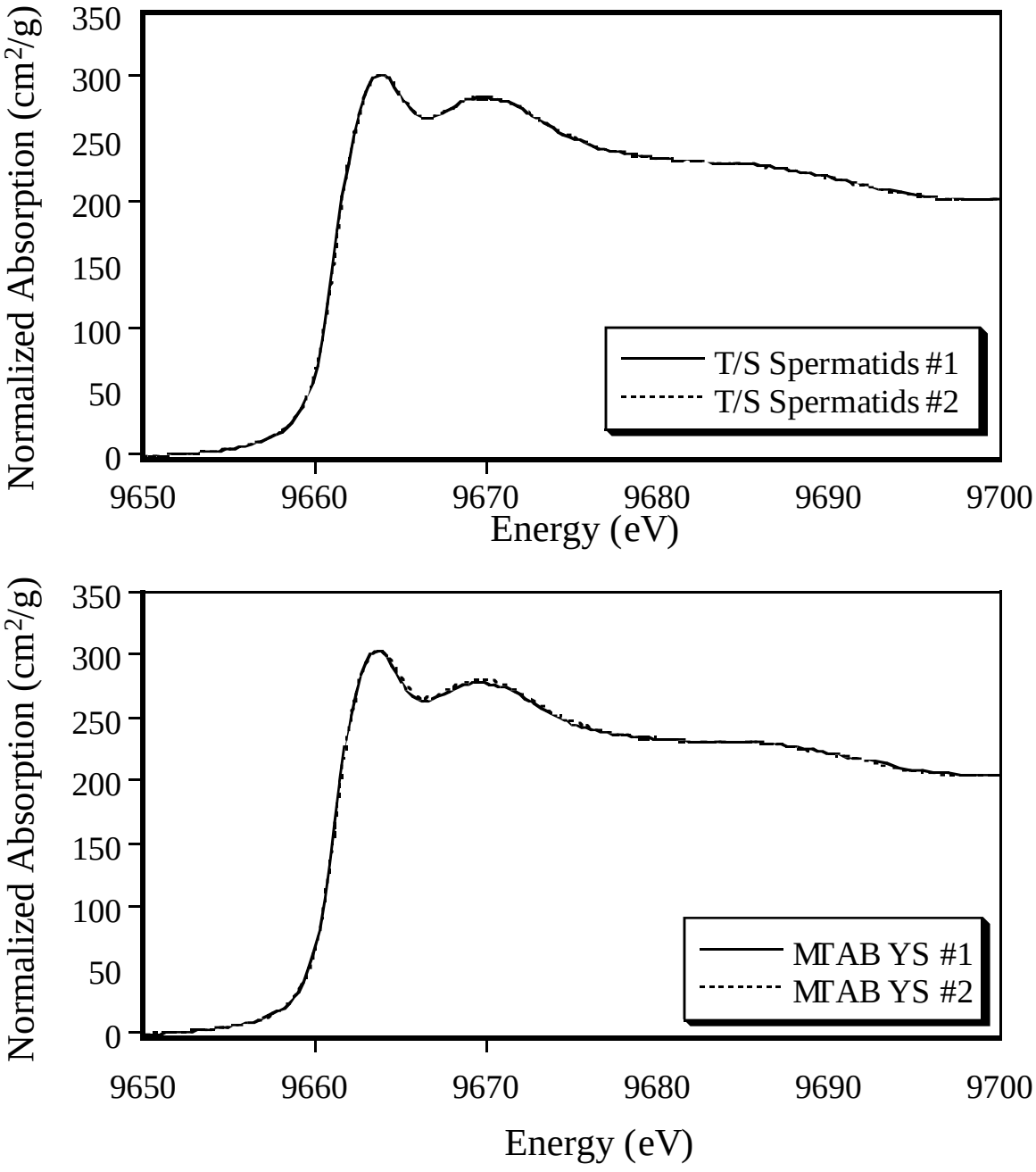

Figure 3. Representative XANES spectra of hamster spermatids incubated in (A) tris -saline (T/S) buffer and (B) mixed alkyl trimethylammonium bromide (MTAB) and β-mercaptoethanol.

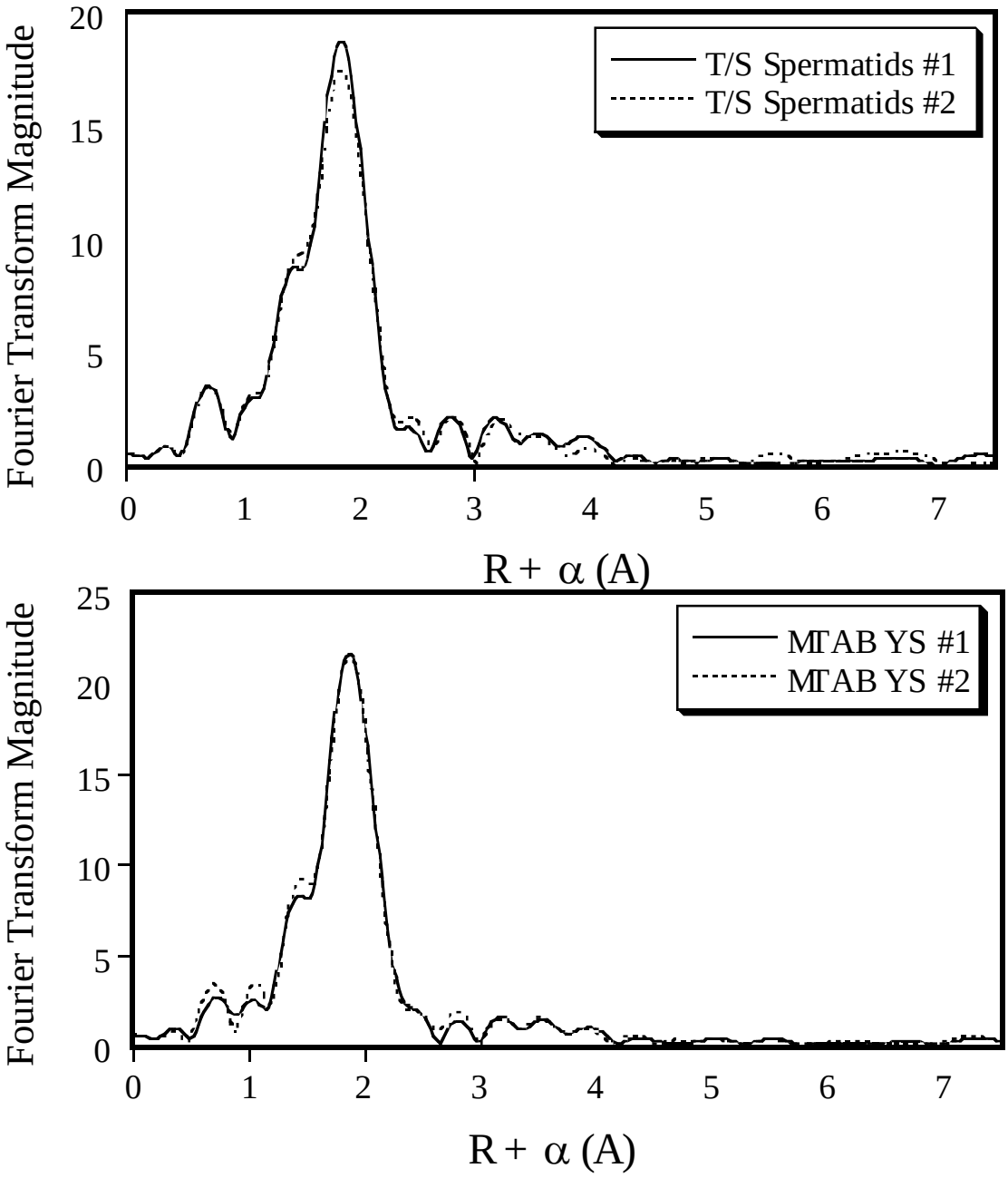

Figure 4. Representative Fourier transformed EXAFS data for hamster spermatids incubated in (A) tris -saline (T/S) buffer and (B) mixed alkyl trimethylammonium bromide (MTAB) and β-mercaptoethanol.

Sample	**Ligand**	**R_{ab} (Å)**	**$\sigma^2 \bullet 10^3$ (Å^2)**	**F'**
T/S Spermatids #1	4S	2.32	6.3	0.021
	3S **1N**	**2.32** **2.05**	**4.2** **5.4**	**0.009**
	2S 2N	2.33 2.07	1.9 5.4	0.014
	1S 3N	2.33 2.10	0 5.8	0.090
T/S Spermatids #2	4S	2.32	6.8	0.027
	3S **1N**	**2.32** **2.03**	**4.3** **3.0**	**0.012**
	2S 2N	2.33 2.06	2.0 4.6	0.011
	1S 3N	2.33 2.09	0 6.0	0.063
MTAB-Treated Spermatids #1	4S	2.33	5.2	0.014
	3S **1N**	**2.33** **2.07**	**3.3** **5.2**	**0.011**
	2S 2N	2.34 2.09	1.1 4.4	0.028
	1S 3N	2.34 2.13	0 4.2	0.141
MTAB-Treated Spermatids #2	4S	2.33	5.2	0.017
	3S **1N**	**2.33** **2.06**	**3.1** **3.9**	**0.008**
	2S 2N	2.33 2.08	0.9 3.9	0.018
	1S 3N	2.34 2.12	0 4.6	0.133

Table 4. Representative EXAFS fitting results for hamster spermatids. Best-fit data denoted in bold.

fits of the MTAB-treated samples, suggesting that the decrease observed in the Fourier transform of the T/S spermatid EXAFS data is due to an increase in the disorder of the S ligands.

Conclusion

We determined by PIXE that zinc is present and associated with the chromatin in early spermatid and sperm before exposure to seminal fluid secreted by the prostate. The mode of zinc binding, identified using EXAFS, changes during maturation of the spermatid to sperm: as the sperm transits the epididymis, disulfide bridges form and the coordination of zinc by protamine 2 switches from 3S + 1 N/O to 1S + 3 N/O. This observation can be experimentally validated by the addition of reducing agents to the sperm cells. Due to the extended conformation of protamines to bind DNA (22), we proposed that zinc binds to the N-terminus of protamine 2 to stabilize a dimerization site and to facilitate and organize binding of protamine 2 onto DNA and the subsequent condensation of the sperm chromatin (Figure 5).

The biological relevance of elucidating the structure of the zinc coordination site of P2 is demonstrated by numerous clinical experiments that have correlated reduced levels of P2 with infertility (29-34). Similar studies comparing human protamines isolated from fertile and infertile males

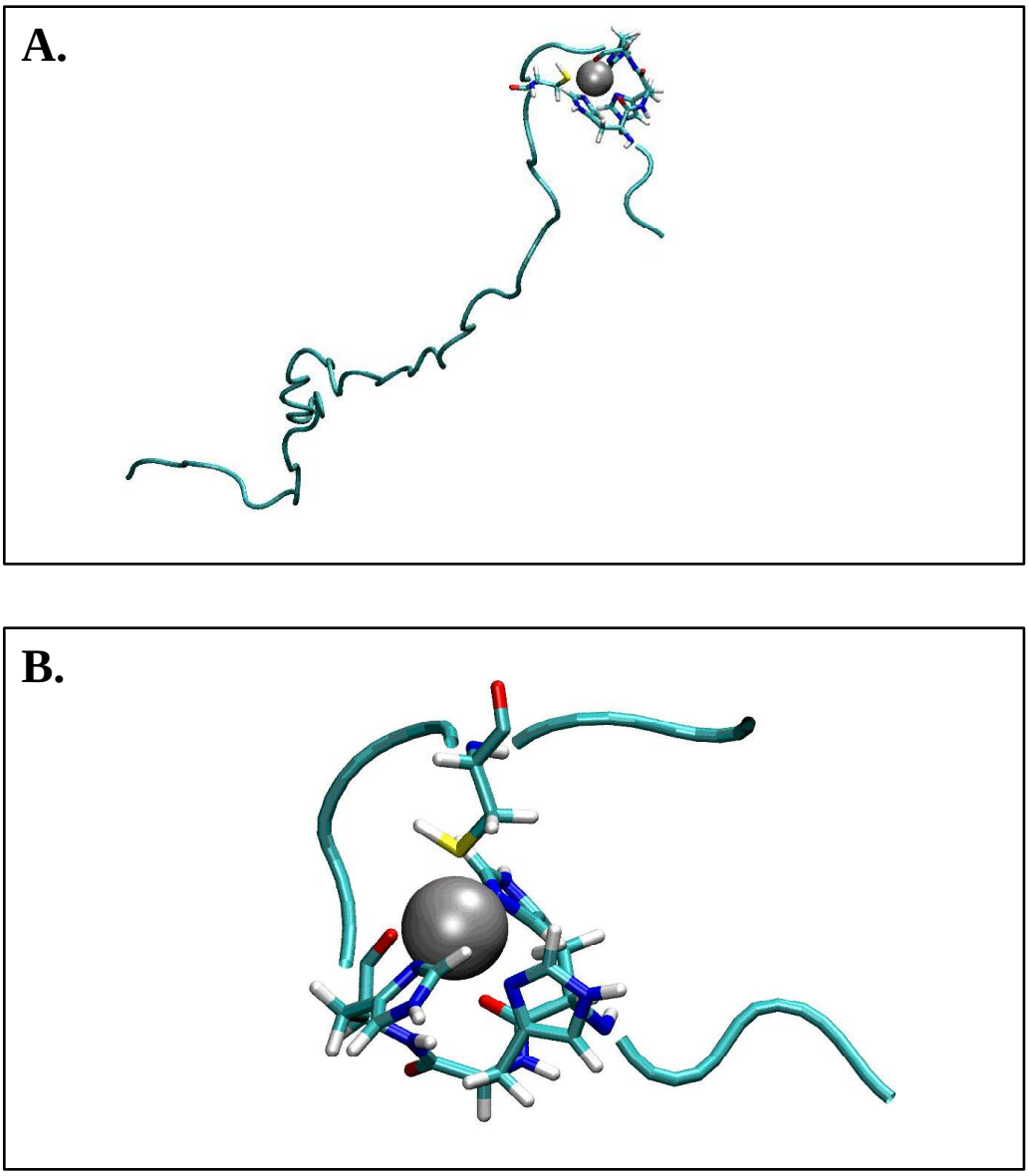

Figure 5. (A) Computer model of hamster protamine 2 with proposed zinc binding domain at N-terminus. Remaining sequence shown in extended conformation. (B) Enlarged view of the zinc ligands, 1 cysteine and 3 histidines, in hamster protamine 2. Legend: oxygen=red, nitrogen=blue, and sulfur=yellow.

should provide insight to the structure of the zinc-binding domain of P2. Mutations within the zinc-binding domain of P2 would affect zinc binding, altering the structure of P2 and reducing the affinity of P2 for DNA. These changes could prevent incorporation of P2 into the sperm chromatin thereby inhibiting DNA condensation by P2. This would explain the positive correlation observed between fertility and the levels of zinc and protamine 2.

Acknowledgements

We gratefully acknowledge Dr. Katrina Peariso for her X-ray Absorption Spectroscopy data collection and interpretation, and Dr. Graham Bench for his Proton-Induced X-Ray Emission data collection and analysis.

We would also like to thank Michele Corzett for her helpful suggestions for the optimization of the sample preparations.

References

1. Balhorn R. Mammalian protamines: structure and molecular interactions. In: Adolph KW, editor. Molecular Biology of Chromosome Function. New York: Springer-Verlag; 1989: 366-395.
2. Bjorndahl L, Kvist U. Loss of an intrinsic capacity for human sperm chromatin decondensation. Acta Physiol Scand 1985; 124:189-194.
3. Kvist U, Bjorndahl L. Zinc preserves an inherent capacity of chromatin decondensation of human spermatozoa. Acta Physiol Scand

1985; 124:195-200.

4. Kvist U, Bjorndahl L, Kjellberg S. Sperm nuclear zinc, chromatin stability, and male fertility. Scanning Microsc 1987; 1:1241-1247.

5. Bjorndahl L, Kjellberg S, Roomans GM, Kvist U. The human sperm nucleus takes up zinc at ejaculation. Int J Androl 1986; 9:77-80.

6. Kvist U, Bjorndahl L. Zinc in sperm chromatin and chromatin stability in fertile men and men in barren unions. Scand J Urol Nephrol 1988; 22:1-6.

7. Gatewood JM, Schroth GP, Schmid CW, Bradbury EM. Zinc-induced secondary structure transitions in human sperm chromatin. J Biol Chem 1990; 265:20667-20672.

8. Bianchi F, Rousseaux-PrevostR, Sautiere P, Rousseaux J. P2 protamines from human sperm are zinc-finger proteins with one CYS2/HIS2 motif. Biochem Biophys Res Commun 1992; 182:540-547.

9. Bal W, Dyba M, Szewczuk Z, Jezowska-Bojczuk M, Lukszo J, Ramakrishna G, Kasprzak S. Differential zinc and DNA binding by partial peptides of human protamine HP2. Mol Cell Biochem 2001; 222:97-106.

10. Brewer L, Corzett M, Balhorn R. Condensation of DNA by

spermatid basic nuclear proteins. J Biol Chem 2002; 277:38895-900.

11. Bench GS, Corzett MH, Kramer CE, Grant PG, Balhorn R. Zinc is sufficiently abundant within mammalian sperm nuclei to bind stoichiometrically with protamine 2. Mol Reprod Dev 2000; 56:512-519.

12. Bench GS, Balhorn R, Friz AM. Nuclear microscopy of sperm cell elemental structure. Nucl Instr Methods 1995; B99:553-556.

13. Balhorn R, Gledhill BL, Wyrobek AJ. Mouse sperm chromatin proteins: quantitative isolation and partial characterization. Biochemistry 1977; 16:4074-4080.

14. Corzett M, Kramer C, Blacher R, Mazrimas J, Balhorn R. Analysis of hamster protamines: primary sequence and species distribution. Mol Reprod Dev 1999; 54:273-282.

15. Peariso K, Goulding CW, Huang S, Matthews RG, Penner-Hahn JE. Characterization of the zinc binding site in methionine synthase enzymes of Escherichia coli: The role of zinc in the methylation of homocysteine. J Am Chem Soc 1998; 120:8410-8416.

16. Teo BK. EXAFS: Basic Principles and Data Analysis. New York: Springer-Verlag; 1986.

17. Rehr JJ, deLeon JM, Zabinsky SI, Albers RC. Theoretical x-ray

absorption fine-structure standards. J Am Chem Soc 1991; 113:5135-5140.

18. Rehr JJ, Albers RC, Zabinsky SI. High-order multiple-scattering calculations of x-ray-absorption fine structure. Phys Rev Lett 1992; 69:3397-3400.

19. Clark-Baldwin K, Tierney DL, Govindaswamy N, Gruff ES, Kim C, Berg J, Koch SA, Penner-Hahn JE. The limitations of X-ray absorption spectroscopy for determining the structure of zinc sites in proteins. When is a tetrathiolate not a tetrathiolate? J Am Chem Soc 1998; 120:8401-8409.

20. Rulisek L, Vondrasek J. Coordination geometries of selected transition metal ions (Co2+, Ni2+, Cu2+, Zn2+, Cd2+, and Hg2+) in metalloproteins. J Inorg Biochem 1998; 71:115-27.

21. Pogany GC, Corzett M, Weston S, Balhorn R. DNA and protein content of mouse sperm: implications regarding sperm chromatin structure. Exp Cell Res 1981; 136:127-136.

22. Bench GS, Friz AM, Corzett MH, Morse DH, Balhorn R. DNA and total protamine masses in individual sperm from fertile mammalian subjects. Cytometry 1996; 23:263-271.

23. Gatewood JM, Cook GR, Balhorn R, Bradbury EM, Schmid CW.

Sequence-specific packaging of DNA in human sperm chromatin. Science 1987; 236:962-964.

24. Pongsawasdi P, Svasti J. The heterogeneity of the protamines from human spermatozoa. Biochim Biophys Acta 1976; 434:462-473.

25. Tamphaichitr N, Sobhon P, Taluppeth N Chalermisarachai P. Basic nuclear proteins in testicular cells and ejaculated spermatozoa in man. Exp Cell Res 1978; 17:347-356.

26. Corwin DT, Gruff ES, Koch SA. Zinc, cobalt and cadmium thiolate complexes – models for the Zn(S-cys)3(his) center in the gene 32 protein. Inorg Chim Acta 1988; 151:5-6.

27. Gruff ES, Koch SA. A trigonal planar [Zn(SR)3]1- complex. A possible new coordination mode for zinc-cysteine centers. J Am Chem Soc 1989; 111:8762-8763.

28. Kawai T, Konishi T, Fujikawa T, Sekine A, Imai L, Akama K. EXAFS Analysis of the Zinc-Binding Domain of Boar Spermatidal Transition Protein 2. J Synchrotron Rad 2001; 8:993-995.

29. Balhorn R, Reed S, Tanphaichitr N. Aberrant protamine 1/protamine 2 ratios in sperm of infertile human males. Experientia 1988; 44: 52-55.

30. Belokopytova IA, Kostyleva EI, Tomilin AN, Vorobev VI. Human male infertility may be due to a decrease of the protamine-P2 content

in sperm chromatin. Mol Reprod Devel 1993; 34:53-57.

31. Blanchard Y, Lescoat D, Le Lannou D. Anomalous distribution of nuclear basic proteins in round-headed human spermatozoa. Andrologia 1990; 22:549-555.

32. de Yebra L, Ballesca JL, Vanrell JA, Bassas L, Oliva R. Complete selective absence of protamine-P2 in humans. J Biol Chem 1993; 268:10553-10557.

33. Bench G, Corzett MH, de Yebra L, Oliva R, Balhorn R. Protein and DNA contents in sperm from an infertile human male possessing protamine defects that vary over time. Mol Reprod Dev 1998; 50:345-353.

34. de Yebra L, Ballesca JL, Vanrell JA, Corzett M, Balhorn R, Oliva R. Detection of P2 precursors in the sperm cells of infertile patients who have reduced protamine P2 levels. Fertil Steril 1998; 69:755-759.

CHAPTER THREE

Characterization of an Atypical Protamine 2 Isolated from Chinchilla Sperm

Abstract

Both protamines 1 (P1) and 2 (P2) package DNA in chinchilla (Chinchilla laniger) sperm. The amino acid compositions, the amino-terminal sequences of the two protamines, and the DNA sequences of P1 and P2 genes demonstrate the sequence conservation of chinchilla P1 compared with P1 present in the sperm of other mammals. Conversely, chinchilla P2 is an anomaly. P2 isolated from the sperm of other rodent and primate species are histidine-rich (13-21%) and contain one zinc atom per molecule of protamine 2 (1,2) whereas chinchilla P2 contains 5% histidine and binds half the amount of zinc. Computer modeling using the data from the P2 gene sequence and X-ray Absorption Spectroscopy (XAS) of sperm heads reveal that the zinc-binding site of chinchilla P2 must be radically different from that of other protamine 2 molecules. The unusual zinc-P2 stoichiometry, the amino acid sequence of chinchilla P2, and the EXAFS data obtained for the zinc coordination by P2 in chinchilla sperm, suggest

that the zinc atom may be tetrahedrally coordinated to symmetric pairs of amino-terminal histidine residues, and that this coordination may facilitate the clustering of P2 molecules as dimers when the proteins bind to DNA in sperm chromatin.

Introduction

The predominant chromatin proteins that package DNA in the sperm of eutherian mammals are either protamine 1 or a species-specific combination of protamine 1 and protamine 2. Protamine 1 contains 5% or less histidine whereas protamine 2 molecules isolated from various species of rodents and primates are extremely rich in histidine (13-21%) (1,3-13).

The amount of protamine 2 in sperm chromatin varies widely among mammalian species, from 0% in sperm of the ungulates, bull and boar, up to 80% in the sperm of some species of primates (14,15). The stringent regulation of protamine expression in mammalian sperm is apparently vital for male fertility. Several studies have reported that aberrant protamine ratios or absence of protamine 2 correlates with infertility in human males (16-19). Clinical studies have demonstrated that protamine-deficient sperm contain DNA that is not properly condensed and is often damaged (20-28). These observations, which have been derived primarily from analyses of human sperm, have been substantiated experimentally by studies using

transgenic mice with reduced amounts of either P1 or P2. The sperm produced by these mice exhibited incomplete chromatin assembly, loss of nuclear DNA integrity and were incapable of producing viable offspring (29). Thus, accumulated evidence supports the idea that perturbations in the precise species-designated proportion of P1 and P2 in mammalian sperm can disrupt the packaging and organization of chromatin structure, increasing the susceptibility of the sperm cell to DNA damage, thereby causing defective sperm function and infertility.

In our earlier study using Proton Induced X-ray Emission (PIXE) to quantitate zinc and protamine 2 in the sperm heads from six mammalian species, we discovered that the zinc content varies proportionately with the amount of protamine 2 present in sperm chromatin (2). An exception was chinchilla chromatin, which contained half the amount of zinc expected based on its protamine 2 content (2). These intriguing results suggested that the amino acid sequence and zinc-binding domain of chinchilla protamine 2 might be unique when compared with other protamine 2 molecules studied to date.

To verify this hypothesis, we isolated the basic nuclear proteins from chinchilla sperm, purified protamines 1 and 2, and partially characterized the protamines by amino acid analysis and amino-terminal sequencing.

Complete putative amino acid sequences were subsequently obtained by sequencing the P1 and P2 genes. The zinc coordination site for P2 was also analyzed in chinchilla sperm heads using XAS. The sequencing and XAS data revealed that the protamine 2 present in chinchilla sperm has features distinctive from the protamine 2 molecules previously isolated and characterized from rodents and primates. The results of these experiments have led to the development of a model that appears to explain the structure of this atypical protamine 2 isolated from chinchilla sperm. In this chapter, we describe these studies, the model, and discuss the unique role protamine 2 appears to have as a DNA packaging protein in mammalian sperm.

Materials & Methods

Protamine Isolation. Sperm were obtained from the cauda epididymides of mature chinchillas (L. Johnson, Beltsville Agricultural Research Center, U.S.D.A., Beltsville, MD) as described previously for the mouse (30). The basic nuclear proteins were isolated as described previously (8).

Gel Electrophoresis and Protamine Quantification by Microdensitometry. The basic nuclear proteins isolated from chinchilla sperm were separated by gel electrophoresis and the relative proportion of the two protamines was determined as previously described for hamster (8).

High-Performance Liquid Chromatography. The sperm basic nuclear proteins were reduced with 10mg dithiothreitol per milligram of protamine in 6M guanidine hydrochloride (GuCl), 0.01M Tris-HCl pH 8, 0.25M ethylenediaminetetraacetic acid (EDTA) for a minimum of 16 hours at 20°C and dialyzed against 2 liters of 10mM HCl one hour prior to chromatography. The proteins were separated by HPLC on a Nucleosil RP-C18 column (7.5mm x 300mm) using an acetonitrile gradient (buffer A = aqueous 0.1% TFA; buffer B = 30% acetonitrile, 0.1% TFA): 40% to 65% Buffer B over 10 minutes, 65% for 20 minutes, 65% to 75% Buffer B in 0.1 minute. Protein elution was monitored at 214 nm.

Western Blotting and Immunostaining. The sperm basic nuclear proteins were separated on acid-urea gels as previously described (31). The proteins were electroblotted onto Immobilon membranes (Millipore Corporation, Burlington, MA) in 0.0009N acetic acid at 50V for 15 minutes. The membranes were air-dried and probed with P1- and P2-specific antibodies as previously described (9,32).

Immunograms. Eighty HPLC fractions (1 ml) were collected across the chromatogram and lyophilized. The protein was dissolved in 200µl distilled water and used as the antigen in an ELISA. The entire sample was applied to a 96-well round-bottom microtiter plate (Nunc Inc., Naperville,

IL), diluted 2-fold across the plate, and allowed to air dry. The plates were blocked in 10mM phosphate buffer (pH 9.5), containing 3% ovalbumin and 10μg/ml calf-thymus DNA for one hour, probed with either with a monoclonal antibody specific for protamine 1 (HuP1N) or protamine 2 (HuP2B) by adding 100μl of mAb (1:500) to each microtiter well for one hour at 37°C, then washed with aqueous 0.05% Tween-20 and incubated with a peroxidase-conjugated anti-mouse immunoglobulin (1:200 dilution) (Sigma Chemicals, St. Louis, MO) for one hour at 37°C. The plates were washed as described above and the amount of mAb bound to the wells was detected using 2,2 azino-di-3-ethylbenzthiazoline sulfonic acid (ABTS) as the substrate.

Amino Acid Analysis and Amino-Terminal Sequencing. The cysteine residues of the HPLC-purified proteins were carboxymethylated by reaction with sodium iodoacetate as described previously for bull protamine (33). The modified proteins were hydrolyzed in 6N HCl for 22 hours at 105°C, lyophilized, and submitted for amino acid composition on a Beckman 6300 analyzer (Protein Structure Laboratory, University of California, Davis, CA). Unmodified samples of the proteins were pretreated with 4-vinylpyridine to modify the cysteine residues and then sequenced using an Applied Biosystems 470A sequencer.

PCR Amplification and DNA Sequencing. Genomic DNA was isolated from Chinchilla testes using a PureGene kit as per manufacturer's instructions (Gentra, Research Triangle Park, NC). The P1/P2 gene cluster was PCR-amplified using an Elongase kit (Gibco BRL Products, Grand Island, NY), primer pair 5'-CAGGTGTGCCCTCTGTTCTGAG-3' and 5'-TTGGCTTGGGCAGGTGACTTC-3', 100 nanograms genomic DNA as template, and the following program: 94°C for 2 minutes; 5 cycles of 94°C for 1.5 minutes and 68°C for 6 minutes; 29 cycles of 94°C for 1 minute, 63°C for 1.5 minutes, and 68°C for 5 minutes; and a final incubation at 72°C for 10 minutes. A single product of 3kb was amplified. Individual P1 and P2 genes were then amplified as a second reaction using the P1/P2 PCR amplicon as template and an Elongase kit (Gibco BRL Products, Grand Island, NY). The P1 gene was amplified using the primers 5'-CAGGTGTGCCCTCTGTTCTGAG-3' and 5'-CCCGAATTCCTTAGCACGCTCCTGTT-3'. The P2 gene was amplified using primers 5'-TCTTCATCCCATCCAGGTCAG-3' and 5'-TTGGCTTGGGCAGGTGACTTC-3'. Both genes were amplified using the following program: 94°C for 2 minutes, 5 cycles at 94°C for 1 minute, 68°C for 2 minutes, and 25 cycles at 94°C for 45 seconds, 65°C for 45 seconds, and 68°C for one minute followed by 68°C for 3 minutes.

Isolation of Chinchilla Sperm Heads. Sperm were obtained from the cauda epididymides of mature chinchillas (L. Johnson, Beltsville Agricultural Research Center, U.S.D.A., Beltsville, MD) as described previously for the mouse (30). The sperm were maintained at 4°C and sonicated in Tris-saline (pH 8.0) 3 times to remove tails from the heads. The suspension was centrifuged at 4000Xg for 5 minutes. The sonication and centrifuge steps were repeated four times. The pellet was resuspended in 10ml Tris-saline by sonication, and 2ml of suspension was applied to 10ml solution of 1M sucrose/10mM Tris-HCl, pH 8.0 (for a total of 10 samples) and centrifuged at 2500g for 5 minutes. The sperm heads were pelleted and the contaminating tails remaining in suspension were carefully aspirated off. The sucrose purification step was repeated three times. The pelleted sperm heads were pooled, washed twice with Tris-saline, pH 8.0, twice with double deionized water (metal-free) and resuspended in 100μl double deionized water for analysis by XAS.

X-ray Absorption Spectra Data Collection and Analysis. A suspension of isolated chinchilla sperm heads was centrifuged at 14,000g for 10 minutes to form a pellet of cells. The supernatant was removed, and the cells were transferred to a Lucite cuvette with a 40 m Kapton window and frozen in liquid nitrogen.

Extended X-ray Absorption Fine Structure (EXAFS) measurements were made on two independently isolated samples of intact chinchilla sperm cells at Stanford Synchrotron Radiation Laboratory on beam-line 9-3 using a Si(220) double crystal monochromator under standard conditions (3.0 GeV, 100 mA). The monochromator was operated fully tuned, and a rhodium coated upstream mirror was used for harmonic rejection. Samples were held at 10 K throughout the measurements in an Oxford Instruments liquid helium flow cryostat. X-ray energies in the individual scans were calibrated by simultaneous measurement of the absorption spectrum of a zinc foil, with the first inflection point of the foil assigned to be 9659 eV. The spectra were measured using 10 eV steps through the pre-edge region, 0.30 eV steps through the edge region, and 0.05k Å^{-1} steps through the EXAFS region with integration times of 1 s, 1 s, and k^3 weighted times from 1-20 s, respectively, giving a total scan time of ~30 min/scan. Data were collected as fluorescence excitation spectra using a 30-element Ge solid-state detector array. The total incident count rates for each channel were held below 75 KHz to avoid saturation. This gave windowed Zn K count rates of 7-9 KHz in the EXAFS region, giving approximately 5x10^6 useful counts per scan at k=13 Å^{-1}. All of the channels in each scan were examined individually for the presence of glitches. For each sample, the good

channels were then averaged (23 channels per scan) to give the final spectrum. Five scans were averaged for each of the chinchilla sperm samples.

EXAFS data reduction was accomplished by first removing the background using a first-order polynomial in the pre-edge region and a two-region cubic spline above the edge, followed by normalization to a Victoreen function (34). The data were converted to *k*-space, where $k=[(2m_e/\hbar^2)(E-E_0)]^{1/2}$, with the threshold energy, E_0, defined as 9675 eV. The EXAFS data were Fourier transformed over a range of 2-12.3 $Å^{-1}$ and then back transformed over the range R=0.8-2.6 Å. Both this filtered data and the raw data were fit to eq. 1 with a nonlinear least-squares algorithm.

In eq. 1, (k) is the fractional modulation in the absorption coefficient above the edge, N_i is the number of scatterers at a distance R_i, $S_i(k)$ is a scale factor unique to the absorber-scatterer pair, $A_i(k)$ is the effective backscattering amplitude, $^2{}_i$ is the mean-square deviation in R_i, and $_i$ is the phase-shift experienced by the photoelectron wave as it passes through the potentials of the absorbing and scattering atoms. The sum is taken over all scattering interactions.

Theoretical EXAFS amplitudes ($A_i(k)$) and phase functions ($_i(k)$) were calculated using FEFF 6.01 (35,36). The experimental data were fit

using single scattering parameters calculated for Zn-O and Zn-N with bond lengths of 2.00 Å and 2.05 Å, respectively. The scale factors used were S=0.9 for O and S=0.85 for N, and the threshold energy was fixed at E_0=9.0 eV. For N, these values were calibrated by fitting EXAFS data for structurally characterized Zn model complexes (37). R and were varied while holding the coordination number fixed at four or five.

Results

The predominant sperm basic nuclear proteins isolated from the cauda epididymides of mature chinchillas resolved into two major bands upon electrophoresis in acid-urea gels (Figure 1). In contrast to the two protamines from mouse and hamster sperm, the two chinchilla protamines separate upon electrophoresis without aminoethylation of the cysteine residues. This indicates that the two chinchilla protamines have different molecular weights and charge densities.

The isolated chinchilla protamines were fractionated by chromatography on a reverse-phase C18 column using a multi-step acetonitrile gradient and the ion–pairing agent trifluoroacetic acid (Figure 2). Three peaks were resolved. The retention time of the first protein eluting from the column was characteristic of protamine 2, but the histidine content

of this protein was much lower than we have observed for other protamine 2 molecules (1). The protein in peak 2 elutes at an acetonitrile concentration

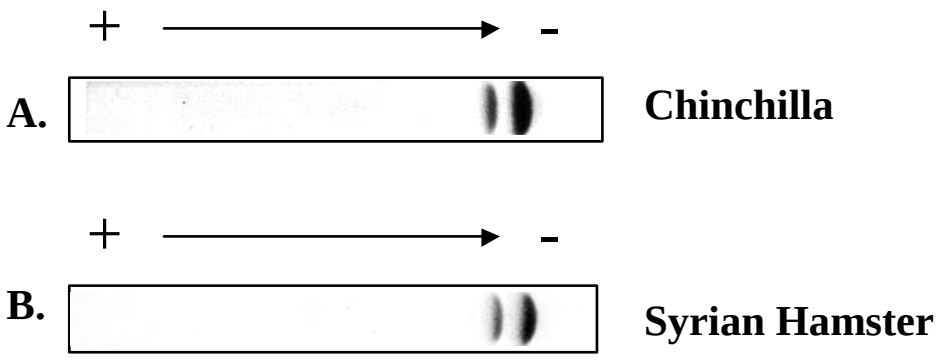

Figure 1. Protamines 1 and 2 isolated from (A) chinchilla sperm separate in acid-urea gels without aminoethylation of the cysteine residues while protamines 1 and 2 isolated from (B) Syrian hamster sperm require modification by ethylenimine to separate into 2 bands.

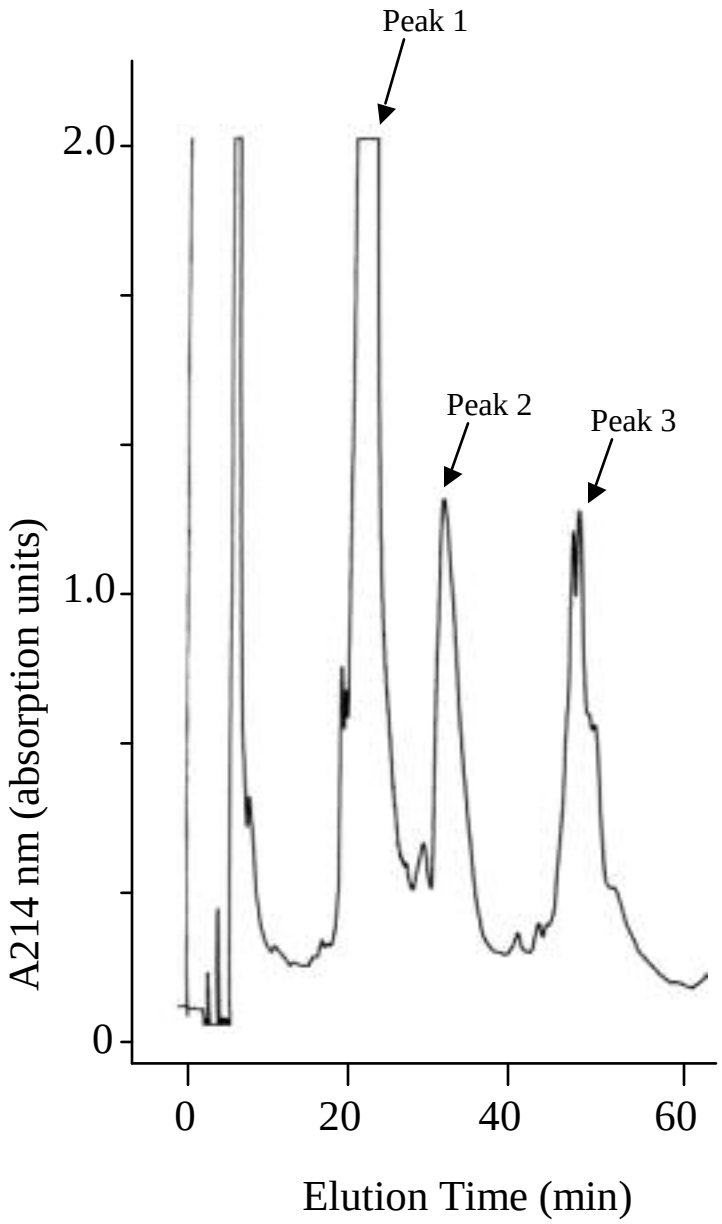

Figure 2. HPLC chromatogram of basic nuclear proteins isolated from chinchilla sperm.

characteristic of protamine 1. Electrophoretic analyses of the proteins eluting from the column as peaks 1 and 2 are consistent with that of protamine 2 and protamine 1, respectively (38,39). The final eluate from the column (peak 3) is resolved by electrophoresis into several bands with substantial slower mobilities than the proteins eluting in the first two peaks (Figure 2). The electrophoretic pattern, gel mobility, and the elution time from the HPLC column of the final eluate are typical of the protamine 2 precursor proteins that have been isolated from rat and mouse sperm (4,40).

To verify the protein fractions were protamines, the three HPLC eluates were analyzed by ELISA using monoclonal antibodies specific for protamine 1 (HuP1N) and protamine 2 (HuP2B) (data not shown). The protein eluting from the column as peak 2 reacted strongly with HuP1N, identifying it as protamine 1. None of the protein peaks reacted with the protamine 2-specific antibody, HuP2B.

The identities of the two proteins eluting as peaks 1 and 2 were confirmed by amino-terminal sequencing. Chinchilla protamine 1, which eluted as peak 2, was identified by its highly conserved, characteristic amino-terminal sequence, ARYRCC (1). The amino acid composition of this protein, in addition to its reaction with HuP1N antibody, suggests that the sequence of chinchilla protamine 1 should be similar to the

sequences of protamine 1 isolated from other rodent species (1). This was verified by sequencing the protamine 1 gene amplified from genomic DNA isolated from chinchilla testes. The gene sequence and predicted amino acid sequence of P1 are shown in Figure 3.

The low histidine content and unusual amino-terminal sequence (KGRYH) of the protein that eluted as peak 1 indicates that the structure of chinchilla protamine 2 is atypical of protamine 2 molecules (1). The protein isolated from chinchilla sperm, in contrast, contains only 5% histidine, yet its retention time (earlier than P1) and electrophoretic mobility (slower than P1) appear characteristic for rodent protamine 2 molecules.

DNA sequencing data obtained for the protamine 2 gene from chinchilla testes confirmed this protein is protamine 2 and revealed the protein contains only three histidine residues in the fully processed P2 (Figure 4). The sequencing data verified that this protein contained the unusual amino-terminal sequence (KGRYH) observed by protein N-terminal sequencing data.

EXAFS data were obtained for chinchilla sperm to identify the ligands (amino acid side chains) that coordinate zinc in protamine 2. Figure 5 shows the raw and Fourier transformed zinc EXAFS data. The Fourier transform exhibits a single narrow peak at ~1.6 Å, suggestive of a single shell of

```
ATGGCCAGATACAGATGCTGCCGCAGCCCAAGCCGGAGCAGATGC    45
 M  A  R  Y  R  C  C  R  S  P  S  R  S  R  C

CGCCGCCGCAGACGGAGATGCCATAGACGAAGGAGGCGGTGCTAT    90
 R  R  R  R  R  R  C  H  R  R  R  R  R  C  Y

CGGAGACGGAGACgtaagcgcgggtgctgctggggtgaggggctg    135
 R  R  R  R

gggctccatggggcccggatggtctctcaacgcctcttgtgcccc    180


tagGGTGCTGCCGCCGCAGGTACACCCGGAGGTGCAGAAGACACtaa 302
   R  C  C  R  R  R  Y  T  R  R  C  R  R  H stop
```

Figure 3. Chinchilla P1 gene sequence. Complete gene sequence is shown with the encoded amino acid sequence below.

```
ATGGTTCGCTGCCGAGTGAGGAGCCCCAGCCATCACCCTCACCAG   45
 M  V  R  C  R  V  R  S  P  S  H  H  P  H  Q

GAGTCTGGTGAGGGCCAGCAGCAGGAGCAGGGGCTGAGCCCAGAG  90
 E  S  G  E  G  Q  Q  Q  E  Q  G  L  S  P  E

CACGGGGAGGCCTACGGGAGGACACACAAAGGTCGCTACCACAGG  135
 H  G  E  A  Y  G  R  T  H  K  G  R  Y  H  R

CGCAGGCGCTGTTCTCGGAGGAGGCCATACCGGATCTACAGGCGG  180
 R  R  R  C  S  R  R  R  P  Y  R  I  Y  R  R

CACAGGTCCTGCCGAAGGCGCAGGAGACGCAGCTGCAGGAGACGC  225
H  R  S  C  R  R  R  R  R  R  S  C  R  R  R

AGCTGCAGGAGGCGACGCCGAGgtctgcctgaactccgccccatc  270
 S  C  R  R  R  R  R

aaccccaggcccttgcacctatgctgctgcacagcagagcagga   315

gggaggctggggttccactgttgtctgagcctaaaccccatcccc  360

acccagatccccccaatgaccccaaatcaacttttcttcccaata  405

gCCTGCAGAAGACGCAGGAGGAGAAGATGCGGGAGGTACCACtaa  450
 A  C  R  R  R  R  R  R  R  C  G  R  Y  H stop
```

Figure 4. Chinchilla P2 gene sequence. Complete gene sequence is shown with the encoded amino acid sequence below. The leader sequence is shown in red.

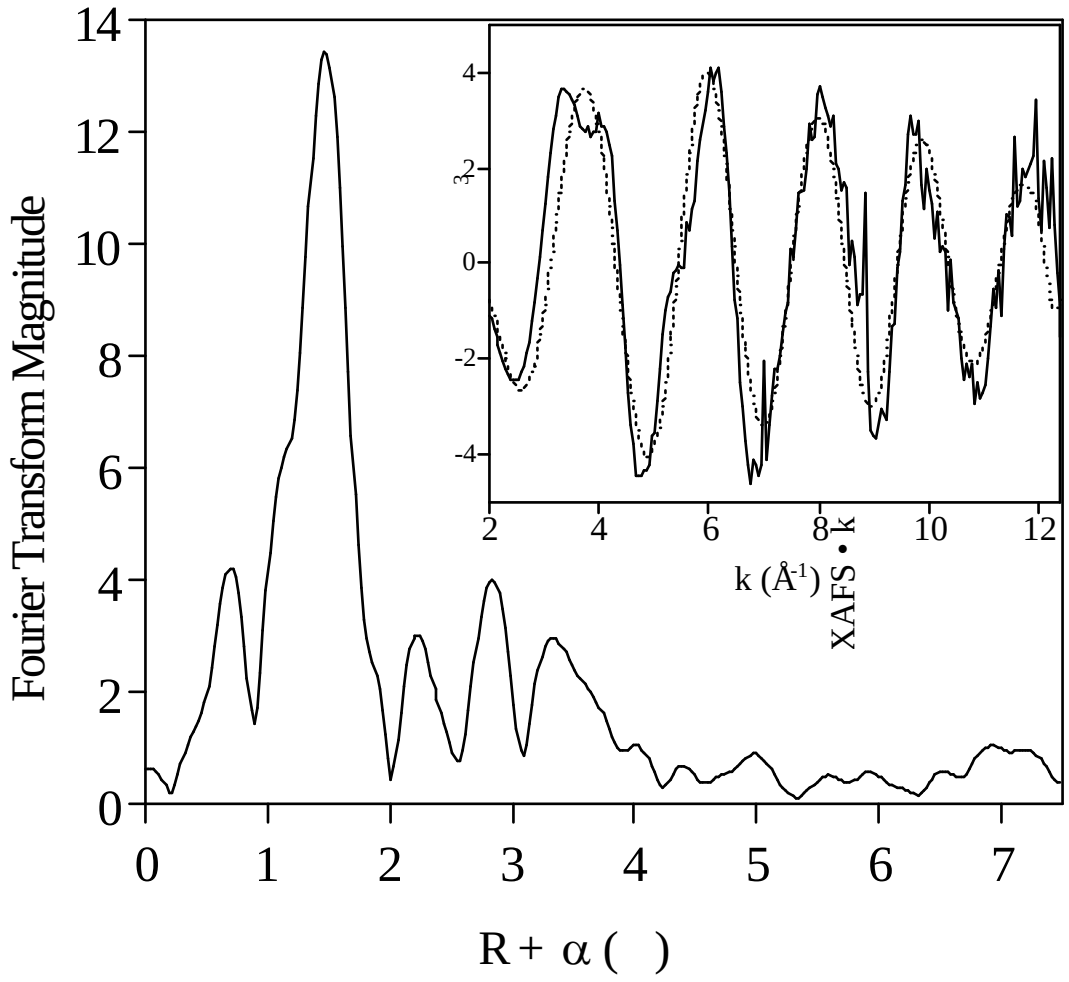

Figure 5. Raw (inset) and Fourier transformed EXAFS data of the zinc ligation in chinchilla sperm.

scatterers. In addition, the structure observed in the EXAFS oscillations as well as the outer-shell features observed in the Fourier transform at R+∝ of ca. 2.2 Å, 2.9 Å, and 3.3 Å have frequencies indicative of coordination by imidazole. Fits to the data (Table 1) show that the spectrum is well modeled as a single shell of four N/O ligands at 2.0 Å with chemically reasonable Debye-Waller factors. The outer-shell scattering obtained for chinchilla P2 is approximately 60% as intense as that observed for a crystallographically characterized zinc tetra-imidazole model, suggesting that there are at least two (and probably more) histidine ligands coordinated to the zinc.

Discussion

The putative amino acid sequence derived from the gene sequence of chinchilla P1 is similar to that for other rodents such as mouse, Syrian hamster, and *R. norvegicus* (Figure 6); however, chinchilla P2 is different from previously described P2 molecules. Although clearly a variant, this protein is one of the predominant nuclear basic proteins in chinchilla sperm comprising 25% of the total protamine in the chromatin of chinchilla (1), and the protein shares some similarities with P2 from other mammals. The chinchilla P2 gene sequence and the N-terminal amino acid sequence of the isolated protein provide evidence that chinchilla P2 must be synthesized as a precursor that is fully processed. The C-terminus of chinchilla P2 also

Ligand	Bond Distance (Å)	$^{2}*10^{3}$ ($Å^{-2}$)	F'[a]
3N	2.00	2.3	0.027
4N	2.00	4.1	0.024
5N	2.00	5.9	0.040
1O	1.96	0	0.021
3N	2.02	7.5	

Table 1. Zinc EXAFS fit table for Chinchilla sperm cells.[b]

[a] F'=$\{[k^6(\text{data-fit})^2]/N\}/(N_{idp}-N_{var})$ where N is the number of data points, $N_{idp}=(2\ \ k\ \ R)/$. is the number of independent data points, and N_{var} is the number of variable fitting parameters.

[b] Fits are given for Fourier filtered EXAFS data. Similar fitting parameters were obtained for fits to the raw data with higher fit residuals due to the inclusion of high-R noise.

Chinchilla
MARYRCCRSPSRSRCRRRRRRCHRRRRRC-YRRRRRCCRRR--YTRRCRRH

Mouse
MARYRCCRSKSRSRCRRRRRRCRRRRRRCCRRRRRRCCRRRRSYTIRCKKY

Syrian hamster
MARYRCCRSKSRSRCRRRRRRCRRRRRRCCRRRRRRCCRRRRTYTLRCKRY

Rat
MARYRCCRSKSRSRCRRRRRRCRRRRRRCCRRRRRRCCRRRRSYTFRCKRY

Figure 6. Alignment of protamine 1 from chinchilla, mouse, Syrian hamster and rat (*Rattus norvegicus*).

contains the polyarginine domains typically associated with functional P2 molecules.

The few biochemical studies of chinchilla sperm that have been conducted demonstrate that the incorporation of this unusual P2 molecule in sperm does not appear to affect chromatin stability. Chinchilla sperm stain normally with DNA dyes for flow cytometry (6). The chromatin in mature sperm is also resistant to disruption in guanidine hydrochloride in the absence of disulfide reducing agents (unpublished observations). In addition, the sperm decondense at a rate characteristic for mouse and hamster sperm containing P2 when injected into hamster eggs (41). Thus, the ratio of zinc to P2 and the sequence variability do not appear to affect the function of chinchilla P2 as a DNA packaging protein.

Using our protein and gene sequence data combined with the electrophoretic mobilities of the isolated proteins in gels, we determined that chinchilla P2 is fully processed and that there are only three histidines in the sequence of the mature protein (Figure 4). However, the low number of histidine residues in this protein, when compared with the known sequences of P2 molecules isolated from the sperm of primates and other rodents suggest that chinchilla P2 must differ significantly in the way it interacts with zinc.

To obtain information about how zinc is coordinated by chinchilla P2, EXAFS data were obtained using the native chinchilla sperm chromatin

complex to identify the amino acids that coordinate zinc. Since the EXAFS data from chinchilla sperm is best fit with the first shell ligands as all low Z, the only ligands that coordinate zinc in chinchilla sperm are nitrogen or oxygen, not sulfur (Table 1). Additionally, the first-shell bond distances are consistent with tetrahedral coordination. Because only one zinc atom is bound to two P2 molecules in chinchilla sperm, there appear to be only two ways in which P2 could bind zinc: either one zinc atom is bound by two P2 molecules, or only half of the P2 molecules bind a zinc atom. The latter possibility seems unlikely since the population of P2 appears homogeneous and zinc would not be expected to bind preferentially to a subpopulation of identical molecules. However, this possibility cannot be ruled out entirely based on limited existing data. Structural and computer modeling studies of the protamine-DNA complex indicate that protamine binds DNA in an extended conformation, and specifically, each protamine 2 molecule covers 15 DNA bases (42-44). The most plausible model, based on our current data, is the zinc atom may be tetrahedrally coordinated to symmetric pairs of histidine residues from the N-terminus of each P2 molecule (Figure 7).

A similar mode of zinc coordination has been demonstrated for an

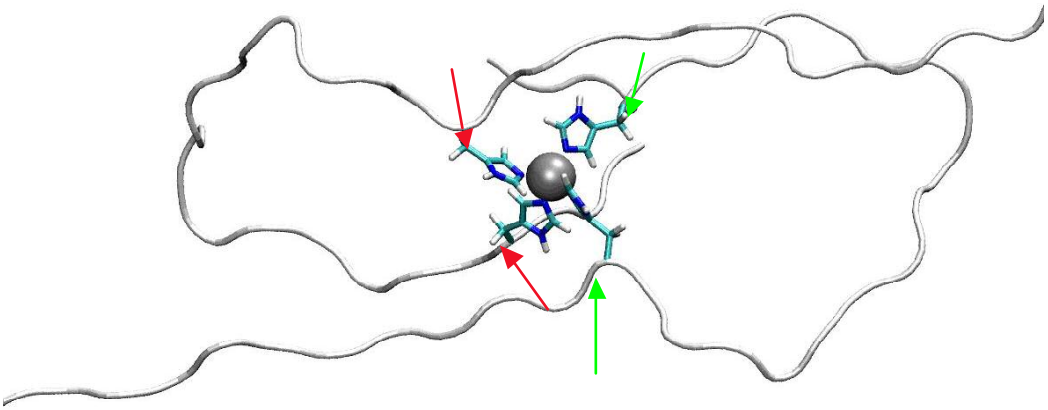

Figure 7. Computer model of two chinchilla protamine 2 molecules bound to one zinc atom by symmetric histidine residues at the amino-terminal regions. Each P2 molecule contributes 2 ligands (shown in red arrows for one molecule and in green arrows for the second P2 molecule. The arginine-rich DNA binding domains are truncated.

unrelated protein, endothelial nitric oxide synthase, in which symmetric pairs of cysteine residues from each monomer bind the zinc ion (45). Other precedents for this unusual formation of dimers by zinc binding include the T cell co-receptors, CD4 and CD8, that form ternary complexes with Lck (the Src-family tyrosine kinase) in the presence of zinc (46). The C-termini of CD4 or CD8 and the N-terminus of Lck in solution are unstructured, but the addition of zinc induces the folding of the proteins into a "clasp"-like structure that wraps around the zinc. However, the interactions of amphipathic helices between CD4 and Lck further stabilize the coordination of zinc whereas the CD8-Lck-Zn^{2+} complex lacks these intermolecular interactions. Preliminary computer modeling results appear consistent with chinchilla P2 binding zinc symmetrically, analogous to nitric oxide synthase. P2 exhibits features that resemble the CD8-Lck-Zn^{2+} in that zinc binding induces a motif in an otherwise unstructured protein.

The data obtained from previous PIXE analyses of chinchilla sperm chromatin combined with the EXAFS and sequence analyses described here provide strong evidence that chinchilla P2 and its interaction with zinc is atypical compared with other protamine 2 molecules. For those species that contain P2 and zinc in the typical 1:1 ratio, we speculate that zinc may play a similar structural role in the formation of P2 homodimers in these species.

Preliminary chemical crosslinking experiments have also indicated that P2 appears to be clustered as dimers when bound to DNA in sperm chromatin (8). In the sperm chromatin of most mammals, these results suggest that each P2 molecule may have a dimerization site whose structure is stabilized by a zinc atom, rather than a coordination site that is shared by two P2 molecules as we have proposed for chinchilla P2.

Acknowledgements

We gratefully acknowledge Dr. Katrina Peariso for collecting and interpreting the X-ray Absorption Spectroscopy data, Drs. Felice Lightstone and Brian Bennion for their computer modeling expertise, and Joe Mazrimas and Michele Corzett for the protein analyses of the chinchilla protamines.

References

1. Balhorn R. Mammalian protamines: structure and molecular interactions. In: Adolph KW (ed), Molecular Biology of Chromosome Function. New York: Springer-Verlag; 1989: 366-395.
2. Bench GS, Corzett MH, Kramer CE, Grant PG, Balhorn R. Zinc is sufficiently abundant within mammalian sperm nuclei to bind stoichiometrically with protamine 2. Mol Reprod Dev 2000; 56:512-519.

3. Kleene LC, Distel RJ, Hecht NB. Nucleotide sequence of a cDNA clone encoding mouse protamine 1. Biochemistry 1985; 24:719-722.

4. Yelick PC, Balhorn R, Johnson M, Corzett M, Mazrimas JA, Kleene KC, Hecht NB. Mouse protamine is synthesized as a precursor whereas mouse protamine 1 is not. Mol Cell Biol 1987; 7:2173-2179.

5. Bellve AR, McKay DJ, Renaux BS, Dixon GH. Purification and characterization of mouse protamines P1 and P2: amino acid sequence of P2. Biochemistry 1988; 27:2890-2897.

6. Johnson PA, Yelick PC, Liem H, Hecht NB. Differential distribution of the P1 and P2 protamine gene sequences in eutherian and marsupial mammals and a monotreme. Gamete Res 1988; 19:169-175.

7. Dolan CE, Fabes SE, Mazrimas JA, Corzett MH, Breed WG, Balhorn R. Variable regulation of protamine 2 gene expression in Muroid rodents. (manuscript in preparation).

8. Corzett M, Kramer C, Blacher R, Mazrimas J, Balhorn R. Hamster protamines sequence and distribution. Mol Reprod Dev 1999; 54:273-282.

9. Retief JD, Winkfein RJ, Dixon GH, Adroer R, Queralt R, Ballabriga J, Oliva R. Evolution of protamine P1 genes in primates. J Mol Evol 1993; 37:426-434.

10. McKay DJ, Renaux BS, Dixon GH. The amino acid sequence of human sperm protamine P1. Biosci Rep 1985; 5:383-391.

11. McKay DJ, Renaux BS, Dixon GH. Human sperm protamines: amino-acid sequences of two forms of protamine P2. Eur J Biochem 1986; 156:5-8.

12. Ammer H, Henschen A, Lee C-H. Isolation and amino acid sequence analysis of human sperm protamines P2 and P2: occurrence of two forms of protamine 2. Biol Chem Hoppe-Seyler 1986; 367:515-522.

13. Gusse M, Sautiere P, Belaiche D, Martinage A, Roux C, Dadoune J-P, Chevaillier P. Purification and characterization of nuclear basic proteins of human sperm. Biochim Biophys Acta 1986; 884:124-134.

14. Maier W-M, Nussbaum G, Domenjoud L, Klemm U, Engel W. The lack of protamine 2 (P2) in boar and bull spermatozoa is due to mutations within the P2 gene. Nucleic Acids Res 1990; 18:1249-1254.

15. Corzett M, Mazrimas JA, Balhorn, R. Protamine 1:protamine 2 stoichiometry in the sperm of eutherian mammals. Mol Reprod Dev 2002; 61:519-527.

16. Balhorn R, Reed S, Tanphaichitr N. Aberrant protamine 1/protamine 2 ratios in sperm of infertile human males. Experientia 1988; 44:52-55.

17. Belokopytova IA, Kostyleva EI, Tomilin AN, Vorobev VI. Human

male infertility may be due to a decrease of the protamine-P2 content in sperm chromatin. Mol Reprod Dev 1993; 34:53-57.

18. de Yebra L, Ballesca JL, Vanrell JA, Bassas L, Oliva R. Complete selective absence of protamine-P2 in humans. J Biol Chem 1993; 268:10553-10557.

19. Carrell DT, Liu L. Altered protamine 2 expression is uncommon in donors of known fertility, but common among men with poor fertilizing capacity, and may reflect other abnormalities of spermiogenesis. J Androl 2001; 22:604-610.

20. Razavi S, Nasr-Esfahani MH, Mardani M, Mafi A, Moghdam A. Effect of human sperm chromatin anomalies on fertilization outcome post-ICSI. Andrologia 2003; 35:238-243.

21. Nasr-Esfahani MH, Razavi S, Mardani M. Relation between different human sperm nuclear maturity tests and in vitro fertilization. J Assist Reprod Genet 2001; 18:219-225.

22. Iranpour FG, Nasr-Esfahani MH, Valojerdi MR, al-Taraihi TM. Chromomycin A3 staining as a useful tool for evaluation of male fertility. J Assist Reprod Genet 2000; 17:60-66.

23. Sakkas D, Urner F, Bizzaro D, Manicardi G, Bianchi PG, Shoukir Y, Campana A. Sperm nuclear DNA damage and altered chromatin

structure: effect on fertilization and embryo development. Hum Reprod 1998; 4:11-19.

24. Bianchi PG, Manicardi GC, Urner F, Campana A, Sakkas D. Chromatin packaging and morphology in ejaculated human spermatozoa: evidence of hidden anomalies in normal spermatozoa. Mol Hum Reprod 1996; 2:139-144.

25. Lolis D, Georgiou I, Syrrou M, Zikopoulos K, Konstantelli M, Messinis I. Chromomycin A3-staining as an indicator of protamine deficiency and fertilization. Int J Androl 1996; 19:23-27.

26. Sailer BL, Jost LK, Evenson DP. Mammalian sperm DNA susceptibility to in situ denaturation associated with the presence of DNA strand breaks as measured by the terminal deoxynucleotidyl transferase assay. J Androl 1995; 16:80-87.

27. Manicardi GC, Bianchi PG, Pantano S, Azzoni P, Bizzaro D, Bianchi U, Sakkas D. Presence of endogenous nicks in DNA of ejaculated human spermatozoa and its relationship to chromomycin A3 accessibility. Biol Reprod 1995; 52:864-867.

28. Gorczyca W, Traganos F, Jesionowska H, Darzynkiewicz Z. Presence of DNA strand breaks and increased sensitivity of DNA *in situ* to of somatic cells. Exp Cell Res 1993; 207:202-205.

29. Cho C, Jung-Ha H, Willis WD, Goulding EH, Stein P, Xu Z, Schultz RM, Hecht NB, Eddy EM. Protamine 2 deficiency leads to sperm DNA damage and embryo death in mice. Biol Reprod 2003; 69:211-217.

30. Balhorn R, Gledhill BL, Wyrobek AJ. Mouse sperm chromatin proteins: quantitative isolation and partial characterization. Biochemistry 1977; 16:4074-4080.

31. Panyim S, Bilek D, Chalkley R. An electrophoretic comparison of vertebrate histones. J Biol Chem 1971; 246:4206-4215.

32. Stanker LH, McKeown C, Balhorn R, Lee C, Mazrimas J, Goralka M, Wyrobek A. Immunological evidence for a P2 protamine precursor in mature rat sperm. Mol Reprod Dev 1992; 33:481-488.

33. Balhorn R, Corzett M, Mazrimas JA. Formation of intraprotamine disulfides in vitro. Arch Biochem Biophys 1992; 296:384-393.

34. Teo BK. EXAFS: Basic Principles and Data Analysis. New York: Springer-Verlag; 1986.

35. Rehr JJ, deLeon JM, Zabinsky SI, Albers RC. Theoretical x-ray absorption fine-structure standards. J Am Chem Soc 1991; 113:5135-5140.

36. Rehr JJ, Albers RC, Zabinsky SI. High-order multiple-scattering

calculations of x-ray-absorption fine structure. Phys Rev Lett 1992; 69:3397-3400.

37. Clark-Baldwin K, Tierney DL, Govindaswamy N, Gruff ES, Kim C, Berg J, Koch SA, Penner-Hahn JE. The limitations of X-ray absorption spectroscopy for determining the structure of zinc sites in proteins. When is a tetrathiolate not a tetrathiolate? J Am Chem Soc 1998; 120:8401-8409.

38. Grimes SR, Meistrich ML, Platz RD, Hnilica LS. Nuclear protein transitions in rat testis spermatids. Exp Cell Res 1977; 110:31-39.

39. Pogany GC, Corzett M, Weston S, Balhorn R. DNA and protein content of mouse sperm: implications regarding sperm chromatin structure. Exp Cell Res 1981; 136:127-136.

40. Bunick D, Balhorn R, Stanker LH, Hecht NB. Expression of the rat protamine 2 gene is suppressed at the level of transcription and translation. Exp Cell Res 1990; 188:147-152.

41. Perreault SD, Barbee RR, Elstein KH, Zucker RM, Keefer CL. Interspecies differences in the stability of mammalian sperm nuclei assessed in vivo by sperm microinjection and in vitro by flow cytometry. Biol Reprod 1988; 39:157-167.

42. Balhorn R, Cosman M, Thornton K, Krishnan VV, Corzett M, Bench

G, Kramer C, Lee J IV, Hud NV, Allen M, Prieto M, Meyer-Ilse W, Brown JT, Kirz J, Zhang X, Bradbury EM, Maki G, Braun RE, Breed W. Protamine mediated condensation of DNA in mammalian sperm. In: Gagnon C (ed), The male gamete: from basic knowledge to clinical applications. Vienna, IL: Cache River Press; 1999: 56-70.

43. Bench GS, Friz AM, Corzett MH, Morse DH, Balhorn R. DNA and total protamine masses in individual sperm from fertile mammalian subjects. Cytometry 1996; 23:263-271.

44. Hud NV, Allen MJ, Downing KH, Lee J, Balhorn R. Identification of the elemental packing unit of DNA in mammalian sperm cells by atomic force microscopy. Biochem Biophys Res Commun 1993; 193:1347-1354.

45. Raman CS, Li H, Martasek P, Kral V, Masters BS, Poulos TL. Crystal structure of constitutive endothelial nitric oxide synthase: a paradigm for pterin function involving a novel metal center. Cell 1998; 95:939-950.

46. Kim PW, Sun ZY, Blacklow SC, Wagner G, Eck MJ. A zinc clasp structure tethers Lck to T cell coreceptors CD4 and CD8. Science 2003; 301:1725-1728.

CHAPTER FOUR

Structural and Functional Studies of Syrian Gold Hamster Protamines with Native Zinc Bound

Abstract

Previous studies of zinc binding to protamine 2 (P2) using peptides and isolated human P2 have demonstrated that protamine 2 has multiple sites that bind zinc *in vitro*. One common feature shared by these experiments is the zinc added to the protein or peptide is maintained in excess, a condition not representative of the *in vivo* zinc environment of P2 inside the heads of the spermatid and mature sperm. Also, since it is likely that P2 adopts a different conformation in solution ("non-native") than when bound to DNA in sperm chromatin ("native"), zinc binding to P2 *in vitro* may not reflect the actual site or mode of binding *in vivo*. Therefore, to determine the role of zinc in stabilizing the sperm chromatin – a process that appears critical for male fertility - it is imperative to obtain structural data from the biologically relevant native state. The goals of this study were to: design a method for extracting protamines off sperm DNA with mild conditions to preserve zinc binding to protamine 2; obtain structural data

using X-ray Absorption Spectroscopy (XAS) for the zinc binding domain of isolated protamines; and analyze the effect of native zinc on protamine 2 binding to DNA. Using P2 extracted from sperm chromatin with calcium and magnesium, we determined the ligands coordinating zinc by EXAFS. From our optical trapping study, we found that zinc facilitates the condensation of lambda-phage DNA by protamine 2, but zinc had no effect on the rate of chromatin decondensation (P2 dissociation from DNA) *in vitro*. Additionally, the rate of DNA condensation was greatly enhanced by the binding of P1 and P2 with native zinc bound compared with the binding of isolated P2 in zinc buffer. The increased rate of condensation may be caused by the native binding of zinc to P2 as well as the presence of P1 which, unlike P2 alone, represents the *in vivo* state of the sperm chromatin.

Introduction

The concentration of zinc is elevated in the male reproductive tract, compared with blood plasma, and has been proposed to function in maintaining the stability of sperm DNA during epididymal storage and ejaculation (1-5). Changes in the decondensation of DNA has been correlated *in vitro* in sperm with the addition of zinc chelators and *in vivo* in sperm from infertile males with impaired secretion of zinc from the prostate (1-5). Fertility has been shown to be dependent on the regulation of the

amount of zinc present throughout spermiogenesis. Both deficiencies and excessive intake of zinc have been demonstrated to have an adverse effect on testicular tissue and sperm function in rodent testes (6,7).

Although zinc has been deemed critical for stabilizing the sperm chromatin for well over a decade, how it functions in maintaining sperm viability is unknown (1-5). Proper DNA condensation is crucial to sperm viability as well, and DNA binding and condensation is the primary function of protamines. While both protamines contain cysteine, protamine 2 also contains multiple histidines, amino acids with functional groups that bind zinc. Additionally, unlike P1, isolated human P2 and synthetic P2 peptides have been demonstrated to bind zinc *in vitro* (8-10).

The zinc coordination site of P2 *in vivo* remains speculative. Results from *in vitro* zinc binding studies using isolated human protamine 2 have provided contrasting models that differ both in the type of ligands that bind zinc and number of zinc coordination site(s) (8,9). Another study using synthetic P2 peptides revealed that only the N-terminal fragment of P2 complexed with zinc binds DNA in oxidizing conditions, the milieu of a sperm cell (10). Furthermore, this study provided evidence that the zinc does bind to protamine 2 and not to DNA (10).

Structural data of protamines have been inconclusive due to the

insolubility of nucleoprotamine. An attempt to bind protamine 2 and zinc to small oligonucleotides resulted in the formation of insoluble complexes (10). Also, the standard methods for dissociating protamines from sperm DNA utilize reducing agents and denaturants, conditions that also disrupt the binding of zinc to protamine 2. To isolate protamines from hamster sperm without dissociating the zinc, we modified a protocol using calcium and magnesium to extract protamines from mouse sperm chromatin (11,12). We monitored zinc binding to protamines by Proton-Induced X-Ray Emission (PIXE) and obtained structural data of the zinc-binding site in protamine 2 by X-ray Absorption Near Edge Structure (XANES) and Extended X-ray Absorption Fine Structure (EXAFS).

The results from this study demonstrated that zinc remains bound to protamine 2 when the protein is extracted from DNA using divalent cations and the ligands coordinating the zinc are the same as in spermatids (Chapter 2). The use of a disulfide reductant, which is required for protamine extraction, caused new thiol groups to become accessible for binding to zinc, mimicking the conditions found *in vivo* in the spermatid. During the later stages of spermiogenesis, as the thiol groups form intra- and inter-protamine disulfide bridges, one ligand coordinating the zinc changes from sulfur to histidine (Chapter 2). Based on these and other studies, we propose that zinc

binding to P2 induces the formation of an amino-terminal conformation that facilitates P2 dimerization or clustering upon binding to DNA.

Materials and Methods

All chemicals were purchased from Sigma Chemical Company (St. Louis, MO) unless otherwise noted. All buffers were screened by PIXE to ensure purity from contaminating metals. All preparative steps were carried out in metal-free conditions to prevent contamination.

Syrian hamster (*Mesocricetus auratus*) epididymides were obtained from adult males (retired breeders) purchased from Simonsen Laboratory (Gilroy, CA).

Protamine Isolation. Sperm were teased from one epididymis, yielding 100-150 million sperm. Sperm were treated with 30mM β-mercaptoethanol (BME) and mixed alkyltrimethylammonium bromide (MTAB) as described previously (13) then the amembraneous sperm heads were rinsed twice in 10mM Tris-HCl pH 8 to remove detergent and reductant.

The pelleted sperm chromatin was resuspended in 3 ml cold 50mM Tris-HCl (pH 8), 25mM BME, and 1mM phenylmethylsulfonyl fluoride (PMSF) by brief sonication using a Teflon tip and placed on ice 30 minutes. While maintaining the concentration of BME, 250mM $CaCl_2$-$MgCl_2$ (3

mol:2 mol) was added and the sample was incubated at room temperature for 30 minutes, swirling occasionally, and cooled on wet ice for 1 hour. The sample was transferred to 13x51mm polycarbonate tubes and centrifuged at 90000 rpm for 30 minutes at 4°C in a TLA-100.3 rotor using a Beckman T100 ultracentrifuge to pellet the DNA. The supernatant containing protamines was transferred to SpectraPor 7 metal-free dialysis tubing with MWCO 1000 (Spectrum, Houston, TX) and dialyzed against 4 liters of double deionized water for 3 hours, changing water every hour. The sample was immediately frozen on dry ice and lyophilized.

The extracted protein was quantitated by UV spectroscopy at 214nm and 230nm wavelengths. An aliquot of the protein (10µg) was air-dried on a nylon foil, and the zinc and sulfur contents were determined by PIXE (11). Another aliquot (100µg) was modified by reaction with aziridine (13), and the proteins were separated by gel electrophoresis in acid-urea gels as previously described (14). The gels were stained with Naphthol Blue Black and destained as previously described (13,14). The gel band was scanned with a Shimadzu Flying Spot microdensitometer (Shimadzu Inc., Pleasanton, CA), and areas under the protamine 1 and protamine 2 peaks were quantitated.

PIXE Analysis. PIXE analysis using the nuclear microprobe at

LLNL has been previously described (15). In brief, PIXE data of isolated protamine samples were obtained using an incident 3 MeV proton beam with a beam current of up to 5 nA over an area of 2 x 2 m . Each irradiated area contained the dried aliquot from a microliter deposit of the protamine solution onto a formvar foil. The samples were covered but not sealed to allow drying but to protect from dust. Background levels of phosphorus, sulfur, and zinc on the formvar foils were typically below minimum detectable limits of 5ng/cm2 for each sample. The details of data analysis have been described previously (11,15).

XAS analysis. Lyophilized samples of isolated protamines 1 and 2 were left as a solid, packed into Lucite cuvettes with a 40μm Kapton window and frozen in liquid nitrogen. EXAFS measurements were made on 3 independently prepared samples of lyophilized protamines 1 and 2 at SSRL on beamline 9-3 using a Si(220) double crystal monochromator under dedicated conditions (3.0 GeV, 55-100 mA). The monochromator was operated fully tuned, and a rhodium coated upstream mirror was used for harmonic rejection. Samples were held at 10 K throughout the measurements in an Oxford Instruments liquid helium flow cryostat. X-ray energies in the individual scans were calibrated by simultaneous measurement of the absorption spectrum of a zinc foil, with the first inflection point of the foil

assigned to be 9659 eV. The spectra were measured using 10 eV steps through the pre-edge region, 0.30 eV steps through the edge region, and 0.05k Å^{-1} steps through the EXAFS region with integration times of 1 s, 1 s, and k^3 weighted times from 1-20 s, respectively, giving a total scan time of ~30 min/scan. Data were collected as fluorescence excitation spectra using a 30-element Ge solid-state detector array on beamline 9-3. The total count rates for each channel in the detector array and the windowed Zn Kα count rates in the EXAFS region are given in Table 1. All of the channels from each scan were examined for the presence of glitches, and the good channels (Table 1) were then averaged for each sample to give the final spectrum. Based on the number of channels used and the measured Zn Kα count rates at k =13Å^{-1}, approximately 1.7-10.5 x 10^6 useful counts were collected per scan on beamline 9-3. The number of scans averaged for each sample is given in Table 1.

X-ray absorption near edge structure (XANES) data normalization and the EXAFS data reduction followed procedures described previously (16). EXAFS data reduction was accomplished by first removing the background using a first-order polynomial in the pre-edge region and a two-region cubic spline above the edge, followed by normalization to a Victoreen function (17). The data were converted to k-space, where

Sample	Zn Kα	ICR	# FF Channels per scan	# Scans
Protamines 1 & 2 (A)	16000	45000	25	4
Protamines 1 & 2 (B)	21000	45000	25	4
Protamines 1 & 2 (C)	3300	34000	25	5

Table 1. EXAFS data collection parameters. All data were collected as fluorescence excitation spectra using a 30-element Ge solid-state detector array on beamline 9-3.

$k = [(2m_e/\hbar^2)(E-E_0)]^{1/2}$, with the threshold energy, E_0, defined as 9675 eV.

The EXAFS data were Fourier transformed over a range of 2-12.3 $Å^{-1}$ and then back transformed over the range R=0.8-2.6 Å. Both this filtered data and the raw data were fit to eq. 1 with a nonlinear least-squares algorithm.

$$\chi(k) = \sum_i \frac{N_i S_i(k) A_i(k)}{kR_i^2} \exp(-2k^2\sigma_i^2) \sin(2kR_i + \phi_i(k)) \qquad (1)$$

In eq. 1, $\chi(k)$ is the fractional modulation in the absorption coefficient above the edge, N_i is the number of scatterers at a distance R_i, $S_i(k)$ is a scale factor unique to the absorber-scatterer pair, $A_i(k)$ is the effective backscattering amplitude, σ^2_i is the mean-square deviation in R_i, and ϕ_i is the phase-shift experienced by the photoelectron wave as it passes through the potentials of the absorbing and scattering atoms. The sum is taken over all scattering interactions.

Theoretical EXAFS amplitudes, $A_i(k)$ and phase functions, $\phi_i(k)$, were calculated using FEFF 6.01 (18,19). The experimental data were fit using single scattering parameters calculated for Zn-N and Zn-S with bond lengths of 2.05 Å and 2.35 Å, respectively. The scale factor, S=0.85 for O and S=1.02 for S, and the threshold energy, E_0=9.0 eV, were calibrated by fitting

EXAFS data for structurally characterized Zn model complexes (20). *R* and σ were varied while holding the coordination number fixed at reasonable integer values (21).

Optical Trapping experiments. Accurate protamine concentrations were obtained by aliquotting known volumes of samples into glass tubes, freezing on dry ice, and lyophilizing overnight. Replicate samples were dissolved in 6N hydrochloric acid and hydrolyzed at 105°C for 16h, and the amino acid content of each tube was determined by AAA Service Laboratory (Boring, OR). The protein content of each sample was calculated using the known amino acid composition derived from the protein sequences of hamster protamines 1 and 2. Due to high salt concentrations remaining after dialysis, accurate quantitation was not determined for these samples.

The preparation of the stained DNA bead sample was as follows. First, lambda phage DNA (Sigma) was dissolved in buffer (degassed 50% sucrose [w/v], 100mM sodium bicarbonate, pH 9, 30mM dithiothreitol), tagged with biotin, and attached to 1µm streptavidin-coated polystyrene spheres as described previously (22). YOYO-1 dye was added to a dye:DNA base pair ratio of 1:4. Experiments performed with salmine and various peptides have shown that this concentration of YOYO-1 does not

alter the kinetics of binding to DNA (22). The protamine samples were dissolved in the same buffer without YOYO-1 dye.

The apparatus used in the condensation and decondensation experiments is identical to that used previously to examine the condensation of individual DNA molecules by salmon protamine (22). Separate solutions containing protamines and DNA molecules attached to polystyrene beads were introduced into a dual port flow cell at a flow velocity of approximately 50μm/s where they flowed side by side, in a laminar fashion, with little mixing. Beads containing individual DNA molecules were trapped using an infrared laser optical trap (λ = 1.047μm). An argon ion laser (λ + 488nm) was used to excite the YOYO-1-stained DNA molecules, and their fluorescence was visualized using an image-intensified CCD camera.

Working at a depth of approximately 20μm below the coverslip (the flow cell depth was 40μm), the DNA molecule was pulled across the interface separating the two flowing buffer solutions, and the shortening of individual DNA molecules was monitored as the protamines bound to it and induced condensation. The condensed DNA was evident as a bright fluorescent spot at the end of the DNA molecule. The length of the stained λ phage DNA molecule (48.5kb) extended by flow was measured to be 19.2

+/- 0.82µm at a flow rate of 72µm/s in 50% sucrose. Under these conditions, the DNA was 95% extended (D. Stigter, personal communication).

Results and Discussion

EXAFS measurements were made on samples of protamines 1 and 2 isolated from Syrian Gold hamster sperm to determine whether the coordination of the zinc by protamine 2 in intact sperm cells was maintained during the isolation of the protamines. Protamines with bound zinc were isolated from epididymal hamster sperm using a modified protocol of Bellve and colleagues (12) developed for extracting protamines from mouse sperm chromatin. Although the use of calcium and magnesium as described in this procedure does not extract protamines from the sperm chromatin as efficiently as using denaturants or acid, the majority of zinc binding to sperm protamines appears to be preserved (11). These samples were first analyzed by PIXE to verify zinc was still present prior to EXAFS analyses (data not shown).

The amplitude and shape of the main peak in the Fourier transform (Figure 1) of the EXAFS data obtained for the extracted P2-zinc complex is nearly identical to that found in the MTAB-treated mature sperm cells and spermatid samples (Chapter 2). Fits to the EXAFS data also show that the

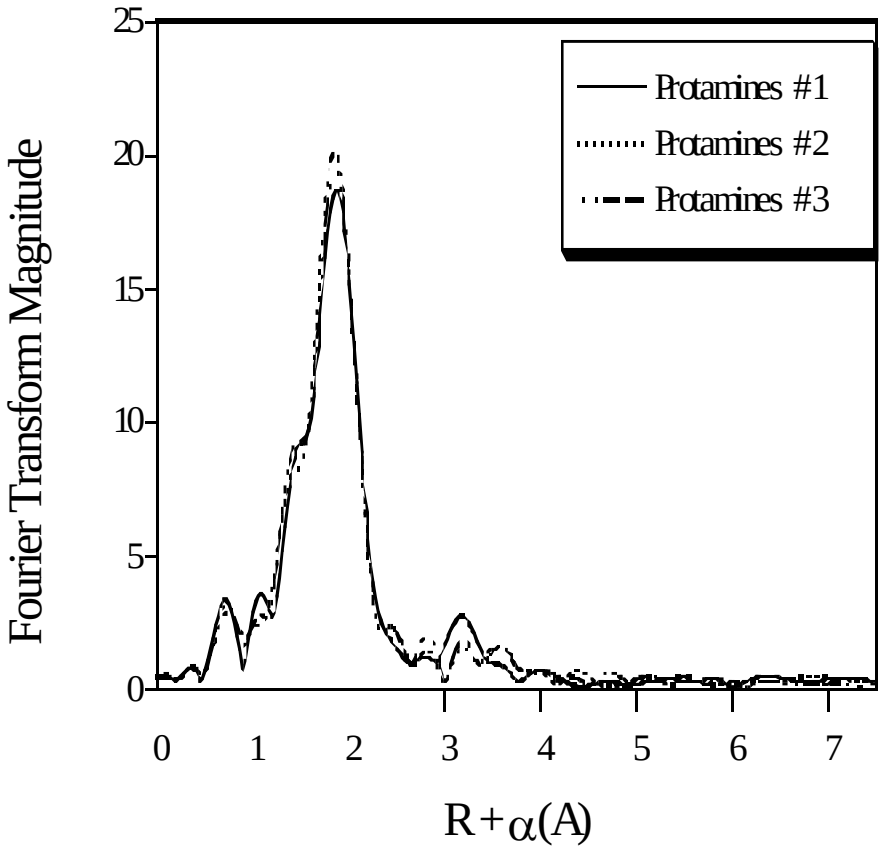

Figure 1. Fourier transformed EXAFS data for protamines 1 and 2 isolated from hamster sperm.

zinc environment is best modeled as 3S + 1(N/O) with bond distances similar to those observed in the other sperm samples (Table 2) and 4-coordinate zinc model complexes (23). Despite the similarity in the fits to the EXAFS data, the XANES spectrum (Figure 2) for the isolated protamines 1 and 2 is very different from those measured for the spermatids and the MTAB-treated mature sperm cells as it lacks the feature at ~9669 eV. Since the XANES region of the spectrum is sensitive to ligand and geometry changes, the fact that the purified protamine XANES spectra are quite different from the other sperm samples suggests that, although the zinc ligands in protamines 1 and 2 are similar to those found for the intact spermatid cells, the zinc environment in purified protamines 1 and 2 is distinct from the average zinc environment in intact cells. While it is possible that the difference observed between the intact cells and the purified protamines 1 and 2 may result in part from differences in sample preparation (i.e. lyophilized vs. solution), it is plausible that the conformation of the zinc binding domain of P2 changes when P2 is bound to DNA**.** This is supported both by the lack of structure P2 adopts when in solution as well as our observation that the zinc dissociates from the protein during prolonged dialysis, a characteristic indicative of the weak binding of zinc to protamine 2 when the protein is not bound to DNA (unpublished observations). Thus,

Samples	**CN**	**R_{ab} (Å)**	**^{2}•10^{3} (Å^{2})**	**CN**	**R_{ab} (Å)**	**^{2}•10^{3} (Å^{2})**	**F'**
Protamines 1 & 2	4S	2.31	5.8				0.017
	3S	**2.31**	**4.0**	**1N**	**2.06**	**5.8**	**0.009**
	2S	2.32	1.6	2N	2.07	4.7	0.017

Table 2. Representative EXAFS fitting results for protamines isolated from hamster sperm. Best-fit data denoted in bold font.

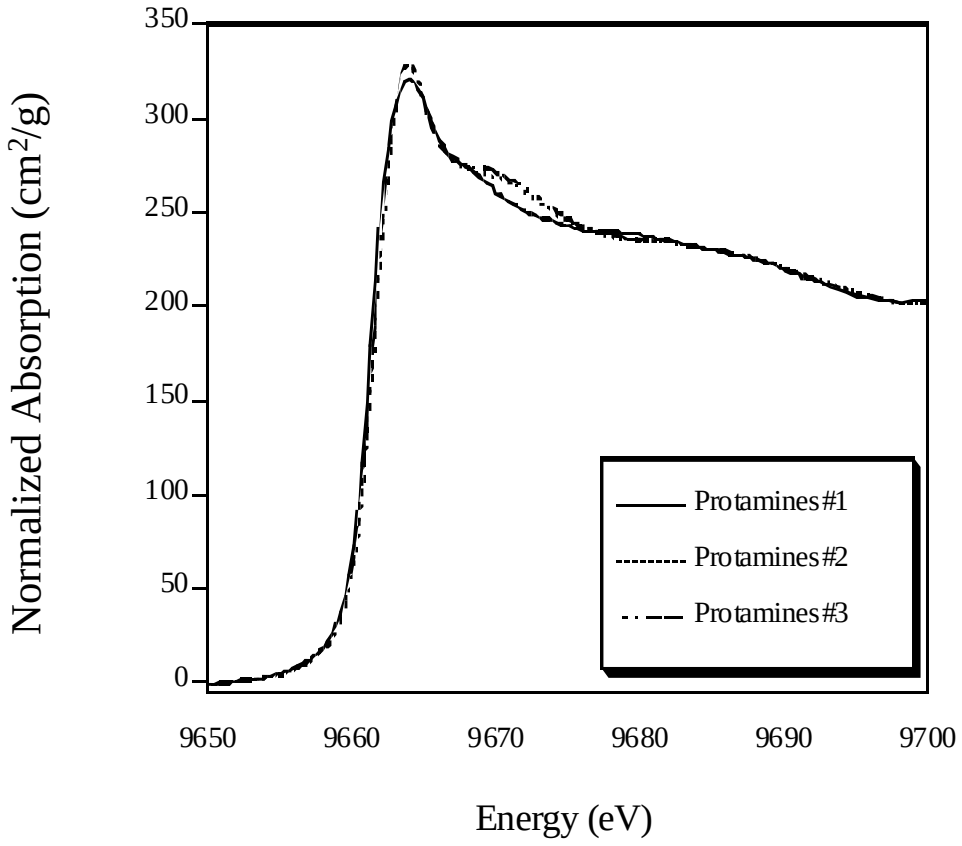

Figure 2. XANES spectra for protamines 1 and 2 isolated from hamster sperm.

we proceeded with our functional studies based on the assumption that, since the zinc binding in the isolated protamines (3S + 1 N/O) represented the early zinc binding to protamine 2 in spermatids, the protamine 2-zinc complex would form the mature structure (1S + 3 N/O) upon DNA binding and intra- and inter-protamine disulfide bond formation.

To gain insight to the functionality of the P2-zinc complex, we performed single DNA molecule experiments to analyze the binding of the protamines with zinc to DNA *in vitro*. In these experiments, an optical trap formed by a focused infrared laser is used to manipulate polystyrene beads with single DNA molecules attached. The experiment is conducted in a dual-port flow cell specifically designed to promote movement of individual DNA molecules between flow streams, with and without protamine. The images of DNA condensation (with protamine) and decondensation (without protamine) are analyzed by real time video. The analyses of DNA condensation induced by proteins binding to single DNA molecules and decondensation by the dissociation of proteins allow quantitation of on- and off-rates when the concentration of protein is known.

We initially measured DNA condensation induced by extracted nuclear proteins, protamines and transition proteins, in buffer with and without zinc, and observed that zinc facilitated DNA condensation by

isolated P2 3-fold (24). Next, we substituted the isolated protamines 1 and 2 with native zinc bound in a zinc-free buffer in an identical experiment and observed a tremendous enhancement of the rate of DNA condensation compared with extracted P2 with and without zinc. Unfortunately, due to the excessive amount of calcium and magnesium required for extracting the protamines from the sperm chromatin, we were unable to quantitate the protein accurately. We are currently optimizing a desalting protocol that will eliminate the salt interfering with protein quantitation, yet retain zinc binding to the protamines. Regardless of the inability to quantitate on- and off-rates, we now have qualitative evidence that native zinc binding to protamine 2 is required to obtain biologically relevant results, as substantiated by the comparison of rates of DNA condensation by the protamine 2-zinc samples. To ensure our results were due to the protamines with zinc and not from any constituent of the buffer, we repeated the experiments with buffer only. No DNA condensation was observed in the presence of buffer alone. Collectively, these exciting *in vitro* results suggest one role of zinc in mammalian sperm chromatin could be to modulate the rate of P2 binding to DNA, thereby directly impacting the rate of DNA condensation.

The enhancement of DNA condensation by the inclusion of zinc with

protamine 2 indicates the formation of a zinc domain in P2 that facilitates DNA binding and subsequent condensation. While zinc typically functions in DNA-binding proteins to create a motif (such as a zinc finger) that interacts directly with DNA, several independent studies do not support that role for zinc in P2. First, lower affinity constants obtained for zinc binding by partial sequences of human P2 using circular dichroism titrations dispute the formation of a typical zinc finger in P2 (10). Second, the sequence of P2 is not homologous to other zinc fingers that have been characterized. Finally, the mass amounts of DNA and protamines present in native sperm chromatin support an extended conformation of the DNA-binding region of protamines, a configuration that must be consistent with the incorporation of zinc. Based on these and other results, we propose that zinc binds to P2 to create a dimerization site, either by forming P2 homodimers prior to DNA binding or by facilitating the dimerization of the P2 molecules when bound to DNA. This arrangement functions to both organize the protamines in the species-specific stoichiometry and increase the affinity of protamine 2 for DNA by creating a protamine 2 dimer with twice the number of electrostatic interactions (arginine side chains bound to DNA phosphates) relative to its monomer counterpart.

Conclusion

Hamster protamines were isolated using conditions that preserved zinc binding, and EXAFS data were obtained for the zinc-binding site in protamine 2 from the isolated protein. The zinc ligands are 3S + 1 N/O, the same as in spermatids, but with different geometry, possibly due to the absence of DNA. Functional single DNA molecule binding studies using optical trapping and real time analysis demonstrate that the rate of DNA condensation is greatly enhanced by protamines 1 and 2 with native zinc bound compared with extracted protamine 2 alone with and without zinc.

Acknowledgements

We gratefully acknowledge Dr. Katrina Peariso for her X-ray Absorption Spectroscopy data collection and interpretation, Dr. Laurence Brewer for conducting the optical trapping experiments, and Drs. Graham Bench and Patrick Grant for collecting and analyzing the Proton-Induced X-Ray Emission data.

We would also like to thank Michele Corzett for her helpful suggestions and discussions to optimize the sample preparations.

References

1. Bjorndahl L, Kvist U. Loss of an intrinsic capacity for human sperm chromatin decondensation. Acta Physiol Scand 1985; 124:189-194.

2. Kvist U, Bjorndahl L. Zinc preserves an inherent capacity of chromatin decondensation of human spermatozoa. Acta Physiol Scand 1985; 124:195-200.

3. Kvist U, Bjorndahl L, Kjellberg S. Sperm nuclear zinc, chromatin stability, and male fertility. Scanning Microsc 1987; 1:1241-1247.

4. Bjorndahl L, Kjellberg S, Roomans GM, Kvist U. The human sperm nucleus takes up zinc at ejaculation. Int J Androl 1986; 9:77-80.

5. Kvist U, Bjorndahl L. Zinc in sperm chromatin and chromatin stability in fertile men and men in barren unions. Scand J Urol Nephrol 1988; 22:1-6.

6. Ozturk A, Baltaci AK, Bediz CS, Mogulkoc R, Gungor S. Effects of zinc and melatonin deficiency on testicular tissue of rats. Biol Trace Elem Res 2003; 96:255-262.

7. Turgut G, Abban G, Turgut S, Take G. Effect of overdose zinc on mouse testis and its relation with sperm count and motility. Biol Trace Elem Res 2003; 96:271-279.

8. Gatewood JM, Schroth GP, Schmid CW, Bradbury EM. Zinc-induced secondary structure transitions in human sperm chromatin. J Biol Chem 1990; 265:20667-20672.

9. Bianchi F, Rousseaux-Prevost R, Sautiere P, Rousseaux J. P2

protamines from human sperm are zinc-finger proteins with one CYS2/HIS2 motif. Biochem Biophys Res Commun 1992; 182:540-547.

10. Bal W, Dyba M, Szewczuk Z, Jezowska-Bojczuk M, Lukszo J, Ramakrishna G, Kasprzak S. Differential zinc and DNA binding by partial peptides of human protamine HP2. Mol Cell Biochem 2001; 222:97-106.

11. Bench GS, Corzett MH, Kramer CE, Grant PG, Balhorn R. Zinc is sufficiently abundant within mammalian sperm nuclei to bind stoichiometrically with protamine 2. Mol Reprod Dev 2000; 56:512-519.

12. Bellve AR, Chandrika R, Martinova YS, Barth AH. The perinuclear matrix as a structural element of the mouse sperm nucleus. Biol Reprod 1992; 47:451-465.

13. Balhorn R, Gledhill BL, Wyrobek AJ. Mouse sperm chromatin proteins: quantitative isolation and partial characterization. Biochemistry 1977; 16:4074-4080.

14. Corzett M, Kramer C, Blacher R, Mazrimas J, Balhorn R. Analysis of hamster protamines: primary sequence and species distribution. Mol Reprod Dev 1999; 54:273-282.

15. Bench GS, Balhorn R, Friz AM. Nuclear microscopy of sperm cell elemental structure. Nucl Instr Methods 1995; B99:553-556.

16. Peariso K, Goulding CW, Huang S, Matthews RG, Penner-Hahn JE. Characterization of the zinc binding site in methionine synthase enzymes of Escherichia coli: The role of zinc in the methylation of homocysteine. J Am Chem Soc 1998; 120:8410-8416.

17. Teo BK. EXAFS: Basic Principles and Data Analysis. New York: Springer-Verlag; 1986.

18. Rehr JJ, deLeon JM, Zabinsky SI, Albers RC. Theoretical x-ray absorption fine-structure standards. J Am Chem Soc 1991; 113:5135-5140.

19. Rehr JJ, Albers RC, Zabinsky SI. High-order multiple-scattering calculations of x-ray-absorption fine structure. Phys Rev Lett 1992; 69:3397-3400.

20. Clark-Baldwin K, Tierney DL, Govindaswamy N, Gruff ES, Kim C, Berg J, Koch SA, Penner-Hahn JE. The limitations of X-ray absorption spectroscopy for determining the structure of zinc sites in proteins. When is a tetrathiolate not a tetrathiolate? J Am Chem Soc 1998; 120:8401-8409.

21. Rulisek L, Vondrasek J. Coordination geometries of selected

transition metal ions (Co^{2+}, Ni^{2+}, Cu^{2+}, Zn^{2+}, Cd^{2+}, and Hg^{2+}) in metalloproteins. J Inorg Biochem 1998; 71:115-127.

22. Brewer LR, Corzett MH, Balhorn R. Protamine-induced condensation and decondensation of the same DNA molecule. Science 1999; 286:120-123.

23. Gruff ES, Koch SA. A trigonal planar $[Zn(SR)_3]^{1-}$ complex. A possible new coordination mode for zinc-cysteine centers. J Am Chem Soc 1989; 111:8762-8763.

24. Brewer L, Corzett M, Balhorn R. Condensation of DNA by spermatid basic nuclear proteins. J Biol Chem 2002; 277:38895-38900.

CHAPTER FIVE

NMR Study of Protamine/DNA Complexes

Abstract

Protamines are small, basic proteins that package DNA in the nuclei of mammalian sperm. Scant details of the molecular structure of nucleoprotamine are known as the structural analyses typically applied to nucleosomes and other protein/DNA complexes have been hindered by the insolubility of the protamine/DNA complex. To circumvent the obstacle of insolubility, we designed DNA hairpins that would allow bull protamine 1 to bind to the duplex stem of the DNA hairpin while retaining the negative charge of the loop region. We analyzed the structure of these soluble complexes using multidimensional Nuclear Magnetic Resonance (NMR) spectroscopy to identify the molecular interactions between the DNA-binding domain of protamine 1 and DNA. The protocol developed to create and optimize the preparation of these soluble complexes and the preliminary structural data obtained for the synthetic protamine 1 peptides bound to hairpin oligos provide information for the preparation of similar complexes using protamine 2 and an oligo with a duplex region the optimal length for binding protamine 2. The protamine 2-DNA complexes will allow analysis

of the zinc-protamine 2 complex and the impact zinc has on the structure of protamine 2 when it is bound to DNA.

Introduction

When histones are replaced by protamines during mammalian spermiogenesis, the nucleosomal organization present in spermatid chromatin is eliminated and the DNA is coiled and condensed into toroids subunits, elliptical structures 50-100nm in diameter (1-6). *In vivo*, the highly compacted sperm chromatin equips the sperm for motility and inactivates the sperm genome until the DNA is decondensed and reactivated in the egg post-fertilization. This reactivation effectively reprograms the sperm genome to express the genes required for cell replication and early development (1,7).

Torus formation is induced by the binding of the regions of consecutive basic arginine residues of protamine to the acidic phosphodiester backbone of both strands of DNA. The electrostatic interactions that stabilize the binding of protamine to DNA, in addition to the extensive crosslinking of neighboring protamines by disulfide bridges, produce a neutral, insoluble complex that limits comprehensive structural studies. The first proposed model of the structure of nucleoprotamine was based on results obtained from X-ray fiber diffraction experiments by

Wilkins and his collaborators, initiated shortly after Watson and Crick elucidated the double helical structure of DNA in 1953. The main features of this model have been both substantiated and challenged in the past 50 years (8,9):

(1) the sugar-phosphate backbone of DNA is in the B-form conformation;

(2) the positively charged guanidinium groups of the arginine residues bind to the negatively charged phosphate groups of DNA;

(3) protamine molecules bind to DNA in an extended conformation;

(4) protamine binds to the minor groove of the DNA double helix.

The conformation of the DNA backbone in the B- form has remained undisputed. Structural data have been obtained for DNA complexes using arginine-rich peptides and salmine (salmon protamine), molecules similar in size to the central polyarginine region in mammalian protamines. Polarized infrared studies of herring and trout nucleoprotamine indicated that the B-form configuration of DNA persists down to 76% relative humidity (10). X-ray diffraction studies confirmed this observation and also revealed that, despite variations in size and amino acid composition of the protamines, all of the complexes analyzed maintained DNA in the B-form, presumably due to stabilization induced by the interaction of sequential arginine residues in

the protamine sequence with DNA since arginine alone did not produce this effect (11). Additional X-ray diffraction studies of DNA complexes with arginine peptides showed that the DNA remained in B-form with 10 base pairs per turn at all relative humidities (12). Raman studies of polyarginine bound to DNA also demonstrated that the DNA was in B-form, but the stacking of the bases was altered in the DNA-salmine complex, creating a modified B-form (13). One explanation for the Raman results may relate to the extensive displacement of water that occurs when protamine binds to DNA, an effect that does not occur when shorter basic peptides bind to DNA. To further extrapolate structural information for DNA-mammalian protamine complexes from analogs is unreliable since neither salmine nor the synthetic arginine peptides contain hydrophobic residues and cysteines. These amino acids change the structure of nucleoprotamine via side chains that interact with DNA and other protamines. Also, other structural differences may be caused by the effect of regularly spaced prolines in fish protamines, which are likely to alter the conformation of the protein backbone, thereby influencing interactions of the side chains with DNA.

The extended conformation model, validated by experimental data and modeling predictions, describes the neutralization of the charge of the phosphodiester chains by the binding of the guanidinium groups of the

arginine-rich regions of the protamines to the phosphates of the DNA backbone in an extended conformation (14). The only other model proposed for a protamine-nucleic acid complex is one in which the protamine adopts an α-helix conformation for protamine when bound to tRNA based on data from single crystal X-ray diffraction (15). However, RNA cannot adopt a conformation equivalent to B-form DNA because the 2'-OH group of the ribose is sterically hindered, forcing double-stranded RNA to adopt an A-DNA-like structure. Since the configuration of the nucleic acid backbone determines the dimension and shape of the minor and major grooves, which are critical in protein binding, the interactions between protamine and the DNA would be expected to be different from those observed in the protamine-tRNA complex. Peptides containing sequential arginine residues have been observed to form alpha helices in solution, and this combined with the structural differences in the RNA groove may explain the α-helices observed in the crystal structure of the protamine-tRNA complex. Also, the fast rate of exchange of deuterium does not support the presence of secondary structural elements in protamine when bound to DNA (10). Moreover, each protamine molecule would be expected to bind to one turn of DNA if it adopted an extended conformation. Calculations based on DNA and protamine masses obtained from mammalian sperm are

consistent with the binding of protamines in an extended conformation (14,16,17).

The major area of debate has been whether protamine binds to the minor and/or the major groove of the DNA helix. At first, studies using chemical reactivity appeared to support the original proposal of minor groove binding. Actinomycin D, a minor groove intercalator, binds readily to DNA in somatic nuclei; however, as spermatids differentiate and the histones are replaced by protamines, the binding of actinomycin diminishes (18,19). While this reduction in binding was originally interpreted to be caused by the binding of the protamine in the minor groove of DNA, further studies revealed that actinomycin D intercalation is blocked by the interlocking of the two phosphodiester strands by the arginine side-chains of protamine. This interlocking prevents the unwinding of the DNA helix, the sliding of the strands in opposite directions relative to each other, and the unstacking of the bases – steps essential for the intercalation of actinomycin D (20,21).

Compelling evidence for the binding of protamine to the major groove was provided by solid-state and solution NMR studies of native bull chromatin and soluble protamine peptide-oligonucleotide complexes in which the methyl group on thymine (located in the major groove) was

observed to be perturbed (1,22). Also, analysis of the binding of the synthetic DNA binding domain of bull protamine to double-stranded poly(dABrdU) by optical detected magnetic resonance suggested that the predominant binding site for protamine is the major groove (23).

The most important insight gained from the nucleoprotamine experiments in the past 50 years has been the recognition that further refinements are needed to complete the structural studies of mammalian sperm chromatin and understand the function of the protamines require the analyses of complexes that contain mammalian protamines, not analogs or modified sequences, as all components contribute to the overall structure of nucleoprotamine. To accomplish this, we devised a novel strategy to obtain soluble protamine-DNA complexes by designing a hairpin DNA oligonucleotide containing a duplex region the appropriate length to bind one protamine molecule. This innovative approach was used to obtain structural data for a synthetic complex of bull P1 peptide bound to an oligonucleotide (1). Results from this study demonstrated directional binding of protamine onto DNA, increased stability of the DNA bases adjacent to the binding site, and the retention of B-form DNA conformation upon protamine binding. Here we present the results of our most recent NMR analyses of synthetic protamine 1 peptides and isolated bull protamine

1 bound to hairpin oligos. Using protamine 1 as our prototype, our ultimate goal is to design soluble complexes of protamine 2 and DNA for structural analyses to determine the role the protamine 2-zinc complex has in mammalian fertility.

Materials and Methods

Preparation of DNA hairpins. The oligodeoxyribonucleotides CCATCGCTACCTTTTTGGTAGCGATGG (designated as C11hp) and GACATGTCTTTTTGACATGTC (designated as G8hp) were synthesized on an Applied Biosystems Model 394 DNA/RNA synthesizer, purified by reverse phase HPLC, and desalted on a Sephadex G25 size exclusion column in series with a Dowex cation exchange column.

Synthesis of protamine peptides. The R_6FGR_6 and R_6GGR_6 peptides were synthesized by SynPep (Dublin, CA) and were quantitated using quantitative amino acid analyses of known aliquots of the peptides (Protein Structure Laboratory, U.C. Davis).

Isolation and purification of bull protamine. Pooled bull semen was purchased from the American Breeders Service (DeFortes, WI) and stored at –20°C until use. The basic nuclear proteins were isolated as previously described (24). The basic nuclear proteins were solubilized in 3M GuCl, 50mM Tris-HCl pH 8.0, and 10mM DTT, and separated from the other basic

nuclear proteins by HPLC using a reverse phase C18 column (Hamilton) and the following multi-step acetonitrile gradient: linear increase of Buffer B (60% acetonitrile, 0.1% trifluoroacetic acid) from 20% to 38% over 20 minutes; isocratic for 20 minutes; and an increase from 38% to 100% Buffer B over 5 minutes. Buffer A = aqueous 0.1% trifluoroacetic acid. Protein elution was monitored at 214 nm. Samples were frozen on dry ice, lyophilized overnight, and analyzed by electrophoresis in acid-urea gels (24) to verify purity.

Methylation of Protamine. The cysteines of purified protamine 1 were methylated with ^{13}C-iodomethane (Sigma) as previously described (25) and purified by HPLC as described above. Accurate protamine concentrations were obtained by aliquotting known volumes of samples into glass tubes, freezing on dry ice, and lyophilizing overnight. Replicate samples were dissolved in 6N hydrochloric acid and hydrolyzed at 105°C for 16h, and the amino acid content of each tube was determined by AAA Service Laboratory (Boring, OR). The protein content of each sample was determined using known sequence of bull protamine 1.

Preparation of complexes. DNA hairpins were dissolved in 10 mM Na_2PO_4, pH 7.0 buffer. Small aliquots of P1 peptide dissolved in water were added to a 500 mL solution of ~0.8 mM DNA hairpin until an equimolar

amount was obtained. Methylated bull protamine 1 (dissolved in water) was complexed with the hairpin oligo C11hp (in water).

NMR Experiments. NMR experiments were performed on a Varian INOVA 600 MHz spectrometer at 37^{o}C and 10^{o}C. A combination of through-space nuclear and rotational Overhauser effect (50 and 300 ms mixing time NOESY and 100 ms spin lock time ROESY) and through-bond correlated (phase sensitive COSY and 40, 60 and 80 ms spin lock time TOCSY) experiments were recorded in the States-TPPI mode on approximately 0.8 mM complex (or control hairpin, P1 or peptide) dissolved in 0.5 ml of D_2O buffer (10 mM Na_2PO_4, pH 7.0). One-dimensional and NOESY (150 ms mixing time) spectra of these samples in 90% H_2O/10% D_2O buffer were collected using a jump-return pulse sequence for solvent suppression. Sweep widths of 6000 Hz and 12000 Hz were used for the sample dissolved in D_2O buffer and H_2O buffer, respectively, with 1024 complex data points and 300 t_1 increments, each having 64 transients and a recycle delay of 1.8 s. The indirect proton-phosphorus correlation spectra were acquired in D_2O and referenced relative to external 10% trimethyl phosphate. Sweep widths of 3600.8 Hz and 1457.7 Hz were used for the ^{1}H and ^{31}P dimensions, respectively, with 1024 complex data points and 128 t_1 increments, each having 128 transients and a recycle delay of 1.3 s. Natural

abundance ^{13}C-carbon-proton heteronuclear multiple quantum coherence (HMQC) spectra were recorded in D_2O buffer with 150 ppm in the ^{13}C dimension. Data sets were processed using the software package VNMR (Varian Inc, Palo Alto, CA), transferred to a SGI workstation, and converted directly into FELIX (MSI, San Diego, CA) matrixes for analysis.

Results and Discussion

Very little is known about the structure and organization of protamines in the sperm chromatin and the interactions that occur between protamines and DNA. Solution studies of the isolated protamines are inadequate because protamines extracted from sperm chromatin lack structure, forming random coils in solution (26,27). It has also been difficult to obtain experimental data from the insoluble, aggregated complexes formed when the highly basic protamines bind and neutralizes the phosphate backbone of DNA. To overcome the inherent insolubility of nucleoprotamine, DNA hairpins were designed to specifically bind protamine peptides (14-16 amino acids) to the duplex stem of a DNA hairpin while retaining the negative charge of the loop region. This design exploits the preference of protamine to bind double-stranded DNA.

The first of these soluble complexes enabled us to analyze the molecular interactions between the C-terminal end of the DNA-binding domain of bull

protamine ($R_3FGR_3SR_2VAR_2$) and an 8bp duplex oligonucleotide (G8hp) by Nuclear Magnetic Resonance (Figure 1)(1). A serine residue (S34) was substituted for one arginine (R34) in the central arginine-rich region of the protamine 1 peptide and two cysteines (C38 and C39) were replaced by alanines to simplify NMR assignments by interrupting the series of six arginines and to prevent cysteine disulfide crosslinking and subsequent aggregation (Figure 1). Binding of the protamine 1 peptide to DNA was specific to the 5bp terminal end of the DNA duplex and the peptide did not interact with the thymine loop region (Figure 2). This result is consistent with previous calculations of DNA and protamine masses from bull sperm indicating that the length of DNA (number of base pairs) covered by protamine corresponds to approximately half the number of arginine residues present in the DNA binding region of the protamine molecule (28). Interestingly, in this particular complex, the specific binding appears to be directed by the intercalation of the phenylalanine between the d(G1•C21) and d(A2•T20) base pairs at the end of the duplex. We also discovered from this homogeneous sample that the chemical shift differences of the thymine methyl groups in the duplex region of the oligonucleotide corresponded to the binding of the peptide in the major groove of the DNA. Finally, the NMR data revealed the conformationof the peptide backbone is extended,

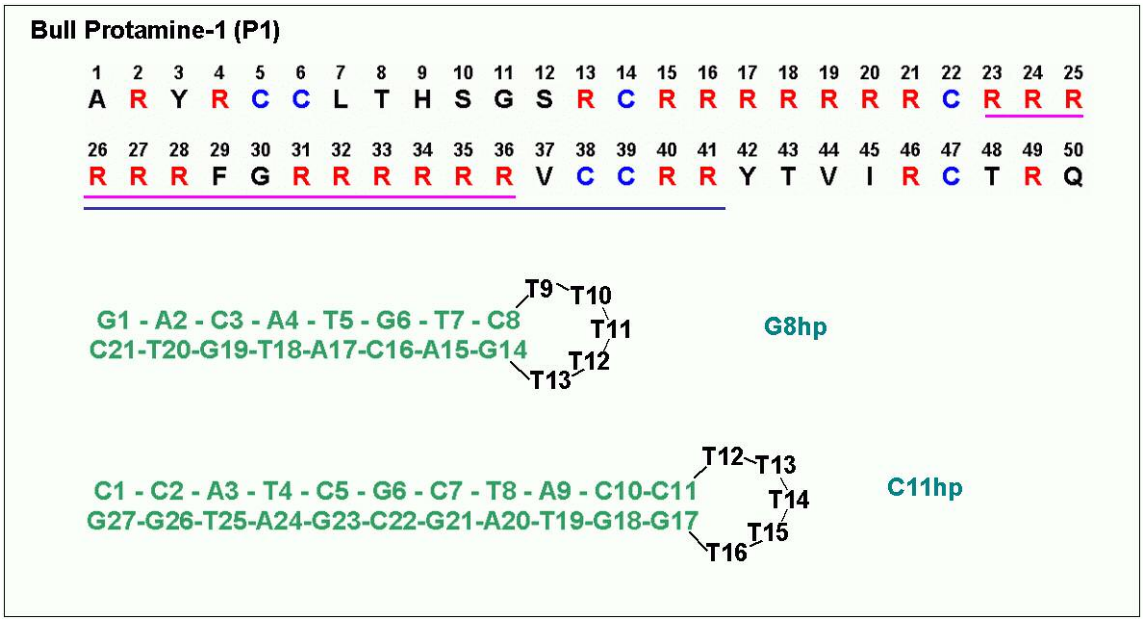

Figure 1. The bull protamine 1 (P1) sequence is shown at the top. Arginines (R) are red and cysteines (C) are blue. The R_6FGR_6 peptide sequence is underlined in pink and the sequence $R_3FGR_3SR_2VA_2R_2$ is underlined in dark blue. S34 was substituted for R34 and A38 and A39 were substituted for C38 and C39. The DNA sequences for the hairpin oligonucleotides, G8hp and C11hp, are also shown.

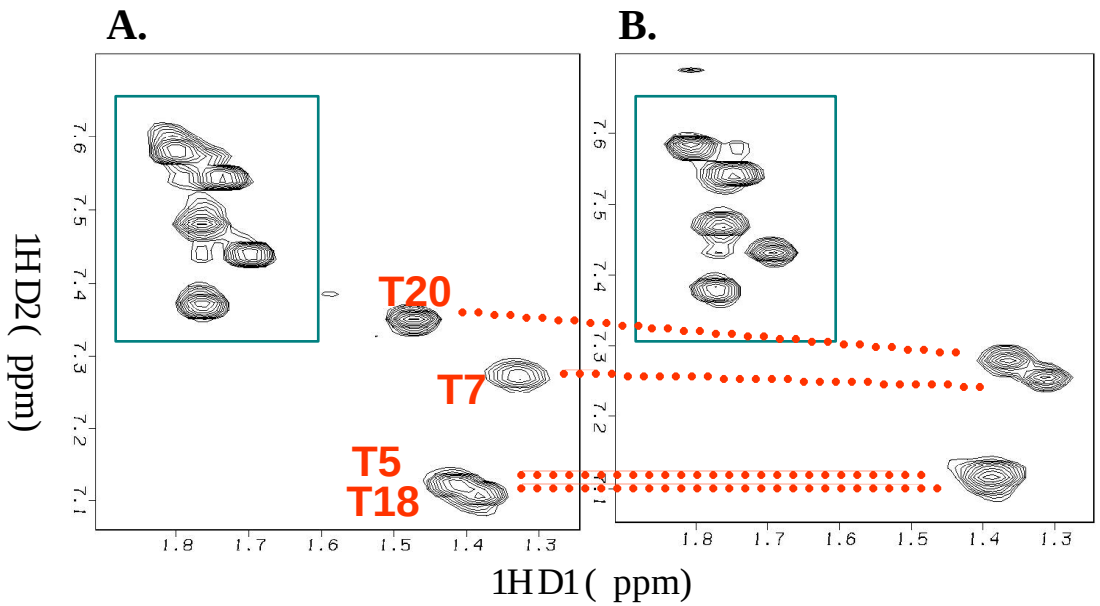

Figure 2. Expanded region of the 300 ms NOESY spectrum of the G8hp+$R_3FGR_3SR_2VA_2R_2$ complex showing the thymine methyl region. A comparison of the chemical shifts of (A) G8hp and (B) G8hp+$R_3FGR_3SR_2VA_2R_2$ complex shows the thymines in the hairpin loop (enclosed in the squares) do not shift, while T5 and T20 in the duplex stem in the complex shift relative to their positions in the control (G8hp).

not helical as previously proposed (1). Subsequent NMR studies of protamine peptides and hairpin DNA complexes were not as informative. Data from the C11HP+R_6GGR_6, and C11HP+R_6FGR_6 samples indicate that the duplex stem is too long to obtain a homogeneous complex required for NMR analysis (Figures 3, 4 and 5). Since protamine binding to DNA is non-specific, multiple forms of complexes involving peptide bound to the duplex or to the loop region can rapidly exchange during the NMR experiments. To resolve the problem of heterogeneity, we plan to repeat these experiments using complexes prepared by binding the peptides to the smaller oligonucleotide, G8HP, to promote position-specific binding and thus obtain a homogeneous sample suitable for NMR analysis.

The next set of experiments focused on conducting structural studies of complexes using the full-length protamine 1 molecule isolated from bull sperm and C11hp (Figure 1). The structural data obtained from these complexes will be more biologically relevant than complexes prepared with subsets of the protamine sequences. Our first attempt to complex purified protamine 1 with C11hp in equal molar amounts resulted in the preparation of a sample with “sticky”, white precipitate that adhered to the glass tube. Heating, reducing the interprotamine disulfide bonds by reductants, and prolonging the incubations of this sample did not induce protein exchange

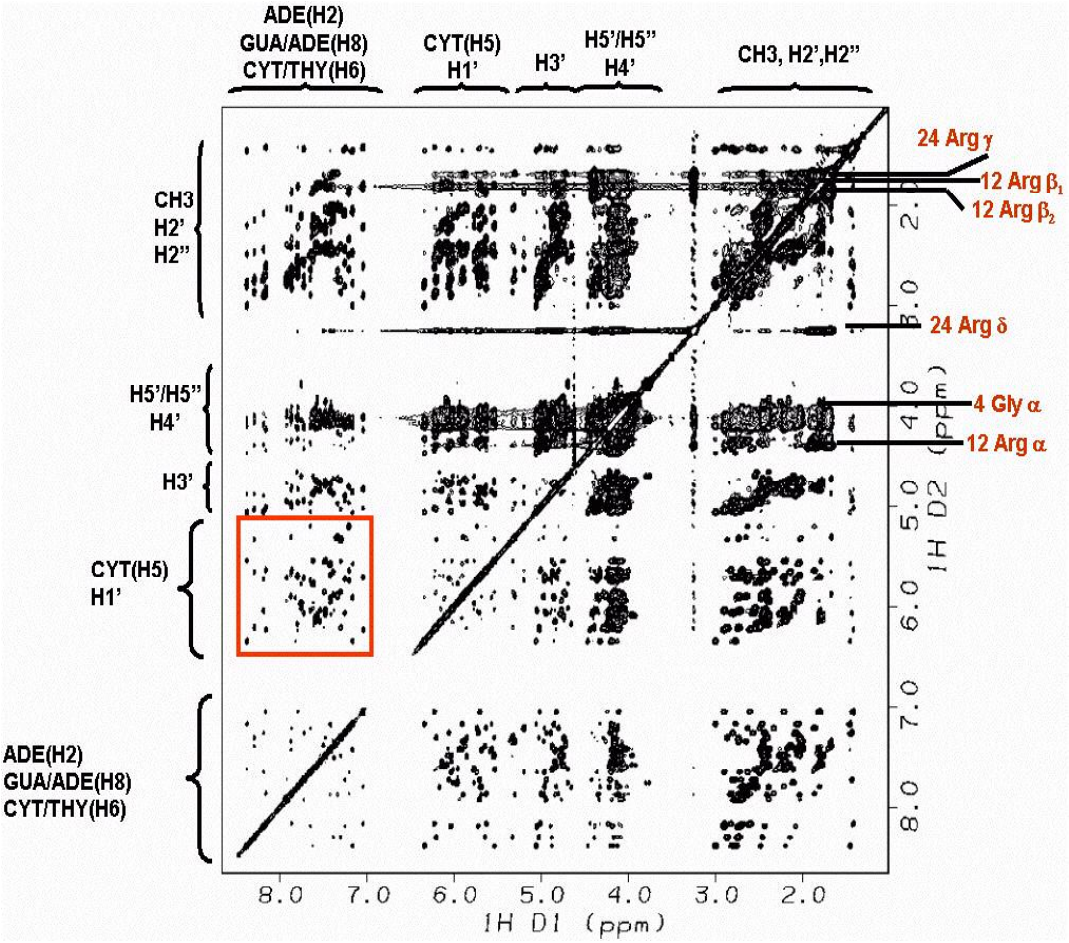

Figure 3. 300 ms mixing time NOESY (nuclear Overhauser effect spectroscopy) at 37°C of the R_6GGR_6/C11hp complex showing showing that the R_6GGR_6 peptide (arginine and glycine protons denoted in red font) is bound to the C11hp DNA hairpin. The fingerprint region for the C11hp is in the red square and expanded in Figure 4.

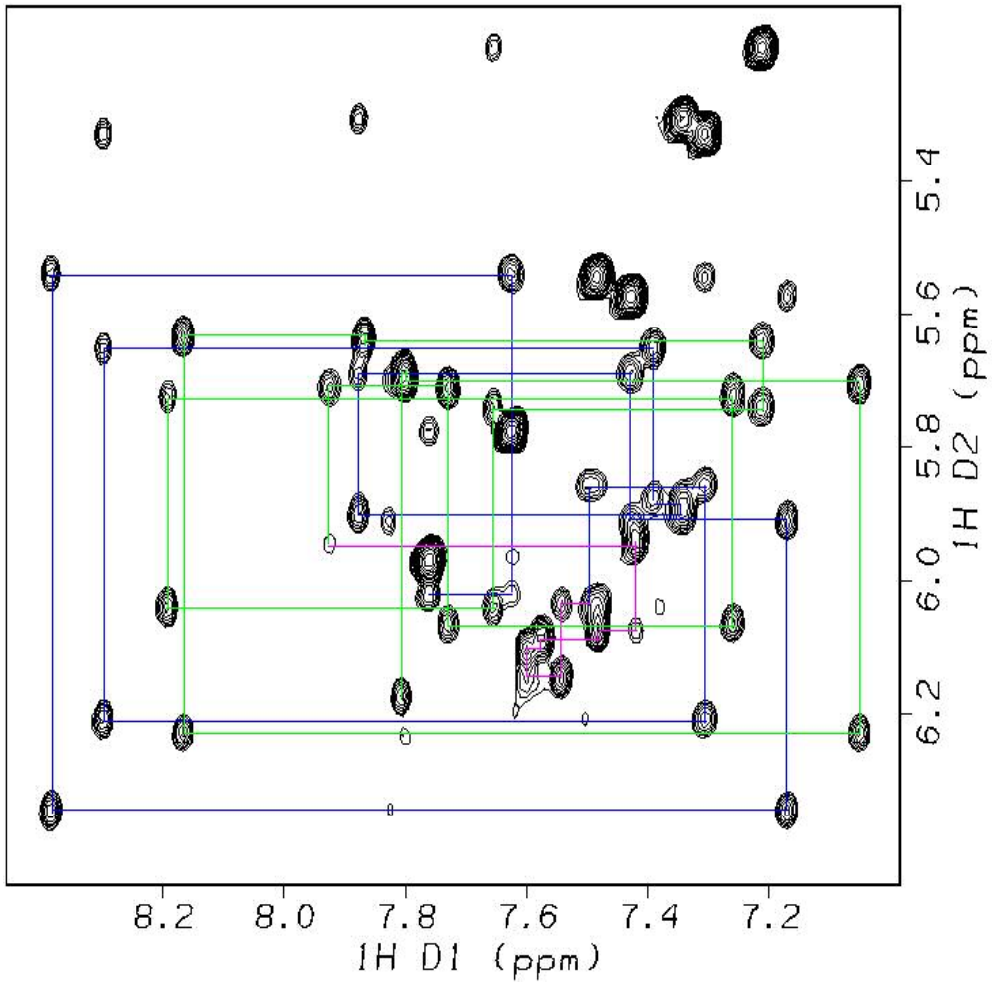

Figure 4. The fingerprint region of R$_6$GGR$_6$/C11hp complex is expanded to show the base (H6/H8) to sugar H1 Õwalk designated by the blue lines for residues C1-C11, purple for T12-T16 and green for G17-G27. The cytosine H5/H6 crosspeaks are labeled by *.

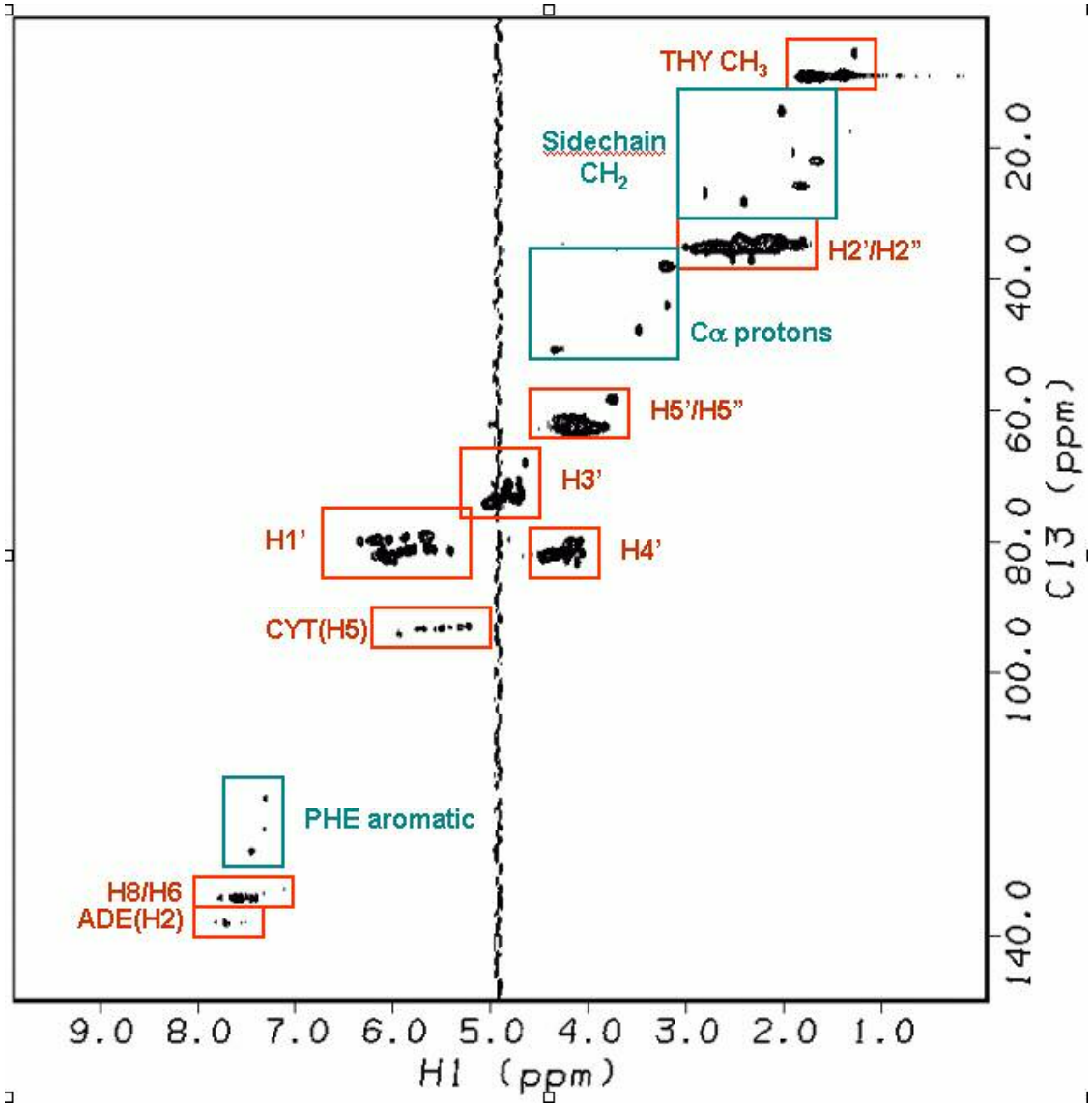

Figure 5. Natural abundance ^{1}H-^{13}C-heteronuclear multiple quantum correlation (HMQC) spectrum at 10 °C of the R_6FGR_6/C11hp complex. Red boxes indicate crosspeaks from C11hp and green boxes indicate those from the protamine peptide R_6FGR_6.

from complexes containing more than one protamine bound per DNA molecule. NMR analysis revealed that only free DNA (in hairpin conformation) remained in solution, verifying that the precipitate contained the protamine-DNA complex. Since the amounts of DNA and protamine were equivalent in this sample and only uncomplexed DNA was soluble, the precipitate obviously contained complexes in which multiple protamine molecules were bound to one oligonucleotide. Collectively, these experiments indicated that the precipitation was caused by intermolecular crosslinking of the protamines during the long incubations required to prepare the samples (the protein was slowly titrated into the DNA sample) and instabilities in pH, which were often suboptimal for the reactivity of the reducing agent (pH 8).

To eliminate the formation of disulfide bonds, we methylated the seven cysteine residues in protamine 1 using methyl iodide. This methylation, in addition to decreasing the DNA:protamine ratio from 1:1 to 2:1 and reducing the concentration of the sample 3-fold, did improve the solubility of the complex somewhat. This sample did not precipitate instantaneously nor did it form the aggregates that previously adhered to the surface to the tube. Instead, an opaque, almost colloidal-type, suspension was obtained. NMR analysis revealed broad peaks, consistent with the

presence of very large structures or aggregates, suggesting that factors other than intermolecular crosslinking contribute to the formation of these aggregates. One plausible explanation suggested by these recent experiments is that the neutralized regions of the duplex DNA with protamine bound interact with each other through hydrophobic van der Waal forces, as the sperm chromatin does when it forms toroids *in vivo*. We envision the complexes might arrange into micelles - analogous to the formation of liposomes by phospholipids. Another possibility we cannot rule out is that the presence of the C-terminal end of the protamine 1, which contains arginines, interacts with the thymine loop thereby neutralizing the charge on the complex and causing the precipitation. A solution for the latter explanation is to selectively methylate the cysteines prior to protamine isolation from sperm chromatin, such that the intramolecular disulfide bridges flanking the DNA binding domain remain intact while disrupting the intermolecular bonds that crosslink the complexes. This would result in the isolation of more compact protamine molecules having amino- and carboxy-terminal sequences sequestered through intramolecular disulfides formed between cysteines in the terminal peptide regions. This can be achieved using folded protamines with the terminal regions locked in place. Such proteins have been prepared in a previous study that characterized disulfide

formation in native bull sperm chromatin (29). However, the most likely scenario is that two protamine molecules bind cooperatively to each hairpin, which would account for the 2 populations in the sample of DNA alone and DNA with multiple protamines bound. This cooperativity may be minimized by adjusting the length of the duplex region of the hairpin to promote binding of one protamine molecule.

The design of an optimal DNA oligonucleotide for creating a complex with the intact protamine 1 or protamine 2 molecules could be problematic if the DNA duplex needs to be slightly longer than the actual protamine binding site, a reasonable assumption when interpreting the results from the NMR analysis of the C-terminal binding site and the G8hp oligonucleotide. First, the peptide bound specifically to the 5bp terminal end, not the entire length of the DNA, leaving 3bp charged and thus adding to the solubility. Second, the isolated bull protamine has regions with 5-6 consecutive arginines, unlike the peptide with no more than 3. The presence of a hydrophobic residue inserted between the clusters of arginine appears to contribute to the solubility of the complex as well. The combined results obtained from our analyses of the various complexes have identified several factors that contribute to the formation of insoluble protamine-DNA hairpin complexes. Applying this information, our future complexes will be

prepared using protamine 1 molecules that retain the two native intramolecular disulfide bonds (29), but have the other cysteine residues methylated. This should prevent the formation of disulfide bonding that leads to the irreversible complex aggregation, while also preventing the arginine residues in the terminal peptide sequences (those outside the DNA-binding domain) from interacting with the thymine loops. Alterations in the base sequence of the duplex region of the hairpin DNA will also be made to optimize the ability of the single phenylalanine residue in protamine 1 to intercalate into the duplex sequence. This may involve, for example, positioning an A:T–G:C junction at the appropriate place in the sequence so the intercalation of the phenylalanine would direct the full protamine 1 molecule onto the DNA such that it preferentially binds starting at the end of the duplex sequence, away from the thymine loop as was observed for the first complex we prepared. If this is insufficient to direct the ordered binding of the protamine to the end of the hairpin sequence, we may need to alter the sequence of the protamine 1 molecule by inserting intermittent hydrophobic residues in between two or more arginine clusters and tailoring the sequence of the DNA, as described above, to direct the binding of the protamine to the end of the sequence through the intercalation of these phenylalanine residues.

Conclusion

Previous studies have shown that the neutralization of the negative charge of the phosphate backbone of DNA upon protamine binding results in the formation of an insoluble protamine/DNA complex. We have demonstrated that we can obtain soluble complexes by designing hairpin DNA sequences that contain loop regions that preclude peptide binding, thus the complexes are not neutralized, and can be analyzed by NMR. To date, we have studied three complexes (G8HP+$R_3FGR_3SR_2VA_2R_2$, C11HP+R_6GGR_6, and C11HP+R_6FGR_6) and all the relevant DNA and peptide controls. Our preliminary studies show that binding of the peptides to the DNA is highly dependent on the peptide sequence and the length of the DNA duplex stem. The most recent experiments performed with the complete protamine 1 molecule, which to date have resulted in the formation of insoluble complexes, have identified several factors that must be overcome to create a soluble complex containing protamine 1.

Acknowledgement

We gratefully acknowledge Dr. Monique Cosman for contributing her NMR expertise to this project and for training and mentoring Cheryl Dolan in structural biology.

References

1. Balhorn R, Cosman M, Thornton K, Krishnan VV, Corzett M, Bench G, Kramer C, Lee J IV, Hud NV, Allen M, Prieto M, Meyer-Ilse W, Brown JT, Kirz J, Zhang X, Bradbury EM, Maki G, Braun RE, Breed W. Protamine mediated condensation of DNA in mammalian sperm. The male gamete: from basic knowledge to clinical applications. Vienna, IL: Cache River Press; 1999: 56-70.

2. Allen MJ, Bradbury EM, Balhorn R. AFM analysis of DNA-protamine complexes bound to mica. Nucleic Acids Res 1997; 25:2221-2226.

3. Hud NV, Allen MJ, Downing KH, Lee J, Balhorn R. Identification of the elemental packing unit of DNA in mammalian sperm cells by atomic force microscopy. Biochem Biophys Res Commun 1993; 193:1347-1354.

4. Hud NV, Downing KH, Balhorn R. A constant radius of curvature model for the organization of DNA in toroidal condensates. Proc Natl Acad Sci USA 1995; 92:3581-3585.

5. Ward WS, Zalensky AO. The unique, complex organization of the transcriptionally silent sperm chromatin. Crit Rev Eukaryot Gene Expr 1996; 6:139-147.

6. Brewer LR, Corzett MH, Balhorn R. Protamine-induced condensation and decondensation of the same DNA molecule. Science 1999; 286:120-123.

7. Cho C, Jung-Ha H, Willis WD, Goulding EH, Stein P, Xu Z, Schultz RM, Hecht NB, Eddy EM. Protamine 2 deficiency leads to sperm DNA damage and embryo death in mice. Biol Reprod 2003; 69:211-217.

8. Feughelman M, Langridge R, Seeds WE, Stokes AR, Wilson HR, Hooper CW, Wilkins MHF, Barclay RK, Hamilton LD. Molecular structure of deoxyribose nucleic acid and nucleoprotein. Nature 1955; 175:834-838.

9. Wilkins MHF. Physical studies of the molecular structure of deoxyribose nucleic acid and nucleoprotein. Cold Spring Harbor Symp Quant Biol 1956; 21:75-90.

10. Bradbury EM, Price WC, Wilkinson GR. Polarized infrared studies of nucleoproteins. J Mol Biol 1962; 4:39-49.

11. Suau P, Subirana JA. X-ray diffraction studies of nucleoprotamine structure. J Mol Biol 1977; 117:909-926.

12. Fita I, Campos JL, Puigjaner LC, Subirana JA. X-ray diffraction study of DNA complexes with arginine peptides and their relation to

nucleoprotamine structure. J Mol Biol 1983; 167:157 -177.

13. Hud NV, Milanovich FP, Balhorn R. Evidence of a novel secondary structure in DNA-bound protamine is revealed by Raman spectroscopy. Biochemistry 1994; 33:7528-7535.
14. Balhorn R. A model for the structure of chromatin in mammalian sperm. J Cell Biol 1982; 93:298-305.
15. Warrant RW, Kim SH. α-Helix-double helix interaction shown in the structure of a protamine-transfer RNA complex and a nucleoprotamine model. Nature 1978; 271:130-135.
16. Bench GS, Friz AM, Corzett MH, Morse DH, Balhorn R. DNA and total protamine masses in individual sperm from fertile mammalian subjects. Cytometry 1996; 23:263-271.
17. Pogany GC, Corzett M, Weston S, Balhorn, R. DNA and protein content of mouse sperm: implications regarding sperm chromatin structure. Exp Cell Res 1981; 136:127-136.
18. Darynkiewicz Z, Gledhill BL, Ringertz NR. Changes in deoxyribonucleoprotein during spermiogenesis in the bull. 3H-actinomycin D binding capacity. Exp Cell Res 1969; 58:435-438.
19. Balhorn R, Kellaris K, Corzett M, Clancy C. 7-Aminoactinomycin D binding and the final stages of sperm chromatin processing in the

mouse. Gam Res 1985; 12:411-422.

20. Puigjaner LC, Fita I, Arnott S, Chandrasekaran R, Subirana JA. Modelling and refinement of the crystal structure of nucleoprotamine from Gibbula divaricata. J Biomol Struct Dyn 1986; 3:1067-1078.

21. Chen H, Liu X, Patel DJ. DNA bending and unwinding associated with actinomycin D antibiotics bound to partially overlapping sites on DNA. J Mol Biol 1996; 258:457-479.

22. Prieto MC. Structural characterization of DNA-protein complexes by optically detected magnetic resonance and nuclear magnetic resonance. Ph.D. thesis. University of California, 1995.

23. Prieto MC, Maki AH, Balhorn R. Analysis of DNA-protamine interactions by optical detection of magnetic resonance. Biochemistry 1997; 36:11944-11951.

24. Corzett M, Kramer C, Blacher R, Mazrimas J, Balhorn R. Analysis of hamster protamines: primary sequence and species distribution. Mol Reprod Dev 1999; 54:273-282.

25. Jung H, Cooper A, Perham RN. Interactions of the peripheral subunit-binding domain of the dihydrolipoyl acetyltransferase component in the assembly of the pyruvate dehydrogenase multienzyme complex of *Bacillus stearothermophilus*. Eur J Biochem 2003; 270:4488-4496.

26. Gatewood JM, Schroth GP, Schmid CW, Bradbury EM. Zinc-induced secondary structure transitions in human sperm chromatin. J Biol Chem 1990; 265:20667-20672.

27. Bal W, Dyba M, Szewczuk Z, Jezowska-Bojczuk M, Lukszo J, Ramakrishna G, Kasprzak S. Differential zinc and DNA binding by partial peptides of human protamine HP2. Mol Cell Biochem 2001; 222:97-106.

28. Bench GS, Friz AM, Corzett MH, Morse DH, Balhorn R. DNA and total protamine masses in individual sperm from fertile mammalian subjects. Cytometry 1996; 23:263-271.

29. Balhorn R, Corzett M, Mazrimas JA. Formation of intraprotamine disulfides *in vitro*. Arch Biochem Biophys 1992; 296:384-393.